

**Impact of hypertonic osmotic stress on bacterial cell physicochemical
properties and the consequences for soil wetting properties**

by

Abd Alaziz Abu Quba (M.Sc.)

from Altall, Syria

Accepted dissertation thesis for the partial fulfilment of the requirements for a

Doctor of Natural Sciences

Fachbereich 7: Natur- und Umweltwissenschaften

Rheinland-Pfälzische Technische Universität Kaiserslautern-Landau (RPTU)

Thesis examiners:

Prof. Dr. Gabriele E. Schaumann, Landau in der Pfalz, Germany

Dr. Doerte Diehl, Landau in der Pfalz, Germany

Date of the oral examination:

15.11.2024

Declaration

I hereby declare that this PhD thesis, entitled “Impact of hypertonic stress on bacterial cell physicochemical properties and the consequences for soil wetting properties”, was conducted and created by my own with some Artificial Intelligence (AI) editing as described below. All assistances, contributors and authors are declared and clearly indicated in this thesis. This PhD thesis has never been submitted elsewhere for an exam.

This work has been subject to some Artificial Intelligence (AI) editing. ChatGPT 3.5 (<https://chat.openai.com/>) was used to improve the text flow. In detail, after writing my own text, I asked ChatGPT 3.5 to improve the flow of the text for readability. I used some expressions or words that better link between sentences than my own text or better emphasize the intended message. In addition, I sometimes accepted changes in the overall structure of the paragraph (order of sentences). I also accepted some singular/plural changes and some suggestions about the length of sentences e.g. dividing long sentences into parts or joining the short ones. Some suggestions about titles of some sections were considered. I critically reviewed all changes such that information is not changed but only the clearness and flow of the text is improved.

Landau in der Pfalz, 23.11.2024

Place, date

Signature (Abd Alaziz Abu Quba)

The following parts of this thesis are published:

Chapter 3: Abu Quba Abd Alaziz, Gabriele E. Schaumann, Mariam Karagulyan, and Doerte Diehl. "A new approach for repeated tip-sample relocation for AFM imaging of nano and micro sized particles and cells in liquid environment." *Ultramicroscopy* 211 (2020): 112945.

Supplemental Information: <https://bit.ly/3CzryZ0>

Abu Quba Abd Alaziz conceived, designed and conducted the experiments. Mariam Karagulyan produced the bacterial cells. The literature review provided in supplemental information for tip-sample relocation methods was made by Abu Quba Abd Alaziz and organized by Doerte Diehl. All authors contributed to the writing of the article.

Chapter 4: Abu Quba Abd Alaziz, Gabriele E. Schaumann, Mariam Karagulyan, and Doerte Diehl. "Quality control of direct cell–mineral adhesion measurements in air and liquid using inverse AFM imaging." *RSC advances* 11.10 (2021): 5384-5392.

Abu Quba Abd Alaziz conceived, designed and conducted the experiments. Mariam Karagulyan produced the bacterial cells. All authors contributed to the writing of the article.

Supplemental Information: <https://bit.ly/48RFWrH>

Chapter 5: Abd Alaziz Abu Quba, Marc-Oliver Goebel, Mariam Karagulyan, Anja Miltner, Matthias Kästner, Jörg Bachmann, Gabriele E. Schaumann, Doerte Diehl. "Changes in cell surface properties of *Pseudomonas fluorescens* by adaptation to NaCl induced hypertonic stress." *FEMS microbes* 4 (2023): xtac028.

Supplemental Information: <https://bit.ly/3YSqvul>

Doerte Diehl, Gabriele E. Schaumann, Marc-Oliver Goebel, Jörg Bachmann, Anja Miltner and Matthias Kästner had the project idea and acquired the funding. Abd Alaziz Abu Quba conducted the AFM/CFM experiments, analyzed the data and wrote the manuscript. Mariam Karagulyan, Anja Miltner and Matthias Kästner produced the bacterial cells and made the contact angle measurements. Marc-Oliver Goebel and Jörg Bachmann made XPS measurements and analyzed the data. Doerte Diehl made statistical analysis. All authors contributed to the writing of the article.

Chapter 6: Abd Alaziz Abu Quba, Marc-Oliver Goebel, Mariam Karagulyan, Anja Miltner, Matthias Kästner, Jörg Bachmann, Gabriele E. Schaumann, Doerte Diehl. "Hypertonic stress induced changes of *Pseudomonas fluorescens* adhesion towards soil minerals studied by AFM." *Scientific Reports* 13.1 (2023): 17146.

Supplemental Information: <https://bit.ly/3AMgmaW>

Doerte Diehl, Gabriele E. Schaumann, Marc-Oliver Goebel, Jörg Bachmann, Anja Miltner and Matthias Kästner had the project idea and acquired the funding. Abd Alaziz Abu Quba developed the method for estimating the contact area. Abd Alaziz Abu Quba, Doerte Diehl and Gabriele E. Schaumann, performed the AFM experiments, analyzed the data, performed the statistical analyses and wrote the paper. Marc-Oliver Goebel and Jörg Bachmann contributed with XPS, zeta potential and contact angle measurements, calculated the energy profiles based on the XDLVO theory and the work of adhesion. Mariam Karagulyan, Anja Miltner and Matthias Kästner prepared the stressed and unstressed bacterial cell suspensions. All co-authors contributed to an internal review of the manuscript.

Besides, Abd Alaziz Abu Quba contributed to the following publication:

Mariam Karagulyan, Marc-Oliver Goebel, Doerte Diehl, Abd Alaziz Abu Quba , Matthias Kästner , Jörg Bachmann, Lukas Y Wick, Gabriele E Schaumann , Anja Miltner. "Water Stress-Driven Changes in Bacterial Cell Surface Properties." *Applied and Environmental Microbiology* 88.21 (2022): e00732-22.

Abd Alaziz Abu Quba carried out the AFM analysis of the *Pseudomonas fluorescens* and *Bacillus subtilis* and contributed to the writing of the article.

Acknowledgements

First of all, I express my heartfelt thanks to God (Allah) for granting me the power to do my job in academic research.

I deeply appreciate my late parents, Mahfouz Abu Quba and Amena Alkahwaji. My father was truly ahead of his time, serving as a supportive figure who consistently encouraged me to pursue my aspirations. He instilled in me the value of striving for excellence and mastery, pushing the boundaries of knowledge, and excelling in my chosen field. I will always remember my mother with love and gratitude. When I was young, in times of economic difficulties, she dedicated herself entirely to support our family, working tirelessly to offer me a good life without burdening me with responsibilities. Her care, love, and encouragement laid the foundation upon which I could completely focus on my studies. Words cannot adequately convey my immense appreciation for her sacrifices. I wish she could share this moment with me; my thesis reflects her dedication.

I am thankful to my siblings for being always supportive. Our shared moments have been an escape from the daily routine; positivity affecting my life. I want to express my deepest gratitude to my brother, Waref Abu Quba, who has been like my twin in every sense, supporting me tirelessly throughout my doctoral journey. I can never forget his devotion whenever I needed him. He went out of his way numerous times, even at the cost of inconveniencing himself, to assist me. I would like to extend my heartfelt gratitude to my elder brother, Samer Abu Quba, whose support has been invaluable to me. I am truly fortunate to have him by my side. I also thank my sister Dr. Rana Abu Quba for the hints during the ups and downs of my work. She provided me with invaluable support and shared her expertise step by step, helping me navigate through obstacles.

With heartfelt love, I express my deepest gratitude to my incredible wife for her support and boundless patience. Her understanding during the periods when I needed to prioritize my writing has been invaluable. She has been a pillar, providing support every step of the way, consistently offering guidance and encouragement. I wholeheartedly wish her the very best in her studies. To my children, I am immensely grateful for your understanding during times when my work commitments created some pressure. The support I feel when I look into your eyes means everything to me. Your ability to adapt to the challenges we faced together is truly remarkable, and I am deeply thankful for your patience.

I want to thank Prof. Dr. Gabriele Ellen Schaumann and Dr. Doerte Diehl for giving me the opportunity to work in their research group. Their guidance and trust throughout my PhD period were reflected positively on my work. I cannot thank Dr. Doerte Diehl enough for enhancing the quality of my research. Her insightful comments and constructive criticism played an important role in the design of my methodological approach and writing of my papers. By working with her, I improved my critical thinking skills and learnt how to precise my research questions and formulate hypotheses. I am also grateful for her support during the review process. Additionally, her expertise in statistics helped me to check statistical significances in my results.

I extend my gratitude to Angelika Holderle for managing all administrative issues. I want to thank our technical assistants for their support and dedication in the laboratory. I thank both student assistants, Selina Morscheid and Lotta Fädler, for their good work. I am also grateful to Dr. Christian Dietz for his fruitful discussion. I thank Robin Kaltenbach and Ahmad Amer for their support in the beginning of my PhD. I thank all members of our working group.

Finally, I express my gratitude to all the funders and cooperation partners involved in the WetBac project. Their efforts are integral to the success and realization of this project.

Abstract

The wettability of soil particles defines important soil processes such as water infiltration in the soil and sorption of various substances on mineral surfaces. Soil water repellency (SWR) significantly impacts soil-water dynamics, often leading to reduced growth rates and crop yields. This phenomenon arises from hydrophobic coatings formed on soil particles by non-living organic compounds such as waxes, alkanes, fatty acids, free lipids and amphiphilic molecules.

While previous research on soil microorganisms mainly focused on their degradation activities, recent findings indicate a neglected aspect: the direct involvement of these microorganisms in hydrophobic interactions with soil particles modifying soil wettability. Specifically, it was found that the coverage of mineral particles by Gram-negative soil bacteria is associated with high water repellency of the produced cell-mineral association. Moreover, bacterial adaptation to drought stress increases cell surface hydrophobicity, suggesting a potential intensification of microbial induced SWR under changing environmental conditions. However, the mechanism, extent, and persistence of SWR caused by bacteria are poorly understood.

The aim of this work is thus to understand how a hypothesized increase of bacterial surface hydrophobicity, as an adaptation strategy to stress, affects cell adsorption onto mineral surfaces. My results are linked to scientific findings about cell growth processes under variations in soil moisture to estimate the short and long-term consequences of the drought stress on soil wetting properties. Key information at the single-cell level including cell size, stiffness, roughness and adhesion, obtained by improved atomic force microscopy (AFM) techniques, were linked to the stress induced changes of the bacterial surface hydrophobicity and surface composition obtained by contact angle and X-ray photoelectron spectroscopy (XPS) analyses, respectively. In addition, for the first time, a new AFM approach was developed to perform direct cell-mineral adhesion measurements taking the effect of contact area of these irregular materials into account. This helped to understand how cell growth environment and mineral type affect adhesion.

The findings of this study provide valuable contributions to both environmental sciences and biology by enhancing our understanding of soil-water dynamics. This knowledge helps to understand how the response of the ecosystem to environmental stress affects biological activities. In addition, it contributes to a broader understanding of soil processes such as the transport of fluids and the sorption of organic molecules and microorganisms on mineral surfaces. The results showed that stressed cells exhibit smaller size, higher stiffness and elevated protein content relative to unstressed cells. In addition, stress increases the contact angle in many strains, which indicates enhanced hydrophobicity due to the changes of the cell envelope structure. Such structural changes at the cell envelope also resulted to higher single-cell adhesion to hydrophobic than hydrophilic nanosurfaces (AFM tips) for stressed cells compared to unstressed cells. It is discussed that cell shrinkage induces protein crowding in the lipid bilayer while potentially releasing lipopolysaccharides (LPS) and lipids as membrane vesicles (MVs). The higher protein content increases the number of hydrophobic nanodomains

per surface area, which enhances hydrophobic interactions and reduces affinity towards aqueous solution.

Considering that by stress the ability of water to spread on cell surfaces becomes weaker, it is addressed that, during drought conditions, cells tend to minimize exposure to the stressful medium (aqueous solution). This is confirmed by increased adhesion pressure of montmorillonite and goethite versus stressed compared to unstressed cells due to increased hydrophobic interactions. In other words, the cells shield themselves from the stressful medium by adsorption to the mineral phase. The role of hydrophobic interactions is evident by the absence of stress induced increase of adhesion pressure towards quartz. Hence, quartz with high hydrophilicity consistently exhibits surface wetting during separation from the cell surface regardless of cell condition. Nevertheless, the unexpected weaker adhesion pressure towards kaolinite under stress could not only be described by its wetting characteristics. The interfacial properties of this mineral are highly affected by the specific surface (basal, edge or both planes) interacting with the cell surface as discussed in the thesis.

Based on my findings and other research, a comprehensive model that elucidates bacterial behavior and function throughout a drying-rewetting cycle is introduced. In conclusion, a microbial induced soil hydrophobizing effect is suggested, albeit its persistence appears to be sensitive to drought periods, showing only transient impacts among frequent shifts in moisture content. Furthermore, the observed increase in cell surface hydrophobicity plays a critical role in enhancing bacterial survival, fostering dynamic “beneficial” interactions within the soil which maintain plant productivity under stress conditions. Nonetheless, extended periods of severe dehydration, surpassing seasonal fluctuations, could lead to the cumulation of hydrophobic materials in the soil matrix upon cell decay, which could feedback into persistent hydrophobizing effect. This emphasizes the importance of understanding the balance between the dynamics of soil microbes and the prolonged environmental stressors for sustaining soil health and productivity.

Table of contents

Declaration	1
Acknowledgements	4
Abstract	6
Table of contents	9
1 Introduction	10
1.1 Soil-water interactions	10
1.2 Properties and composition of soil organic matter (SOM)	11
1.3 Causes of soil water repellency (SWR)	13
1.4 The potential role of microbial biomass for SWR	14
1.4.1 <i>Fungi and bacteria: reviewing the bacterial contribution</i>	14
1.4.2 <i>Mechanisms of bacterial adaptation to stress and the impact on soil properties</i>	16
1.4.3 <i>Microbial mobility and colonization in the soil matrix</i>	17
1.5 Atomic force microscopy (AFM)	19
1.6 Chemical force microscopy (CFM)	21
1.7 Force spectroscopy	22
1.8 Determination of cell shape and nanomechanical properties with AFM	24
1.9 Use of AFM to measure cell-mineral interaction (CMI)	25
1.9.1 <i>Concept and application examples</i>	25
1.9.2 <i>The effect of roughness on CMI</i>	25
1.9.3 <i>The effect of irregular surface geometry on CMI</i>	26
1.9.4 <i>Quality control of CMI</i>	27
2 Research questions, hypotheses and approach	29
2.1 Research questions	29
2.2 Hypotheses	30
2.3 Approach	31
3 A new approach for repeated tip-sample relocation for AFM imaging of nano and micro sized particles and cells in liquid environment	33
4 Quality control of direct cell–mineral adhesion measurements in air and liquid using inverse AFM imaging	42
5 Changes in cell surface properties of <i>Pseudomonas fluorescens</i> by adaptation to NaCl induced hypertonic stress	52
6 Hypertonic stress induced changes of <i>Pseudomonas fluorescens</i> adhesion towards soil minerals studied by AFM	62
7 Synthesis and Conclusions	80
7.1 Relevance of relocation and inverse imaging methods for life and environmental sciences	80
7.2 How to normalize adhesion? by tip radius or contact area?	81
7.3 Theoretical model of bacterial growth under stress condition	85
8 References	92
9 Annex	108
9.1 List of abbreviations	108
9.2 List of figures	109
9.3 Curriculum vitae	111

1 Introduction

1.1 Soil-water interactions

One of the most fundamental soil functions is to absorb and retain water and nutrients which are subsequently accessed by the plant roots providing necessary elements for plant growth and food production (Fageria & Moreira, 2011; Waraich *et al.*, 2011). The availability of water at the soil surface varies, ranging from situations of unlimited water, when water is ponded above the soil, to limited water originating from rainfall, irrigation, condensation, snowmelt or other sources (Nimmo & Shillito, 2023). However, the maximum amount of water that can infiltrate into the subsoil is constrained by the water retention capacity, which in some cases might be insufficient to accommodate the incoming water supply, resulting in runoff processes (Nimmo & Shillito, 2023). The water retention capacity is influenced by various soil characteristics, including soil hydraulic conductivity, sorptivity, hydrophobicity, layer structure and water as well as air content (Gupta & Larson, 1979; Nimmo & Shillito, 2023).

The fraction of the interstitial spaces between the soil particles (pores) that is occupied by gas, liquid solution, ice or a combination of these media can vary significantly, depending on the type of soil and environmental conditions (Ball *et al.*, 1988; Watanabe & Flury, 2008; Keller & Håkansson, 2010). Typically, soil exhibits a porosity ranging from at least 30% to as much as 70% (Nimmo, 2013). This porous soil structure serves multiple purposes, including the retention of water and microorganisms within soil aggregates (Carter & Gregorich, 2007). Furthermore, it facilitates the transportation of nutrients and chemicals through the soil pore network (Petersen *et al.*, 1996; Bronick & Lal, 2005). The specific surface area of soil is influenced by the composition (clay and organic matter content) among other factors (Petersen *et al.*, 1996). Nevertheless, soil matrix is generally featured by a large specific surface area where numerous physiological activities take place (Bachmann *et al.*, 2021). Particularly, the boundaries of soil's solid particles serve as sites for interactions such as adsorption, hydrolysis and condensation processes which impact capillary actions and soil properties like hydrophobicity (Lambert, 2008; Majid *et al.*, 2023). Therefore, a comprehensive understanding of the interfacial properties of soil and the underlying interactions with the surrounding environment is crucial for advancing our knowledge in the field of soil science and can help humans to do management practices for improving crop yields and soil fertility (Fundamentals of Soil Physics - 1st Edition).

In general, most mineral particles are originally wettable meaning that water can readily spread out on their particle surfaces after dry periods (Lewin *et al.*, 2005; Uddin, 2008; Adamczuk *et al.*, 2022). High wettability of soil is conducive to water storage between soil particles (Heidar Barghi, 2019). At low to moderate water content, water forms bridges or clusters that are held against the force of gravity, partially due to capillary attractive forces toward the mineral phase and partially due to cohesive forces between water molecules, referred to as surface tension (Heidar Barghi, 2019). Soil water repellency (SWR) is defined as a reduction in the soil ability to absorb water, to the extent that it either limits water infiltration into the soil or completely prevents soil wetting and water retention for a duration that may last for few seconds, extend up to weeks or even longer periods (Doerr *et al.*, 2000; Hallett, 2007; Diehl, 2013; Caltabellotta *et al.*, 2022). Reports about SWR date as far back as 1917, but it was only after 1960, and particularly in the 1980s it has been realized that water repellency is more widespread than previously believed heading to an extensive research of this phenomenon (Doerr *et al.*, 2000).

It is agreed that SWR affects the availability and distribution of water in the soil matrix (Doerr *et al.*, 2000; Diehl, 2013). The consequences of this can be significant, as it can result in a decrease of the soil fertility, formation of persistent preferential flow paths and changes in the microbial community compositions (Doerr *et al.*, 2000; Morales *et al.*, 2010; Goebel *et al.*, 2011). In soils exhibiting high levels of SWR, water tends to form droplets or intermittent water films rather than continuous films on mineral surfaces (Goebel *et al.*, 2007). Moreover, soil that repels water can impede the infiltration of water causing increased runoff and soil erosion (Doerr *et al.*, 2000; Braun *et al.*, 2010). If water repellent properties persist over time, plants might experience water stress due to reduced moisture availability, resulting in decreased growth rates and lower yields (Goebel *et al.*, 2011). Nonetheless, a certain level of water repellency can be beneficial for protecting soil aggregates and enhancing soil stability (Tisdall, 1995; Hallett & Young, 1999). In addition, SWR can assist in minimizing water loss from the soil through evaporation (Bachmann & van der Ploeg, 2001).

1.2 Properties and composition of soil organic matter (SOM)

Soil organic matter (SOM) refers to the complex blend of all organic materials found in soils regardless of their source or level of decomposition (Navarro-Pedreño *et al.*, 2021). These substances can occur naturally like decomposing plant and animal matter or be introduced into the soil through human activities, such as the application of fertilizers or other processes (de Brogniez *et al.*, 2015; Navarro-Pedreño *et al.*, 2021). The chemical interactions between these

compounds and the different components of the soil play a role in various essential aspects of soil health and productivity including aggregate stability, water retention capacity, nutrient cycling frequency and cation exchange capacity (Lal, 2009; Murphy, 2015). This dynamic interplay between SOM and soil functions can be attributed to that any change in the quantity and nature of SOM leads to immediate impact on soil properties in contrast to other long-term processes like weathering (Lauber *et al.*, 2008; Navarro-Pedreño *et al.*, 2021).

The presence of microorganisms, such, as fungi and bacteria has an impact on the size of carbon stock and the composition of SOM (Kabiri *et al.*, 2016; Furtak & Gajda, 2018). The relative abundance of bacteria and fungi varies based on factors like moisture content, soil type and pH, density of cultivation, grazing pressure, nitrogen fertilization inputs, successional age and other environmental factors, but they together make more than 90% of the total soil microbial biomass (Bailey *et al.*, 2002; Six *et al.*, 2006; Lauber *et al.*, 2008). Bacteria are the predominant microorganisms inhabiting the root zones of plants alongside fungi (Furtak & Gajda, 2018). Among these bacteria in the rhizosphere is the genus *Pseudomonas* that produces substances including antibiotics, lytic enzymes, ethylene, auxin, and gibberellin (Ramos, 2004). Remarkably, studies have shown that a large number of species of around 5×10^{11} can be present in just 30 grams of soil, with the common species typically account for between only 1% to 0.1% of this count (Dykhuizen, 2005). This high level of diversity is crucial for soil functions as these microorganisms actively participate in nutrient cycles and help maintain soil quality by aiding in detoxification processes (Silveira *et al.*, 2006; Ko *et al.*, 2017). They also contribute to plant growth by creating suitable conditions for seed germination, root development and exchange of chemicals released by plants (Girvan *et al.*, 2003; Furtak & Gajda, 2018).

In soil ecosystem, it is suggested that most bacteria have closer associations with dissolved organic matter, specifically the hydrophilic pool that contains a substantial portion of low molecular weight compounds characterized by high carboxyl functional groups to carbon ratios (Xia *et al.*, 2020). However, the adaptation of bacteria to stress conditions leads to the production of several compounds in the soil solution which may include: extracellular polymeric substances (EPS), osmolytes, biosurfactants in addition to other compounds with hydrophobic nature (Baumgarten *et al.*, 2012; Miltner *et al.*, 2012; Achtenhagen *et al.*, 2015). Furthermore, in conditions marked by frequent drying and rewetting cycles, cells may undergo damage, releasing significant quantities of microbial residues, predominantly cell wall fragments, into the SOM which increase its lipids content (Miltner *et al.*, 2012).

1.3 Causes of soil water repellency (SWR)

The study of causes of SWR is complicated (Caltabellotta *et al.*, 2022) due to its association with numerous factors including moisture content (Weber *et al.*, 2021), soil texture and structure (Harper & Gilkes, 1994; Vogelmann *et al.*, 2013), soil temperature and its gradient (DeBano, 1981), soil management practices (Hallett *et al.*, 2001), vegetation type (Dekker & Jungerius, 1990), fire severity (Caltabellotta *et al.*, 2022), drying and wetting cycle frequency (Caltabellotta *et al.*, 2022), contaminations by petroleum hydrocarbons (Roy *et al.*, 1999) or microplastics (Cramer *et al.*, 2023) and finally amount as well as composition of the SOM (Davari *et al.*, 2022). Intensive research has been conducted to unravel the potential causes of SWR. Initially, researchers proposed that SWR originates from hydrophobic organic compounds such as waxes, alkanes, alkanols, fatty acids, and humic acids which are either parts of leaf surfaces or result from the microbial degradation of plant exudates (Doerr *et al.*, 2000; Six *et al.*, 2006; Goebel *et al.*, 2011; Mao *et al.*, 2019). This has been observed by experiments in which the originally wettable soil exhibited increased hydrophobicity when such water repellent materials were added into the soil (Doerr *et al.*, 2005; Achtenhagen *et al.*, 2015). In some soil sites, the adsorption of the organic molecules onto mineral surfaces can lead to enhanced hydrophobicity. In details, when the soil dries, the amphiphilic molecules can form hydrogen bonds between their polar ends, causing them to contract and reveal some sites of the hydrophobic SOM layers underneath them (Horne & McIntosh, 2000; Doerr *et al.*, 2000; Mao *et al.*, 2019). During the subsequent rewetting event, water has reduced affinity to interact with these low energy surfaces, resulting in decreased water availability within these hydrophobic domains of the soil (Diehl, 2013; Seaton *et al.*, 2019).

When exploring how organic matter affects soil wettability, it is important to take into account the type of soil because it affects the extent to which the hydrophobic compounds adhere to the particle surfaces (Chenu *et al.*, 2000; Adamczuk *et al.*, 2022). For instance, sandy soils with large particles are more likely to develop SWR compared to loamy and clayey soils with smaller particles (Majid *et al.*, 2023). In addition, an experiment demonstrated that even a small amount of microbial coating on mineral surfaces can notably increase the hydrophobicity of quartz particles (Achtenhagen *et al.*, 2015). Interestingly, this effect was not observed in silt and clay minerals, since the microbial coverage was insufficient to induce substantial changes in their surface properties because of their large surface area (Achtenhagen *et al.*, 2015).

As research on SWR progressed, it became evident that soil surface chemistry is quite complex. SWR cannot be only attributed to root and plant secretions; instead, recent studies have indicated that soil may become repellent through hydrophobic or amphiphilic substances that were previously not considered, including microplastics (Cramer *et al.*, 2023) and cell membranes of certain fungi and bacteria (Achtenhagen *et al.*, 2015). Changing the environmental conditions is also known to have an impact on the wettability of soil and may lead to the induction of SWR (Diehl, 2013; Bachmann *et al.*, 2021).

1.4 The potential role of microbial biomass for SWR

1.4.1 Fungi and bacteria: reviewing the bacterial contribution

The interaction between microorganisms and their surroundings is complex and there are many factors that can affect the properties of the cell-mineral association (CMA) including primarily the availability of food and water, the physicochemical characteristics of the soil, the type and composition of the microbial community, and the presence of stress environments (Miltner *et al.*, 2012; Furtak & Gajda, 2018; Seaton *et al.*, 2019). Considerable research has been devoted to exploring the impact of fungi on soil wetting properties. Fungi receive attention for several reasons: they constitute a substantial portion of soil biomass, they are believed to be more hydrophobic than bacteria, and they have the potential to manipulate soil hydrophobicity, stability, and water infiltration (Furtak & Gajda, 2018; Xia *et al.*, 2020; Salifu & El Mountassir, 2021). Indeed, it has been observed that certain fungi can hydrophobize initially wettable surfaces through the secretion of proteins known as hydrophobins (Chau *et al.*, 2012; Park & Lin, 2022). This phenomenon implies that the wetting nature of the specific fungal strain dominates the wetting properties of the soil they inhabit. For instance, research by Chau *et al.* demonstrated that after fungal incubation in sandy soil, chrono-amphiphilic fungi reduced SWR in originally repellent soil while increasing it in originally wettable soil (Chau *et al.*, 2012). The induced repellency by fungal treatment reduces the soil hydraulic conductivity maintaining higher shear strength following rainfall events which helps for the deployment of a cost-effective method to enhance the stability of slopes and retaining walls (Salifu & El Mountassir, 2021; Park & Lin, 2022; Salifu *et al.*, 2022).

Initially, it was suggested that living bacteria could enhance soil wettability due to their involvement in various biological processes in the soil. Early studies suggested that bacteria, rather than fungi, play a key role in degrading soil hydrophobic compounds, thereby reducing SWR (Hallett, 2001; Roper, 2004). To experimentally confirm this, Hallett *et al.* employed

biocide treatment to inhibit the activities of specific microorganism. They demonstrated that soil wettability was improved when fungal activities were suppressed, while soil hydrophobicity was increased when bacterial activities were suppressed (Hallett, 2001). However, arguments arose later challenging the notion of estimating the effect of microorganisms on soil wettability based solely on their metabolic activities neglecting the effect of their surface properties (Achtenhagen *et al.*, 2015; Seaton *et al.*, 2019). It is proposed that if a particular microbial species is itself characterized by a hydrophobic cell wall, it could be involved in hydrophobic interactions, thereby increasing the water repellent property of the soil, even though it might partially decompose non living organic matter (Chau *et al.*, 2012). Thus, for example, improving infiltration in severely repellent soil may require the use of a microbial strain with robust degrading capabilities coupled with wettable cell surfaces (Chau *et al.*, 2012). Apart from that, bacteria can form biofilms with advanced water resistant properties. According to Epstein *et al.*, *Bacillus subtilis* can generate highly repellent biofilms that also inhibit the penetration of antimicrobial agents into the soil (Epstein *et al.*, 2011). These characteristics are attributed to an interplay between multiple factors including cell surface chemistry (the molecular composition and arrangement of the extracellular matrix), multiscale roughness and the reentrant topography that prevents the liquid from contacting the whole biofilm surface (Epstein *et al.*, 2011). However, the concept of biofilms acting as "diffusion barriers" against other materials should not be generalized to all microbial communities in the soil network, as this phenomenon is specific to certain species (Seaton *et al.*, 2019).

In recent years, there has been an emerging concept that environmental stress can significantly influence the characteristics of soil bacteria thus affecting soil properties (Achtenhagen *et al.*, 2015). This has motivated new research that deepens our knowledge regarding microbial interactions in soil ecosystems. Unlike fungi, bacterial communities are known to be highly dynamic (Seaton *et al.*, 2019) and respond quickly to changes in environmental conditions. For example, Rousk *et al.* found that as soil pH levels increased from 4 to 8 both the abundance and diversity of bacteria also increased, while fungi remained relatively stable within this pH range (Rousk *et al.*, 2010). This leads to the conclusion that bacteria have greater ability to adapt to stress conditions compared to fungi. In fact, the fungal cell membranes consist of melanin and chitin polymers and are more complex than the bacterial cell membranes which are composed of phospholipids with embedded proteins and extended lipopolysaccharides (Koebnik *et al.*, 2000; Bailey *et al.*, 2002; Six *et al.*, 2006). The polymers in fungi are more resistant to

degradation compared to phospholipids but less adaptable to various stress conditions (Bailey *et al.*, 2002; Six *et al.*, 2006).

1.4.2 Mechanisms of bacterial adaptation to stress and the impact on soil properties

As a reaction to drought stress, soil microbes can produce EPS that might be hydrophobic, especially when they get dried (Hallett, 2001). The cover of lipopolysaccharide (LPS) extracted from cultures of bacteria such as *Pseudomonas aeruginosa*, *Pseudomonas fluorescens* and *Escherichia coli* on minerals like kaolinite and montmorillonite resulted in decreased contact angles as detected by diiodomethane and formamide drops, along with an increased water contact angle (Chen & Zhu, 2004). This emphasizes the significance of non-polar interactions of cell-mineral associations. Drying and rewetting cycles have been shown to cause significant changes in the microbial community composition, which in turn explain the observed modifications in soil functions and processes (Fierer *et al.*, 2003; Braun *et al.*, 2010; Seaton *et al.*, 2019).

A common feature of Gram-negative bacteria is the production of membrane vesicles (MVs) as an adaptive mechanism to osmotic stress. These released vesicles consist of proteins and fatty acids, which increase cell hydrophobicity and promote biofilm formation (Baumgarten *et al.*, 2012; Mozaheb & Mingeot-Leclercq, 2020). In addition, water stress can stimulate the release of cytosolic compounds or the production of biosurfactants (Morales *et al.*, 2010; Achtenhagen *et al.*, 2015). The latter is known to reduce water surface tension at the adjacent regions which can reach as low as 50 % of the original surface tension level (Morales *et al.*, 2010). Biosurfactants, associated with organisms like *P. fluorescens*, are known to significantly impact cell surface properties, including hydrophobicity (Tuleva *et al.*, 2002; Vasileva-Tonkova *et al.*, 2006).

A review proposing a significant role of microbial biomass residues on SOM pointed that the hydrophobicity in soil particles is partially attributed to the formation of cell envelope fragments (Miltner *et al.*, 2012). When bacterial cells die and decompose, their cell envelopes can fragment releasing the lipid bilayers into the surrounding surfaces (Fierer *et al.*, 2003; Michel *et al.*, 2017). Upon interaction with the particle surfaces and subsequent drying, the adsorbed cell wall fragments can render certain areas of the soil hydrophobic (Miltner *et al.*, 2012).

Furthermore, it is well accepted that the stress leads to a reduction in bacterial growth rate (Jozefczuk *et al.*, 2010; Hachicho *et al.*, 2017) due to limited energy resources available for new biomass production, resulting in reduced cell maintenance activities (Oren, 1999). In such low energy environments, bacteria may exhibit smaller sizes, with membrane adjusted turgor pressure levels (Deng *et al.*, 2011), compared to unstressed conditions, either through increased cell division (Amy *et al.*, 1993) or shrinking processes (Spagnoli *et al.*, 2008; Francius *et al.*, 2011). Such changes in cell morphology are often associated with modifications in the community composition and can influence the configurations as well as functions of the membrane proteins (Lang, 2007; Miller *et al.*, 2016). While the shrinkage of bacteria can result in protein crowding or degradation to its basic structure, cell swelling stimulates higher protein production to maintain the same density at the cell surface (Lang, 2007).

So far, there has been no study concentrated on the bacterial cells themselves, particularly on whether they change the composition and structure of their cell walls to increase surface hydrophobicity in response to stress. Besides, the broader implications of these potential modifications at the microscale on the characteristics of the entire microbial colony at the macroscopic level remain unexplored. Solving those research gaps illustrates if the bacterial cell walls, which represent a significant portion of the SOM (Miltner *et al.*, 2012), contribute to the commonly observed decrease of soil wettability after severe dehydration.

However, how stress influences cell wettability at the single-cell level has not been tested yet. This is because traditional soil science techniques do not capture fine-scale interactions or the fast dynamics of microbial responses to environmental stressors. Atomic Force Microscopy (AFM) provides detailed images and force measurements at the nanoscale. Additionally, advanced analysis techniques enable the study of these phenomena on a larger scale, integrating biological and chemical processes such as changes in charge, chemical composition, and macroscopic wettability, upon stress which is complementary to the localized AFM information. Nonetheless, there are no straightforward protocols to directly address these research gaps, highlighting the need for the development of new methodologies.

1.4.3 Microbial mobility and colonization in the soil matrix

Many microorganisms live freely in a planktonic state within fluid environments before initiating the process of adhesion and colonization on solid surfaces (Oh *et al.*, 2007; Tuson & Weibel, 2013). The motion of bacteria towards these substratum surfaces can be driven by self-motorized activates of the pili known as “twitching” as well as external factors including

gravitational or hydrodynamic forces (Anselme *et al.*, 2010; Talà *et al.*, 2019). To survive in stress conditions related to limited water availability, high acidity, or extreme salinity, bacteria often form complex surface associated colonies called biofilms where they interact with each other by membrane organelles and chemical signals (Anselme *et al.*, 2010) ensuring higher stability and increased resistance mechanisms in comparison to individual cells (Oh *et al.*, 2007; Tuson & Weibel, 2013). Nevertheless, it has been suggested that even isolated, randomly adhered single-cells on surfaces can exhibit improved resistance properties in certain bacterial strains (John *et al.*, 2011). Hence, adhesion plays a pivotal role in the initial retention of individual cells on solid surfaces until they firmly adhere, giving rise to the formation of larger communities (Aguayo *et al.*, 2015; Mulansky *et al.*, 2017).

In soil ecosystems, bacterial adhesion can impact soil properties and functions significantly. For example, the capability of cells to colonize mineral surfaces and the pore spaces of minerals contributes to the development of soil aggregates and mineral weathering (Huang *et al.*, 2015). *P. fluorescens* shows a remarkable ability in colonization on soil, roots, and various biotic and abiotic surfaces because of its biofilm development capability (El-Kirat-Chatel *et al.*, 2014a). At suitable environmental conditions, *P. fluorescens* cells produce surface proteins, which are known for their role in promoting cell attachment towards both hydrophobic and hydrophilic substrates (El-Kirat-Chatel *et al.*, 2014a). In fact, even a slight enrichment of cells (Achtenhagen *et al.*, 2015) and biological molecules (Chen & Zhu, 2004; El-Kirat-Chatel *et al.*, 2014b) at mineral surfaces can lead to massive changes in surface properties, like surface roughness, charge, adsorption affinities, and wettability. Consequently, bacterial adhesion plays a crucial role in soil ecosystems (Cao *et al.*, 2006; Elbourne *et al.*, 2019).

The substrate surface properties such as morphology, roughness, chemistry, and initial protein content on cell adhesion have been thoroughly studied (Mitik-Dineva *et al.*, 2009; Anselme *et al.*, 2010; El-Kirat-Chatel *et al.*, 2014a). The role of cell surface extracellular appendages including flagella, pili, and curli, is believed to be significant in mediating bacterial adhesion to abiotic surfaces (Berne *et al.*, 2018). Apart from that, the environmental conditions in the vicinity, including factors like the ionic strength, the nutrient availability, the acidity level and the osmotic stress potential, have a direct impact on the kinetics of bacterial accumulation on solid surfaces and the subsequent processes of bacterial adhesion and biofilm formation (Hinsa *et al.*, 2003; Oh *et al.*, 2007; Anselme *et al.*, 2010; Baumgarten *et al.*, 2012).

Understanding how cell wall properties change in response to stress, and how these changes affect the interactions between cell surfaces and soil particles is crucial. Nevertheless, there has been no study to elucidate how stress affects the kinetics of bacteria to adhere to minerals surfaces. Additionally, the fate of the microbial colony after adsorption to the mineral phase is largely unknown. In details, it is not explored whether the hydrophobizing effect induced by bacteria translates to persistent SWR or if improved environmental conditions enable the cells to recover their unstressed physiology; featured by higher water content, reduced hydrophobicity and new biomass production. Again, AFM is promising to understand these complex interactions by allowing direct measurement of interaction forces between colloids under environmental conditions. However, absolute quantification of adhesion forces between natural materials must account for the "irregular" contact areas created by their morphological heterogeneity. This research area is difficult and there has been no suitable approach for it, in contrast to the intensive AFM research on engineered surfaces with well-defined shapes.

1.5 Atomic force microscopy (AFM)

Atomic force microscopy (AFM) belongs to the family of scanning probe microscopy (SPM) and is well established in the scientific community as powerful tool for surface analysis (Meyer, 1992). It provides the capability for imaging with sub-nanometer/nanonewton resolution (Meyer, 1992; Sullan *et al.*, 2013b). In comparison with scanning electron microscopy (SEM) and transmission electron microscopy (TEM) it has a greater number of applications in chemistry, physics, materials science, life and environmental sciences, biotechnology and medicine because of its unique ability to study solid, molecular and bioengineered materials for not only their nanostructures but also physicochemical properties (Yamashita *et al.*, 2012; Toca-Herrera, 2019; Yang *et al.*, 2019). Along with the minimal sample preparation required for AFM measurements, the advantage in microbiology research is the possibility to image the cell wall ultrastructure without staining or labelling and under the native physiological conditions; a critical aspect for understanding cellular functions (Dufrêne, 2014; Alsteens *et al.*, 2017; Qiu *et al.*, 2022). Taken together, AFM has revolutionized nanotechnology and opened new avenues for discoveries in nanoworld (Green *et al.*, 2003; Meister *et al.*, 2009; Sun *et al.*, 2011; Alsteens *et al.*, 2013; Longo & Kasas, 2014; Dufrêne *et al.*, 2017). With the continued development of AFM techniques, it is anticipated that AFM will be used more in the future becoming fundamental in the research of biointerfaces, which involve interactions between cells and biotic/abiotic surfaces (Variola, 2015; Alsteens *et al.*, 2017).

AFM instrumentation is rather simple (Neuman & Nagy, 2008). It is based on nano sharp tips fabricated at the very end of a beam or V-sharped micro sized spring (cantilever) fixed at a rigid chip at the end opposite to the side where the tip is located (Meyer, 1992; Lévy & Maaloum, 2001). This entire system is referred to as probe and can be mounted to an AFM machine using tweezers so that the tip is oriented towards the sample, which is placed on the AFM stage. The deflection of the cantilever due to tip-sample interactions when scanning over the sample surface is detected and magnified by a laser beam directed towards the end of the cantilever's backside and reflected back to a position sensitive detector made of 2 or 4 segmented photodiode (Meyer, 1992). A piezoelectric actuator (scanner) is normally used to drive the cantilever in XYZ motion (Trache & Meininger, 2008). For the operation mode PeakForce Quantitative Nanomechanical Mapping (PFQNM), the tip scans over the sample surface in XY raster motion (mapping) coupled with Z oscillations with low frequency in comparison to the resonance frequency (Meyer, 1992; Lévy & Maaloum, 2001). During each oscillation cycle, the sample shape as well as the tip-sample interaction forces are simultaneously captured (Allegrini *et al.*, 1992). Although the design of AFM probes can vary significantly with respect to factors such as the tip position, height, and the cantilever spring constant in order to accommodate a wide range of applications, producers seek to achieve the utmost tip sharpness, aiming to provide the highest spatial accuracy possible (Yan *et al.*, 2015). Even single atom terminated tips have been developed and demonstrated the capability to expand our understanding of the lattice structures of single crystals and the configurations of organic molecules (Sun *et al.*, 2011). Most commercial AFM tips, however, possess a tip radius of around 2 nm (information available online from Nanoworld and Bruker probes).

Nevertheless, a number of practical challenges can impact resolution. For instance, highly elastic materials, such as bacterial cells, may undergo deformation (Touhami *et al.*, 2004) causing lateral movement alongside the tip, resulting in poor quality of tracking of the cell shape (**Fig. 1**). Additionally, surface features with elevations greater than the tip radius become enlarged due to interactions with the conical sides of the tip which is referred to as tip-sample deconvolution (Markiewicz & Goh, 1994; Westra & Thomson, 1994). Due to matter with matter collision, the tip may also modify the surface or get contaminated leading to changes in resolution and altering the nature of the interaction (Pethica & Oliver, 1987).

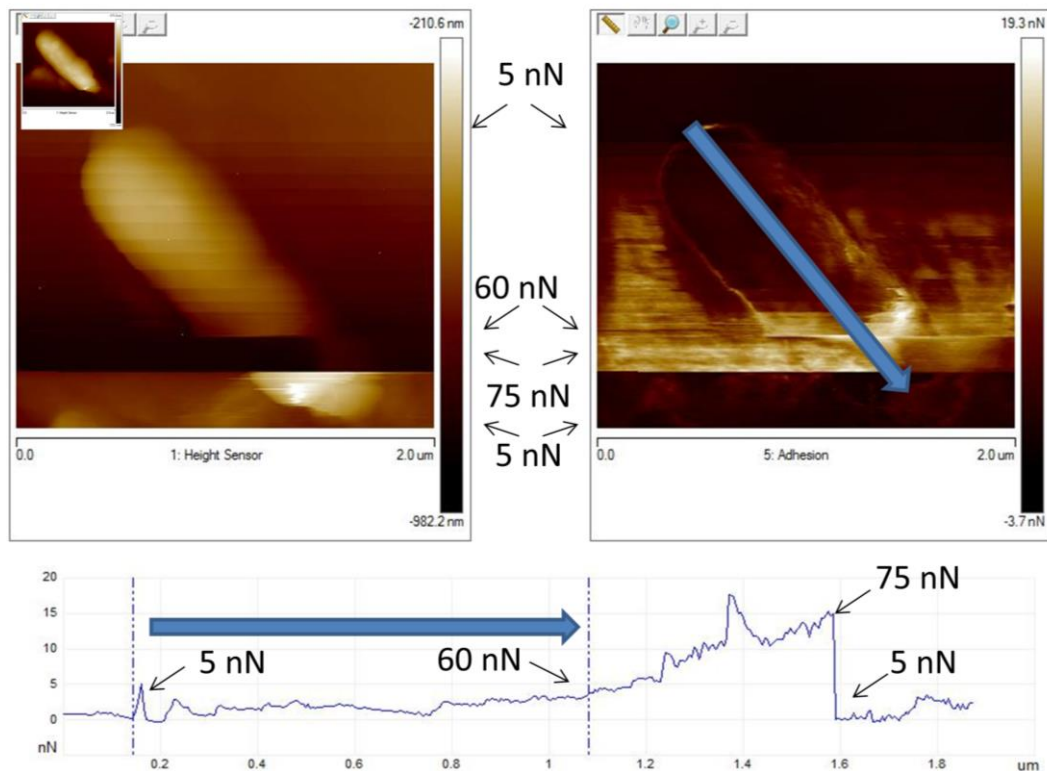


Fig. 1. Top left: single bacterial cell scanned with increased loading force from 5 to 75 nN in increments of 5 nN. High loading forces lead to cell deformation, which affects the quality of cell profiling negatively. The inset (top left) shows a subsequent scan of the cell at 5 nN, where the cell remains undamaged. Adhesion is influenced by the loading force, as seen in the brighter color of the adhesion channel (top right) and increased adhesion forces along the line scan (bottom) which is aligned with the direction of increased loading force (blue arrow).

1.6 Chemical force microscopy (CFM)

Chemical force microscopy (CFM) is similar to AFM system except the chemical functionalization of the tip which allows it be sensitive to specific interaction forces (Frisbie *et al.*, 1994; Beaussart *et al.*, 2020). One example is the study of the mutation of *Aspergillus fumigatus* Conidia cells induced by Sodium dodecyl sulfate (Dague *et al.*, 2007). Topography images showed damage to the outer membrane exposing the smooth cell wall polysaccharide underneath leading to reduced hydrophobic forces in comparison to intact regions (Dague *et al.*, 2007).

It is postulated that the strength of the bond formed when the interacting molecules on the tip come into contact with the sample surface is initially determined by the balance between several forces including electrostatic interactions, hydrophilic interactions (van der Waals forces and hydrogen bonding) and specific non-polar interactions linked to the interfacial free energies of

the two adhering surfaces (Xu & Logan, 2006; El-Kirat-Chatel *et al.*, 2013). The dynamic nature of organic molecules permits them to adjust their orientations, thereby optimizing their adsorption to apolar sites or reducing their contact with the surrounding polar medium (Xu & Logan, 2006; Huang *et al.*, 2015). As the contact time between the tip and the surface increases, these dynamic activities lead to a growing number of molecules from the tip being adsorbed to their conjugate partners on the surface. Simultaneously, interfacial water is gradually displaced, resulting in enhanced adhesion forces, until a saturation point is reached, at which all potential bond partners have interacted (Xu & Logan, 2006; Huang *et al.*, 2015). This phenomenon is referred to as "bond strengthening" and it exhibits variations in terms of its extent and saturation time among various bacterial strains (Meinders *et al.*, 1995; Xu & Logan, 2006).

In fact, the capability of CFM to explore the mechanisms of complex phenomena along with its high resolution makes it suitable for investigating the changes of the molecular interactions on cell surfaces as they adapt to stress, an area where our knowledge is still limited.

1.7 Force spectroscopy

In force spectroscopy experiments, the CFM or AFM tip moves towards the cell surface in a downward direction and then retracts upwards to its original position. Throughout this process, the forces acting on the tip are measured in a relation to the separation distance from the sample surface creation force-distance (FD) curve (**Fig. 2**). The series of events offers insights into how the tip interacts with the sample. When the tip comes into contact with the cell surface, molecules from the cell surface adsorb onto the tip (position 1 to 2, **Fig. 2**). During a short delay at position 2, additional molecules diffuse within the contact zone and adhere to the tip. This leads to bond strengthening (Huang *et al.*, 2015). When the tip is withdrawn, it reaches position 3 of zero force. More retraction leads to opposing (negative) forces (position 4). The peak of adhesion force is observed when the restoring force of the cantilever is equivalent to the maximum adhesion force (position 5). At this point, the number of chemical bonds in the stretched state reaches its maximum. Subsequently, the tip begins to detach from the cell surface in a step-like fashion, involving rupture events that correspond to a gradual unbinding of adsorbed molecules from the tip surface. This leads to a gradual shrinkage of the tip-sample contact area which culminates in the final rupture event, that takes place a few hundred of nanometers away from the surface just before complete separation (position 6). For details, please refer to the works (Baumgartner *et al.*, 2000; Dufrene, 2008; Sullan *et al.*, 2013a).

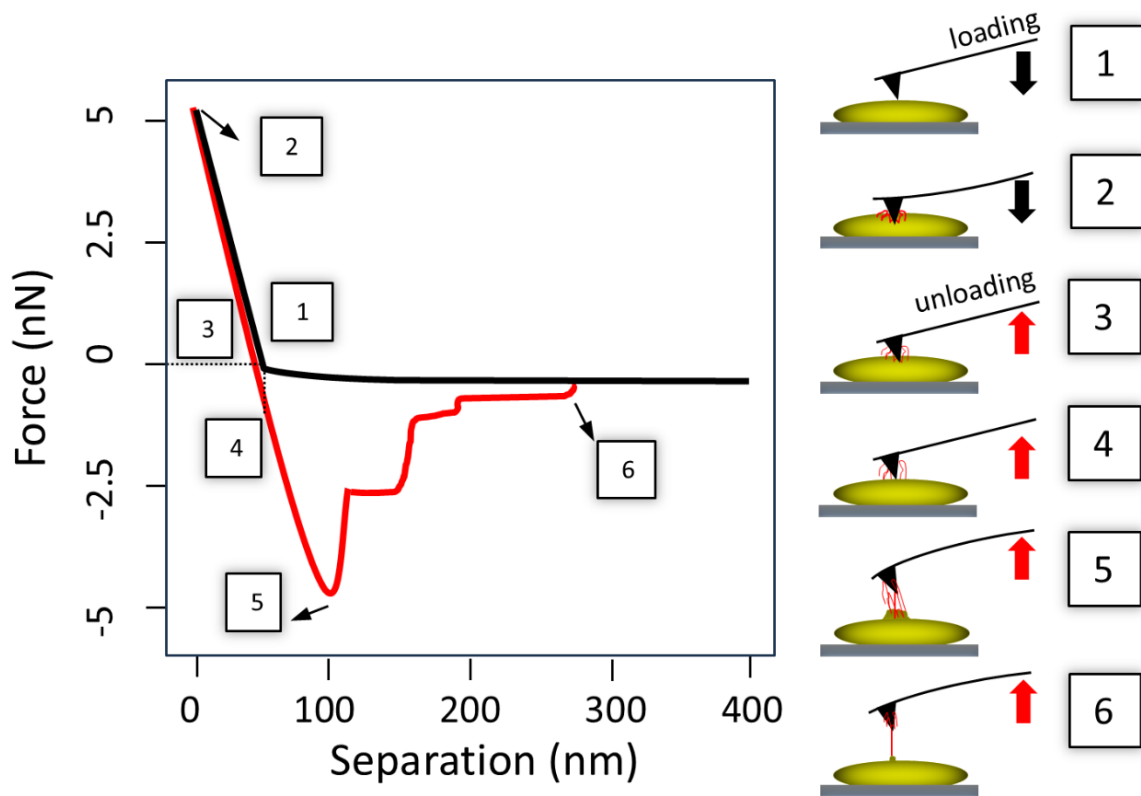


Fig. 2. FD curve (left) obtained between a CFM probe and a bacterial cell with sketches of tip-cell configuration (right) at the corresponding positions (numbers). The black curve illustrates the approach of the probe towards the cell surface, marking the point of initial tip-cell contact (1). Continuing the approach, the tip deforms the surface until reaching a predefined force setpoint (2). Subsequent retraction (red curve) shows force reduction, reaching zero (3), followed by a slight negative (attractive) force at the cell surface position (4). This is followed by a maximum adhesion peak (5). Then, a gradual unbinding of adsorbed molecules occurs reaching the rupture of the final bond leading to a complete separation (6). Note: Positions 1, 3, and 4 merge to the same point when there is no energy dissipation on the cell surface.

Force spectroscopy measurements have become a routine approach for exploring phenomena such as ligand binding, antibody-antigen interactions, and protein unfolding (Neuman & Nagy, 2008). Thereby, the maximum adhesion peak along with the number and magnitude of secondary adhesion peaks could be evaluated statistically (Chen *et al.*, 2011) to identify tip-sample long and short range forces or quantitatively (Alsteens *et al.*, 2017; Awassa *et al.*, 2022) to assign the type, length and stretching behavior of the specific molecules that promote cell adhesion. Furthermore, the integration over the area between approach and retraction curves gives the total energy required to break the tip completely free from the cell surface (Thewes *et al.*, 2015).

1.8 Determination of cell shape and nanomechanical properties with AFM

Bacterial interfacial properties are determined by the specific chemical composition and morphological features of the outer membrane e.g. the presence of various compounds which consist of functional groups (Rijnaarts *et al.*, 1999) creating certain patterns (Variola, 2015; Alsteens *et al.*, 2017) or inducing roughness (Alsteens *et al.*, 2013) on the cell surface. In this context, AFM research of the individual cells gave profound insights into the macromolecules architecture of the cell membrane including teichoic acids, extracellular polysaccharides networks and peptidoglycan cables with involved protein domains (Beaussart *et al.*, 2013; Alsteens *et al.*, 2013). For example, various Gram-positive species displayed major differences in the cell wall composition reflecting distinct approaches to the assembly of these structural elements on the microbial surface (Beaussart *et al.*, 2013; Alsteens *et al.*, 2013). It is well established that the cellular molecules are susceptible to the influence of osmotic stress, leading to phenomena such as conformational change of proteins (Lu & Schulten, 1999; Bremer & Krämer, 2019). The RmmH protein was observed to lose its highly ordered nanotubes configuration through increasing NaCl concentration from 50 to 500 mM (Faulkner *et al.*, 2019). Beyond the examination of bacterial responses to stress conditions, the protein segments were found to be sensitive to the scanning parameters of the AFM tip highlighting an urgent need for deeper understanding of their characteristics. For instance, AFM high resolution images (resolution 8 Å) revealed reversible geometrical transformations of the membrane proteins induced solely by changing the force applied to the scanning probe from 300 to 100 pN (Müller *et al.*, 1997).

The nanomechanical properties such as cell deformation, stiffness (defined by the elastic modulus) and viscoelasticity have been investigated using AFM indentation experiments (Shibata-Seki *et al.*, 2015; Efremov *et al.*, 2017; Li *et al.*, 2021). Apart from the quantification of the rigidity of the cell outer membrane and the underlying core layers cells, stiffness measurements facilitate the calculation of non-directly measurable parameters such as cell's circumferential surface tension and turgor pressure (Deng *et al.*, 2011; Chen *et al.*, 2012). The study of bacterial adhesion offers novel insights into the functional properties of surface polymers and appendages at both the single-cell and single-molecule levels (Alsteens *et al.*, 2013; El-Kirat-Chatel *et al.*, 2014a). Researchers have explored the role of surface biopolymers such as pili (Sullan *et al.*, 2013a), proteins (El-Kirat-Chatel *et al.*, 2014a) and glycopolymers (Beaussart *et al.*, 2013) in facilitating adhesion by changing the chemistry of the surface interacting with bacterial probes to selectively adhere to specific biopolymers.

1.9 Use of AFM to measure cell-mineral interaction (CMI)

1.9.1 Concept and application examples

AFM is the only technique for the study of interaction forces within biological systems at nanometer resolution and in aqueous solutions (Jaschke *et al.*, 1996; Beaussart *et al.*, 2013). In this regard, the tip is normally modified with microorganisms facilitating the mapping of flat or irregularly shaped natural surfaces (Huang *et al.*, 2015). Alternatively, a less frequent approach involves the attachment of a colloidal or mineral particle to the AFM probe to scan over bacterial cells or other solid surfaces (Long *et al.*, 2006; Feng *et al.*, 2020). In both methodologies, measured adhesion forces between the two interacting objects are theoretically independent on the experimental design (which object is at the tip and which one is at the sample). Instead, their interaction depends on their ability to adsorb to each other during contact. Numerous research groups have used AFM to study how variations in surface characteristics of cells, arising from changes in environmental conditions, impact microbial adhesion. Diao *et al.*, constructed various *Acidithiobacillus thiooxidans* bacterial coated probes and investigated their interactions with pyrite mineral showing a negative dependency between pH levels and adhesion forces (Diao *et al.*, 2014). Bowen *et al.* developed a probe featuring a single active yeast cell and quantified higher adhesion towards processed (hydrophobic) mica surface compared to freshly cleaved (hydrophilic) mica surface in an aqueous environment (Bowen *et al.*, 2001). In fact, it turned out that bacterial strains irrespective of their wide range of surface charges and hydrophobicity generally adhere preferentially to apolar surfaces compared to hydrophilic surfaces (van Loosdrecht *et al.*, 1990).

1.9.2 The effect of roughness on CMI

In my exploration of AFM research, it has become evident that the impact of surface roughness and irregular shapes on adhesion strength is a relatively less explored area. The effect of surface roughness, however, is more discussed than the contact geometry on irregular surface features. Xu *et al.*, reported a significant decrease of adhesion of *Staphylococcus epidermidis* and *Staphylococcus aureus* Newman cells on textured surfaces compared to the smooth controls shedding light on the role of surface topography in microbial adhesion (Xu & Siedlecki, 2012). Medilanski *et al.*, addressed that bacteria adhere more strongly to grooved and braided surfaces compared to the flat ones (Medilanski *et al.*, 2002). Edwards *et al.*, highlighted that a significant roughness effect takes place when the sample grooves or scratches conform with the cell morphology (Edwards & Rutenberg, 2001). These observations were discussed in terms of the

effective area available for bacteria-substratum interface. However, it was found that both surface topography and the specific cell type play crucial roles in governing bacterial adhesion to biomaterial surfaces (Abu-Lail & Beyenal, 2013). In cases when the bacterial cells attach firmly on the rough surfaces, it has been postulated that not only the out-of-plane (adhesion) forces but also the resistance to in-plane (shearing) forces increases (Berne *et al.*, 2018). SEM micrographs showed that a single *S. aureus* cell produces EPS if it gets compressed against a surface with rough pattern; a phenomenon that is absent at a smooth surface (Hizal *et al.*, 2016). A more comprehensive understanding of the nature of microbial adhesion on rough surfaces was addressed by Mitik-Dineva *et al.* who revealed that the alterations in cell interaction forces induced by surface roughness are not solely attributed to changes in the effective contact area but also involve substantial changes in cellular metabolic activities including modifications in the cell shape and the production of EPSs (Mitik-Dineva *et al.*, 2008).

1.9.3 The effect of irregular surface geometry on CMI

Incorporating the effect of the contact area is fundamental for describing the mechanisms of CMI. Especially, as soon as it touches a solid surface with high adhesion affinity, the cell progressively exposes its most binding sites towards the respective surface (Berne *et al.*, 2018). Such process is mediated by long range forces (Chen *et al.*, 2014) attracting, thus deforming, the cell surface in the vicinity of the initial contact area and eventually ends up with maximizing the cell-surface contact area until a balance occurs between the attractive force from the host surface and the counter membrane forces dictated by the rigid peptidoglycan layer (Carniello *et al.*, 2018). Consequences of this nanoscale deformation on the cell physiochemical properties have been reported including changes of the cell shape, viability (Chen *et al.*, 2014), viscoelasticity (Chen *et al.*, 2012), the polymer density (Berne *et al.*, 2018) as well as configuration (Carniello *et al.*, 2018) at the cell-surface interface. Firstly, for instance, the lateral extension of the original round cell modifies its profile into an ellipsoidal shape (Chen *et al.*, 2014). Secondly, under nutrient-rich conditions and appropriate temperatures, the increase in membrane tension, driven by the expansion of the cell, triggers the activation of membrane bound sensors, thereby, stimulating the adhering bacteria to produce surface polymers that firmly anchor the cells to the surface (Carniello *et al.*, 2018). The stimulated increase of the adhesion affinity due to the dynamic processes addressed above is indispensable for initially securing the cell to the surface until the irreversible adhesion processes evolve (Berne *et al.*, 2018; Carniello *et al.*, 2018). The latter takes place through “bond strengthening” processes and requires prolonged contact periods (Berne *et al.*, 2018; Carniello *et al.*, 2018).

In contrast to the controlled flat surfaces with specific roughness levels, natural materials with irregular shapes pose a greater challenge to quantitatively decipher tip-sample interactions as they can have multiple contact points (Neal *et al.*, 2005), resulting to a more complex contact geometry (Huang *et al.*, 2015). For instance, a study has illuminated that *E. coli* cells exhibit higher adhesion to needle-like goethite particles in comparison to the flat surfaces of goethite crystals (Huang *et al.*, 2015). In line with this, fewer number of contact points and, consequently, a reduced overall contact area elucidate why *E. coli* adhered less to larger nanoparticles in contrast to smaller ones (Zhang *et al.*, 2011).

The effect of the contact area is normally not considered primarily due to the lack of suitable approaches to visualize and quantify it. Neglecting this factor still permits the determination of the effect of changing the environmental conditions, e.g. solution pH (Chen *et al.*, 2021), on the adhesion forces between two interacting surfaces under identical experimental parameters i.e. where variations in contact area can be excluded. But meaningful comparison of the adhesion affinities between different samples, thus potentially with different contact areas and number of contact sites, under the same environmental condition is not possible (Lau *et al.*, 2009). Some studies have successfully addressed this challenge and explored the adhesion mechanisms by considering the effective tip-sample contact area. But such methods require at least one surface of either the tip or the sample to have an ideal shape; normally flat or sphere (Zhang *et al.*, 2011; Chen *et al.*, 2012; Spengler *et al.*, 2017). Normalizing the adhesion force by the contact area to get the so called adhesion pressure (P_{ad}) was proposed by Lau *et al.* to study the effect of cell maturation on biofilm-glass interaction of the *P. aeruginosa* strain (Lau *et al.*, 2009). To the best of my knowledge, no efforts have been made so far to estimate the contact area between two interacting "non-ideal" systems, such as a single rod-shaped cell interacting with needle-like goethite particles (Huang *et al.*, 2015), pseudo-hexagonal shaped kaolinite particles (Lázaro, 2015) or other particles with diverse shapes.

1.9.4 Quality control of CMI

While AFM is a powerful tool to perform interaction experiments between potentially any kind of biological and abiotic materials, a valid concern arises regarding the reliability of the observed results as long as it is not ensured that they are free from potential artifacts stemming from improper experimental design or other factors. For example, in a relatively straightforward scenario involving the interaction between a single-cell attached to the cantilever versus a flat sample surface, artifacts can occur if the respective cell is killed (Beaussart *et al.*, 2013) or

degraded (Thewes *et al.*, 2014) likely due to the heat generated by the laser beam (Beaussart *et al.*, 2013), detaches from the tip during measurements (Neal *et al.*, 2005) or loses its biopolymers due to binding with the sample surface (Thewes *et al.*, 2015). In addition, given the tiny thickness of the bacterial cell, qualified user should consider cell positioning at the very end of the cantilever, otherwise the latter might touch the sample surface instead of the cell (Thewes *et al.*, 2014). The process of calibrating the deflection sensitivity necessitates both the tip and the sample to be rigid, thereby permitting calibration before the probe is modified with biological materials. This means after calibrating it without a cell, the probe must be removed from AFM for modification and then remounted potentially resulting in laser misalignment that could introduce errors into the measurements (Ricci & Braga, 2004). These challenges already pose considerable complexities when conducting AFM spectroscopy in simplified systems. The situation becomes even more complex when investigating interactions between two materials with irregular shapes. Huang *et al.*, suggested that the cantilever surface should be uniformly coated with a bacterial film when scanning graphite particles, which could potentially make contact with the cantilever surface at any point within the end zone (Huang *et al.*, 2015).

In fact, scientists developed several strategies to avoid artifacts and verify the reliability of the results. One straightforward approach involves confirming the specificity of the FD curves achieved by bacterial probe by comparing their characteristics with those acquired using an unmodified tipless probe (Thewes *et al.*, 2014). Additionally, performing FD curves on a calibration surface both before and after an experiment proves to be a rapid and effective method (Chen *et al.*, 2014). In the context of interaction between diverse natural materials under environmental conditions, the shape and viability of the cells at the modified probes are normally assessed before and after the application of the probes for AFM interactions through one or multiple correlative techniques such as optical microscopy (Zeng *et al.*, 2014), fluorescence microscopy (Beaussart *et al.*, 2013; Zeng *et al.*, 2014; Diao *et al.*, 2014) and scanning electron microscopy (Sheng *et al.*, 2007; Diao *et al.*, 2014; Gultekinoglu *et al.*, 2016). The advantages and limitations of the probe type used in the modification process (Mulansky *et al.*, 2017) as well as the method for the quality control (Vahabi *et al.*, 2013; Jost & Waters, 2019) of the AFM experiments, have been thoroughly examined. Nevertheless, current methods provide only information about the general stability of the modified probes and do not have enough resolution to visualize if the 3D nanostructure of the contacting segments between the tip and the sample are stable during CMI. In addition, a validation method that can be applied without the need to remove probe from the liquid medium is needed.

2 Research questions, hypotheses and approach

2.1 Research questions

Soil bacteria frequently face suboptimal growth conditions due to the competition for resources under stress. While it is known that the cell wall configuration and its functions are modified during drying, the specific changes in hydrophobicity directly at the cell surface i.e. before potential cell damage processes, remain unclear. Investigating the stress effects at the single-cell level and how they are correlated to the macroscopic scale, such as to bacterial films, may highlight a potential hydrophobizing effect of the cells. That means even stressed “intact” cells may contribute to the occurrence of SWR. Thus, the first focus of this study is to understand the process and identify the extent of the development of repellent properties on single bacterial cell surfaces due to hypertonic osmotic stress. In addition, how micro-scale microbial adaptations processes, potentially leading to changes of the cell hydrophobicity, chemistry, charge, morphology and stiffness, impact the culture on the macroscopic scale is to be understood.

For a deeper understanding of the ecosystem response to the environmental stressors, it is crucial to explore the effect of stress on cell adsorption at the mineral surfaces. The second aim is to identify the specific adhesion forces that promote cell attachment to mineral surfaces under varying environmental conditions. Thereby, the influence of cell history (stressed or unstressed) and the properties of different mineral species (shape, wettability and charge) on adhesion strength is addressed. To overcome cell-mineral interaction (CMI) research gaps, development of a measurement procedure enabling the consideration of the effect of contact area between irregular interacting materials is to be conducted. It is aimed to determine i) whether by stress the cell-mineral adhesion increases leading to a more stable association ii) which mineral classes adhere stronger to bacteria making them less susceptible to degradation, ultimately leading to an increased persistence of SWR.

The final objective is to enhance awareness about the long-term consequences of the drought stress on the wetting properties of soil and thus conclude concerning the relation between bacteria and SWR. This involves understanding how modifications in microbial hydrophobicity and other interfacial properties due to changing moisture content affect soil-water dynamics. Specifically, it is addressed whether the induced SWR persists following a rewetting event and to what extent bacteria can survive leading to reversible processes which may potentially

decrease their surface hydrophobicity.

2.2 Hypotheses

It has been accepted that the outer membrane plays a vital role in the cellular response to stresses. I generally expect that the severity of SWR induced by bacteria in the soil matrix strongly depends on the ability of cells to increase their surface hydrophobicity upon stress. It is hypothesized that the hydrophobicity of individual cell surfaces increases by stress (H1). It is further hypothesized that this increase is driven by changes in the physicochemical properties of the “self” cells (H2), rather than by external factors. In chapter 5, more details about the specific hypothesized changes of the cell properties that engage the cell in more hydrophobic interactions due to stress are addressed. In addition, the stress induced SWR of single-cells is expected to cumulatively lead to an enhancement of the microbial hydrophobicity at the macroscopic scale (H3).

The extent to which bacterial cells adhere to mineral surfaces plays an important role in the development of SWR at the mineral surfaces because it reduces the hydrophilic space available for mineral-water interactions. However, direct comparison of cell-mineral adhesion necessities considering the effect of contact size in adhesion forces. I suggest that the larger the interacting surfaces, the larger their adhesion forces. Thereby, adhesion forces are hypothesized to increase linearly with increasing the cell-mineral contact area, whereas the ratio adhesion force / contact area (adhesion pressure P_{ad}) is constant (H4). I also checked the commonly accepted hypothesis that adhesion forces increase with increasing cell-mineral contact time due to bond strengthening (H5). P_{ad} was used to understand how cell growth environment and mineral type affect adhesion. In aqueous dispersions, the level of cell-mineral P_{ad} is hypothesized to increase with increasing cell hydrophobicity (H6). In addition, the formation of the stable bacterial coverage requires some sort of hydrophobicity of the hosting surface. Thus, the hypothesis that less wettable minerals offer higher molecular interactions improving adhesion towards cells is tested (H7).

2.3 Approach

The focus of this work is to investigate the changes that happen directly at the cell surfaces when the cells grow in stress compared to unstressed medium. Therefore, the commonly known rod-shaped cells were tested in terms of the physiochemical properties, whereas those cells with apparent damage of the cell wall as well as the heterogeneous features that are smaller in size compared to the cell were not analyzed. These materials were more abundant in stress clusters than unstressed ones and are likely lysis products from some cells that die and decay during growth processes.

For the main hypothesis of the change of hydrophobicity at the cell surfaces (H1), chemical force microscopy (CFM) was applied on single *Pseudomonas fluorescens* cells with the expectation of enhanced adhesion forces towards the hydrophobic group $-\text{CH}_3$ and reduced forces towards the hydrophilic groups $-\text{COOH}$ and $-\text{NH}_2$ due to stress. Furthermore, cell properties including size and stiffness together with the cell surface composition were extracted by atomic force microscopy (AFM) and X-ray photoelectron spectroscopy (XPS) analyses (chapter 5), respectively. This helped to check if the specific structural changes operated at the cell surface when they grow in stress relative to unstress medium may explain the enhanced cell surface hydrophobicity (H2). Lastly, to address the issue of “scale effect” in (H3), the trend of the change in hydrophobicity of bacterial cultures was directly correlated with the one at the single-cell level. For that, the macroscopic contact angle (CA) detected by sessile drop measurements on dried films of bacterial cells grown unstressed or under osmotic stress was employed.

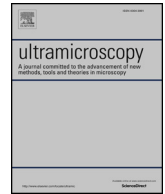
In the context of exploring CMI, I developed AFM methodology that allows measuring adhesion forces between a single mineral particle and a single bacterial cell consideration the effect of the “complex” contact area. This involved improvements to relocate nanosized objects by multiple AFM probes using a reference grid system (chapter 3) and a method to modify AFM tips with mineral particles which are then qualified by improved inverse imaging (chapter 4). A description of the method for estimating the contact area and the underlying assumptions are outlined in [Supplemental Information](#) of chapter 6. Briefly, a correlation between the 3D area of the mineral tip versus the tip height enabled estimating of the contact area at specific deformation level.

In chapter 6, Force-distance (FD) curves using mineral modified probes (kaolinite, montmorillonite, goethite or quartz) were obtained on stressed or unstressed cells in

10 mM KNO₃ solution. The cell-mineral contact area was increased by applying FD curves with incremental increasing loading forces to assess whether the adhesion force increases linearly with increasing the contact area. In addition, each adhesion force was normalized by the respective contact area to get P_{ad} which is assumed to be constant independent of the loading force (H4) and thus allows meaningful comparison of adhesion between colloids (Lau *et al.*, 2009). In addition, the hypothesis that increased contact time results in higher cell-mineral adhesion (H5) was investigated by increasing the contact time of the FD curves.

That the stress promotes greater adhesion of bacterial cells to mineral particle surfaces (H6) was checked by comparing P_{ad} values of stressed cells with those of unstressed cells for interaction with the specific mineral species. P_{ad} values were also compared between the various minerals interacting with stressed or unstressed cells to check if the reduced wettability of the mineral surfaces leads to higher adhesion affinity (P_{ad}) with the cell surfaces (H7).

3 A new approach for repeated tip-sample relocation for AFM imaging of nano and micro sized particles and cells in liquid environment



A new approach for repeated tip-sample relocation for AFM imaging of nano and micro sized particles and cells in liquid environment



Abd Alaziz Abu Quba^a, Gabriele E. Schaumann^a, Mariam Karagulyan^b, Dörte Diehl^{a,*}

^a University of Koblenz-Landau, iES Institute for Environmental Sciences, Environmental and Soil Chemistry Group, Fortstr. 7, 76829 Landau, Germany

^b Helmholtz Centre for Environmental Research – UFZ, Department of Environmental Biotechnology, Leipzig, Germany

ARTICLE INFO

Keywords:

Atomic force microscopy
Relocation
Chemically functionalized tip
Mineral
Bacteria
Liquid environment

ABSTRACT

The ability to repeatedly find exact the same nano region-of-interest (nROI) is essential for atomic force microscopy (AFM) studies of heterogeneous environmental samples. The large variety of methods makes it difficult to find the most suitable one for a specific research question. We thus conducted a literature research for nROI relocation methods and organized the found references in order to give an overview over relocation methods including the advantages, limitations and documented applications. This survey of nROI relocation methods and their key information facilitates the selection of appropriate methods with respect to a specific research question. Based on this survey, we developed a new AFM relocation approach urgently needed for the study of nano and micro sized particles and cells in air and aqueous environment. This approach uses commercially available TEM grids fully embedded in a semitransparent resin as a glue body on top of which particles and cells are fixed. Relocation of nROI within one grid is based on easily recognizable sample features in micro and nanometer scale. The stable sticking of the studied mineral particles and bacterial cells allows repeated measurements of the same nROI with differently functionalized tips in air as well as in water. Our simple, fast, and cost-effective method allows relocation with an accuracy of 10–40 nm and enables the implementation of AFM/ESEM correlative microscopy.

1. Introduction

Atomic force microscopy (AFM) is proven to be a powerful tool for the study of biological systems at the nano scale under different environmental conditions and temperatures [e.g., 1].

In general, prior to AFM scans, the surface of the sample is visualized by an optical microscope integrated into most AFM devices to choose a clean and proper sample area where the tip can engage. However, images produced by the tip consist of nanofeatures that are not detectable by the optical microscope [2]. This means that the optical microscope is "blind" for AFM features due to a "gap" between the magnification range of both techniques. This causes one of the main limitations of AFM: It is difficult to relocate the same sample area once the AFM probe is withdrawn from the surface [2–6]. Such an issue becomes more challenging or even impossible if the sample was removed from the AFM and returned with an angular rotation and positional offset [7–11]. However, the capability to find the same nano-target has a great advantage. It significantly broadens AFM applications because it allows the implementation of complementary AFM experiments as well as correlative microscopy [12]. Correlative microscopy is

defined as "... the application of two or more distinct microscopy techniques to the same region of a sample, generating complementary morphological, structural and chemical information that exceeds what is possible with any single technique..." [13]. Furthermore, in contrast to homogeneous and flat surfaces, natural samples are heterogeneous. Thus it is even more important to relocate the same area and map it under different conditions or after different treatments or using various probes in order to detect small changes in, e.g., adhesion in an environment with high spatial variations.

Thus, in order to bridge the gap of relocation, researchers have developed relocation methods with different strategies. However, the large variety of methods makes it difficult to find the most suitable one for a specific research question. Thus, the present study aims at giving an organized overview over repositioning methods including the advantages, limitations and documented applications. This will facilitate the selection and further development of relocation methods suitable for a variety of research questions.

* Corresponding author.

E-mail address: diehl@uni-landau.de (D. Diehl).

<https://doi.org/10.1016/j.ultramic.2020.112945>

Received 13 March 2019; Received in revised form 13 November 2019; Accepted 21 January 2020

Available online 22 January 2020

0304-3991/ © 2020 Elsevier B.V. All rights reserved.

2. State of the art: relocation methods

2.1. Literature research

In order to discover already existing relocation methods, we performed a literature research (for more details, please refer to Supplemental Information SI-1). The literature research showed that relocation strategies opened the way for numerous new applications, e.g., performing AFM nanomanipulation [14], studying bioelectrocatalytic surface activity [15], and investigating surface modifications as a function of external treatment such as annealing [6], freezing [16], solvent fumigating [3], bacterial infection [12], etc. Furthermore, numerous examples regarding correlative microscopy setups are covered.

As a general approach, the majority of relocation methods create pattern or marker on the sample surface near the region of interest (ROI). These markers can be relocated by the AFM optics in order to move the probe to the desired position (micro-alignment). This is normally followed by fast mapping of a large low-resolution AFM image including the desired region and a nano-alignment process by which the nanofeatures that need relocation are matched (with previous images) navigating the tip by the piezo tube to the desired location. Finally, a high-resolution scan of the desired region is performed. For most commercial AFMs, the last steps are facilitated by user friendly interfaces that enable rotational as well as positional tip offsets.

2.2. Categorization and evaluation of relocation methods

For a more detailed presentation of advantages and limitations, we classified the methods by their methodical approach into the following six categories (for a detailed list of methods and their applications and requirements, please refer to Table SI-1 in Supplemental Information):

- (i) reference relocation markers in the front side of the sample substrate,
- (ii) reference relocation markers in the backside of the sample substrate,
- (iii) large and fine markers in the back- and front side,
- (iv) progressively smaller alignment patterns,
- (v) particles solution drop-on-grid-and-dry procedure,
- (vi) non-marker principle.

Although some advantages of their methods over others are discussed by several authors, this seems to be not straightforward as each method has a functional specialty and thus a comparison of methods with different applications would not be very helpful. For instance, the method of Wu et al. [7] uses alpha-numeric relocation labels on mica surfaces to provide a higher relocation accuracy compared to the grid-guide relocation setup employed by Markiewicz und Goh [6]. In contrast, the method of Liu et al. [8] requires constructing a homemade grid in the backside of a mica sheet as a guide to accurately marking the front side by AFM nanolithography. Thus it was suggested to give a better distinguishable markers at the substrate surface compared to the methods of Markiewicz und Goh [6] and Wu et al. [7]. Nonetheless, the method of Markiewicz und Goh [6] was used to study the influence of annealing on a latex monolayer of polystyrene spheres and polybutylmethacrylate (PBMA) at temperatures up to 120 °C, whereas the experiments of Wu et al. [7] and Liu et al. [8] were done at room temperature. Therefore, the method of Markiewicz und Goh [6] is better qualified for experiments at elevated temperatures. The method of Su et al. [9] was stable even at 500 °C, a temperature that causes failures in other relocation constructions. As a consequence, insights into the different approaches with their advantages and limitations are not given in comparison to others works, but rather in relation to their potential applications. In this way, the working principle of each relocation group is characterized by their specific advantages and limits.

In category (i) the markers on the front side might damage the sample surface or could be harmful to the tip if the markers have sharp edges or rough character. However, if suitable markers were chosen, having markers inside the image turns to an advantage in some cases: E.g., by studying the impact of chemical etching on the nanoscale surface morphology, characteristic sample nanofeatures normally used to relocate the target area may be washed away whereas stronger pronounced markers remain allowing the relocation [17]. A general disadvantage of categories (ii) and (iii) is that they require a transparent substrate to observe the markers on the backside. Categories (iii) and (iv) lead to a fast relocation procedure, nevertheless, mostly involving time-consuming marking procedures. Finally, category (vi) without markers avoids artificial and maybe harmful alterations of the target surface and has a long term stability compared to other methods with markers as the latter may vanish after treatment [8].

2.3. Relocation methods suitable for our research question

In general, the background of our research is to understand which role bacterial cells and their cell wall debris have for surface properties of mineral surfaces in soil. For this aim we need to repeat measurements of adhesion forces at exact the same location on bacterial cells or mineral surfaces with AFM probes functionalized by different chemical groups. In addition, we want to compare these measurements obtained in air with others done in liquid environment in order to assess the effect of capillary forces of water films. Therefore, a relocation method is needed by which mineral particles and bacterial cells are fixed and measured on the same sample holder in air as well as in liquid. Several works discussed the relocation ability in fluids [9,12,16,18]. Both studies, of Su et al. [9] and of Kao et al. [16], require a configuration equipped with a flat sample surface rather than powder systems as we intend to investigate. The work of Janel et al. [12] allowed bacteria imaging in buffer, but requires a special method for fixation and incubation of the cells on photo etched coverslips at certain conditions. The method of Hagan et al. [18] was used to investigated rat intestinal epithelial cells which were properly attached at the substrate but such cells are much larger than the set of particles and cells analyzed here. Because none of the presented methods was suitable for our special application, we developed an additional new method that is essential for the relocation of nano and micro particles and biological materials fixed on a sample holder for AFM measurement in aqueous solutions. A successful method ensures the firm fixation of the investigated samples at the glue surface as well as a repeated relocation of exact the same sample region. Thus, our AFM experiments were divided into two phases. The first phase aims at the shape of the investigated substances, their fixation reliability and their adhesion properties. The second phase aims at the error of the proposed relocation method.

3. Methods

3.1. Fabrication of a relocation system for liquid environment

Fig. 1a illustrates the fabrication of a relocation system. (1) Inspired by Huang et al. [19], a small piece of the adhesive resin glue (tempfix, PLANO GmbH, Wetzlar, Germany) was set on a steel disk (Stainless Steel Metal Specimen Support Disc, 16,207-M, NanoAndMore GmbH, Wetzlar, Germany), and (2) heated up to 130°C for 30 s to melt the glue and form a flat glue surface. (3) After cooling to room temperature, a locator numeric-indexed-grid (Gilder Finder Grid, G400F1-Cu, 400 mesh, copper, Science Services, München, Germany) was set on the center of the hard glue body and (4) the system was again heated up to 130°C for 20 s to melt the glue, let the grid sinking inside it, and form a smooth glue surface over the grid. (5) A mica sheet (Mica Sheet, V5 Quality, Science Services, München, Germany) was set near the grid and fixed by heating the system up to 80°C rendering the glue more adhesive but not melted. The hard mica surface enables a direct

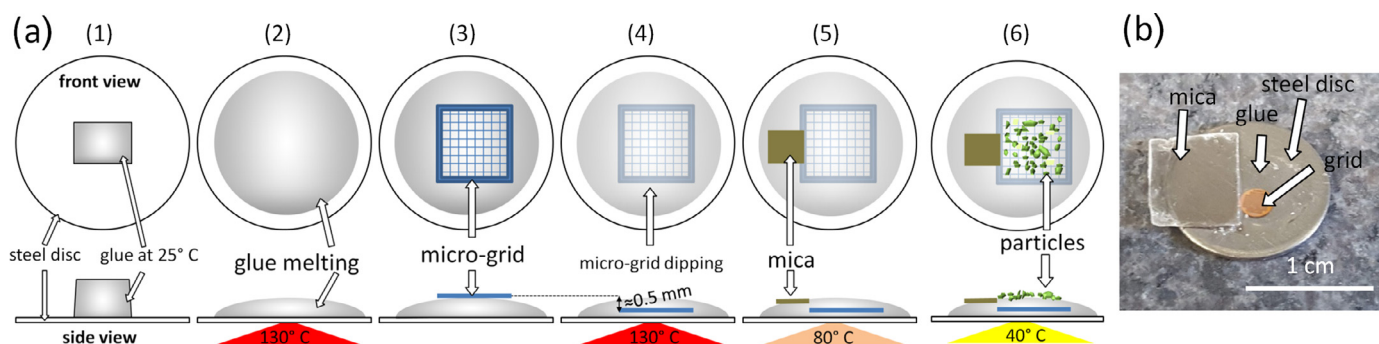


Fig. 1. (a) Fabrication steps for a relocation unit (see further description in Section 3.1), (b) camera image of the sample illustrated in step (6).

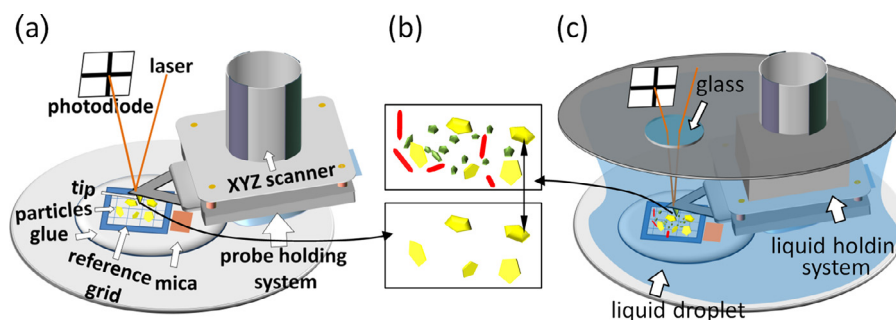


Fig. 2. Experimental approach by a multi-loaded system: (a) AFM system operating in air and (c) in a liquid meniscus, (b) relocation system with a single particle species scanned in air (down) and multi-particle species scanned in liquid (up) with a double arrow indicating the same particle in both systems.

calibration of the probe in water without changing the samples.

3.2. Fixation of minerals and bacteria on a relocation system

In order to fix quartz, montmorillonite, goethite and kaolinite particles on the surface of the glue, we followed the method described by Huang et al. [19]. Briefly, a droplet of particles suspension with concentration of 2 g L^{-1} was set over the grid spot and dried in air for 15 min in a laminar flow box (Figs. 1a and 6 b). The system was subsequently heated up to 38°C for 10 min to fix the particles at the surface of the glue. This was followed by rinsing the surface with ultrapure water (18.2 MO-cm, MilliQ®, Merck Chemicals GmbH, Darmstadt, German) and air drying for 15 min.

The used bacteria cells *Pseudomonas putida* mt-2 KT2440 (DSM 6125), *Rhodococcus erythropolis* (DSM 43066), *Pseudomonas fluorescens* (DSM 50090), and *Bacillus subtilis* (DSM 10) were grown following the method of Hartmans et al. [20]. In order to avoid effects on their bio-films and ultra-structures by an elevated fixation temperature, bacterial cells were adhered to the glue surface by air drying a bacterial suspension (tenfold diluted suspension in ultrapure water with an original optical density of 0.9) at room temperature for 20–30 min followed by rinsing the surface with ultrapure water. For *P. fluorescens* cells we prolonged the time of air drying to 30 min and increased repetition (3 times) and the impact of ultrapure water rinsing using a washing bottle.

3.3. AFM and ESEM imaging

AFM images were obtained by the Peak Force Quantitative Nanomechanical Mapping (PFQNM) mode using atomic force microscope (AFM, Dimension Icon, Bruker Corporation, USA). Prior to scan, the deflection sensitivity (Sv) was calibrated by averaging the slopes of the linear deformation regimes of at least 7 force-distance curves performed at different spots of a freshly cleaved mica sheet integrated in the relocation system (Fig. 1a, step 5). The spring constant (k) was determined by the thermal tune method taking into account at least 5 replicates resulting in less than 15% and 7% standard errors of Sv and k,

respectively. The tip radii (R) were measured by scanning a titanium roughness sample (RS-12 M, Bruker, Santa Barbara, CA, USA) and applying a blind tip reconstruction algorithm into the resultant images leading to ($R = 3\text{--}10 \text{ nm}$) for silicon nitride probes (Bruker, SNL) probes and ($R = 30\text{--}60 \text{ nm}$) for functionalized probes (chemical functionalized Pyrex-Nitride probes ST-PNP-CH₃, -NH₂, -COOH, SmartTips®, NanoAndMore GmbH, Wetzlar, Germany). For imaging in liquid (ultrapure water), we used the Bruker protocol with fluid meniscus [21].

In order to test AFM/ESEM correlative setup, the specific goethite particle pattern was imaged using an environmental scanning electron microscope FEI Quanta 250 ESEM (FEI Company, Hillsboro, United States) in low vacuum mode (acceleration voltage 15 kV, pressure 100 Pa). These acquisition parameters ensured non-destructive imaging of the goethite cluster avoiding degradation caused by the E-beam.

3.4. Experimental approach to test the fixation and relocation method

To reduce tip contamination, wear or degradation (especially for the sensitive chemically functionalized tips), we constructed a single system that contained different sample specimen and scanned them at once. We started from a simple relocation system that was loaded only with one type of particles or bacteria (Fig. 2b, down) and performed AFM images in air of some areas of these specimen (Fig. 2a). The relocation system was then removed from the AFM and other sample specimens were successively added using the drop and dry method mentioned above. After rinsing with ultrapure water, the reference area was probed in ultrapure water yielding an image that contains all added sample specimen (Fig. 2c and b, up, respectively). By matching AFM images in air and water (Fig. 2b up and down, respectively), it was possible to distinguish the first added samples from the newly added ones and prove their fixation ability and their relocation during the measurement in liquid environment. As a proof of concept, the fixation and repeated relocation of 8 model particles and cells with various surface properties were tested.

In addition, we produced relocation systems of individual minerals

and relocated inner micro and nano areas by three functionalized probes. We used notable surface features as correlations to align the relocated frames. To estimate the relocation accuracy (or error), we calculated the maximum possible drift between the relocated images. Thereby, the size of the particles scanned by the three probes had a slight deviation depending on the sharpness of the respective probes. Thus, among the repeated images of the same object, we took the smallest particle size (which reflects the sharpest tip) as a reference and calculated the accuracy as the dimensional enlargement of this particle in the other images with respect to the reference (measured at the fast scan direction).

4. Results and discussion

4.1. Fixation of samples for measurements in air and water

Since the shapes of particles have a strong effect on their adhesion properties, we employed eight samples with various forms in order to test the functionality of the method with a variety of minerals and bacteria (as described in Sections 3.1–3.2). To identify the different mineral particles and their fixation ability, a multi-loaded system was produced. We started with a simple system with one mineral type (kaolinite particles) that was scanned in air (Fig. 3a and b). After goethite and montmorillonite addition, the system was scanned in water (Fig. 3c, d and e). While the same two kaolinite particles were still observable in the same place, additionally, two goethite clusters and one montmorillonite particle were added to the depicted area (indicated by blue and orange frames in Fig. 3a and c). Discrimination between montmorillonite and goethite was straightforward due to their different shapes. The average adhesion of the minerals was calculated and is given by the representative value nearby each particle or cluster (Fig. 3e). The adhesion level of kaolinite and goethite is comparable to each other, but is much higher compared to that of montmorillonite. This highlights the power of the glue to adhere powders of different shapes and surface properties.

All measurements of the adhesion properties of the minerals were performed in liquid phase to exclude capillary forces always in present in ambient air. By using the multi-loaded relocation system, the uncertainty in adhesion calculations is minimized due to different reasons. First, the number of AFM images, necessary to study the three minerals, is reduced from three to one. This leads to a less scan-induced tip wear such that we can assume a constant tip radius for one image. In addition, tip wear is also reduced because only one essential preliminary relocation scan is needed to find the ROI. Finally, since we used the same probe for all minerals, we exclude additional errors sources in the determination of (k), (Sv) and (R) of various probes.

A system of two bacteria strains was prepared by the same strategy. The subsequent fixation of *P. putida* and *R. erythropolis* for imaging in

air worked very well (first and second rows of Fig. 4a–c). However, during imaging in water only *R. erythropolis* remained fixed whereas the culture *P. putida* became fully de-attached from the surface (third row of Fig. 4a–c). Probably, *P. putida* exhibits a lower sticking ability than *R. erythropolis*. This is further supported by a line scan of the adhesion channel across the two different strains (see corresponding black and blue line for scan in air and water in Fig. 4c). The level of adhesion of *R. erythropolis* (measured at the cell center) is with 7.8 nN higher than that of 4.9 nN for *P. putida* (Fig. 4d, black curve). Thus, only the cells with high surface adhesion towards the SNL tips remained at the glue surface after water addition. In order to improve the fixation of *P. putida* in water, we optimized the fixation method as mentioned in Section 3.2 allowing imaging of *P. putida* in air and liquid (Fig. 4e). We also proved the water fixation ability of *P. fluorescens* and *B. subtilis* (results not shown).

The topographical images of *P. putida* and *R. erythropolis* in air and water in Fig. 4a (second and third rows) and Fig. 4e (first and second rows), respectively, show that the cells exhibit larger heights in liquid than in air as observed by the higher brightness of the respective cells in water than in air. In addition, *R. erythropolis* cells exhibit lower adhesion in water than in air (Fig. 4c). As a result, our relocation method opens a gateway to study responses of the same species to changes in environmental conditions.

In order to compare our bacteria fixation method with methods from another study [22], we determined the cell-shape-preservation factor, i.e., the ratio of the cell dimensions width/height (W/H) ratio and the root mean square (RMS) roughness. Naturally, W/H ratio is close to 1 for an intact cell and rod-shaped bacteria [22]. This value however increases after fixation as the cells become flattened on the surface. For *P. putida*, the W/H ratio was with 4.6 ± 0.5 (mean \pm standard error of 11 cells) in good agreement to the suggested best fixation solution of the study of Chao and Zhang [22] with a W/H ratio in the range of 3.2–4.5 for the same strain. Moreover, the cell RMS roughness was with 8.7 in our method close to the value for no fixation in the study of Chao and Zhang [22] of 8.10 nm. The use of all other tested fixation solutions in this study resulted in much higher RMS roughness between 13 and 23 nm [22]. This highlights that our method is promising as it combines good W/H ratio and RMS roughness values indicating minimal disturbance of the natural morphology of the bacteria and thus of their natural surface properties.

4.2. Repeated relocation of μ ROI and nROI

Using the light microscope integrated to the AFM, we visualized the relocation systems. Although focus of the optics was set at the particles plane (see white arrows indicating kaolinite particles in Fig. 5a) the grid was still visible through the semi-transparent glue in which it was embedded. Due to changes of optical focus, the same area appeared

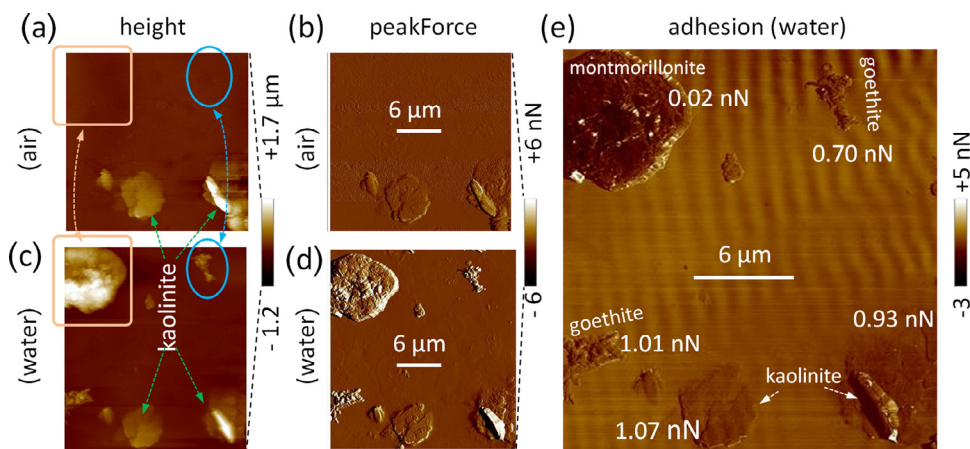


Fig. 3. AFM images of a multi-loaded system used to distinguish three kinds of minerals and their adhesion properties measured with the same tip: (a) height and (b) peakforce image in air of an area loaded with kaolinite particles, (c) height, (d) peakforce, and (e) adhesion image in water of the same area after the addition of montmorillonite and goethite.

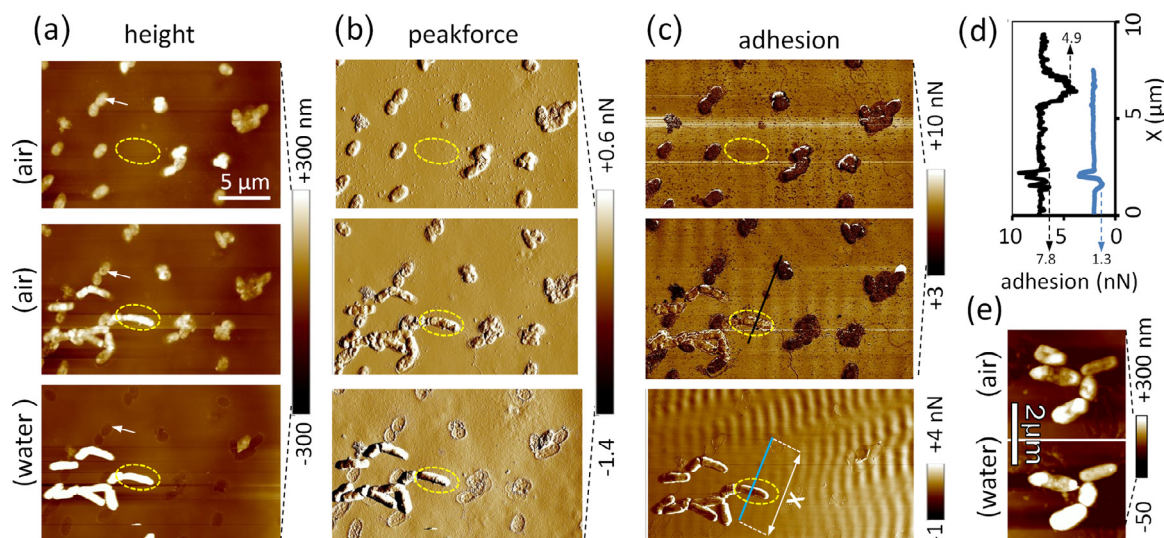


Fig. 4. AFM images of a multi-loaded system used to study the fixation ability of two bacteria strains *P. putida* and *R. erythropolis* in air and water: (a) height (b) peakforce, and (c) adhesion image of the system loaded with *P. putida* probed in air (upper row), after the addition of *R. erythropolis* in air (middle row) and in water (lower row). The dashed yellow markers and white arrows highlight the same positions. (d) Adhesion line scans at black and blue line in (c) middle and lower row, respectively, and (e) height image in air (up) and water (down) of *P. putida* after optimization of the fixation method.

different when a water droplet was introduced for imaging in liquid (Fig. 5b). Thereby, the particles seemed to vanish while the grid remained visible and enables the relocation of the region of interest at the microscale (μ ROI). Using higher magnification in the optical microscope (Fig. 5c and d), a region with specific particle pattern was chosen (see e.g., “ ϵ ” shaped goethite cluster in the inset in Fig. 5f) and scanned in a preliminary large-fast-low-resolution AFM map ($20 \times 20 \mu\text{m}$) made in the corresponding grid-square. Once re-found, the pattern was positioned in the center of the image of a high-resolution smaller scan ($6 \times 6 \mu\text{m}$) using X/Y piezo-offsets. Within this μ ROI, further piezo tunes were made to select a nano region (nROI) and to study the nanostructure of the goethite. The relative position of the nROI within the μ ROI was memorized by taking a screenshot of the latter indicating the scan area of the nROI by a zoom-square. Relocation of kaolinite and montmorillonite together with the bacteria samples was conducted similarly using first the “grid index” and second the “cluster or particle pattern”. However, since the size of the quartz particles is much larger, for the relocation procedure on their surfaces specific edge notches (Fig. 5e) are used as references to relocate an adjacent area.

To study the relocation ability, we used three chemically modified probes and investigated the same sample areas on four different minerals. These results are summarized in Fig. 6 where each row shows images of the same chemical probe (NH_2 , COOH , CH_3) and media

(water, air) while each column shows the same area of the same mineral with its respective inset referenced by a blue square. For instance, the image with a star is an inset of a goethite particle that is scanned by COOH probe in air. To find the same area of a “big” quartz particle, we used a notable surface notch as relocation marker (indicated by the blue arrow in the light microscope image in Fig. 5e and in the AFM image in Fig. 6a). The other clay minerals, however, were small enough to fit into one grid square and could be relocated only by the grid (Fig. 6b, c and d). The “ ϵ ” shape of goethite which was noted in Fig. 5f by the integrated optical microscope of the AFM could be accurately observed (Fig. 6c).

In order to investigate the relocation limitation, we performed local scans as shown in the right columns Fig. 6a, b, c and d. The three white arrows of each column highlight a surface feature that was used to align the images. For quartz, the nanostructure is made of linear pattern as can be observed by the CH_3 and COOH groups (Fig. 2a). By the NH_2 group in water, however, this pattern vanishes. To investigate the reason, we made a subsequent air scan at the same area using a sharp SNL probe and found that there is no pattern anymore and the surface appears flat just similar to the NH_2 image (result not shown). It is thus most likely that adding water to the surface has induced structural changes and caused detachment or a drift of surface features. Thus, the relocation accuracy decreases from $\sim 10 \text{ nm}$ for both, CH_3 and COOH

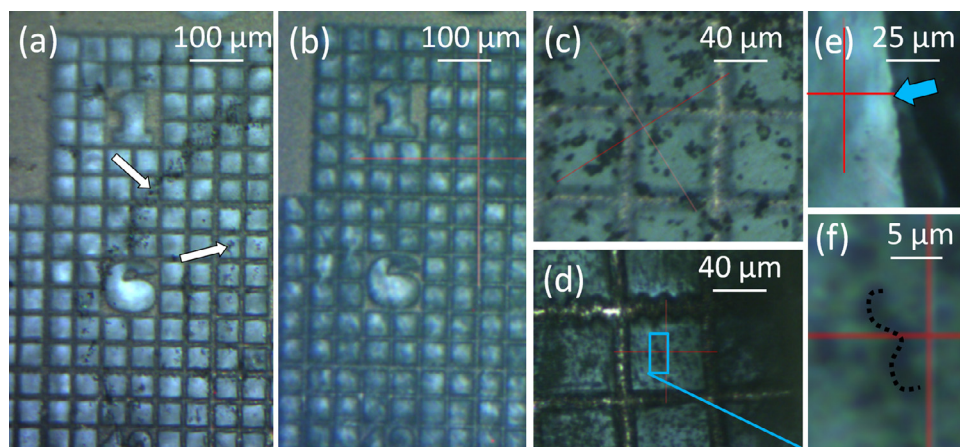


Fig. 5. Optical images of relocation samples with a focus on the top surface of the glue: (a) low magnification image of a sample with kaolinite particles in air, (b) the same area as (a) in water, (c) high magnification image of kaolinite particles, (d) high magnification image of goethite particles with (f) an inset of an area forming an “ ϵ ” cluster, (e) high magnification image of a part of a single quartz particle with the arrow indicating an “edge notch” used as a marker to relocate the same area.

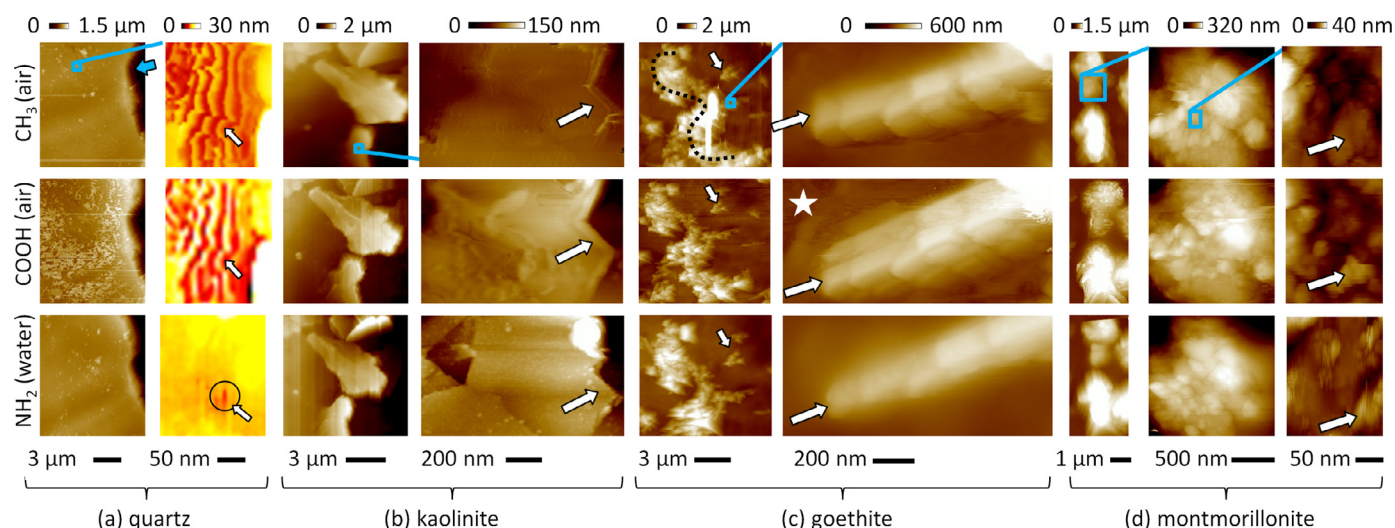


Fig. 6. Study of the relocation accuracy using three chemically modified probes. Height images on (a) quartz, (b) kaolinite, (c) goethite, and (d) montmorillonite obtained in air by CH₃ tip (upper row), by COOH tip (middle row) and in water by NH₂ tip (lower row). As indicated by the blue squares, the right columns of each mineral show insets of local areas of the images in the left columns. The three white arrows of each right column indicate the same position.

Table 1

Relocation error as the maximal enlargement of the smallest particle size between 3 repeated measurements.

Relocation error	Kaolinite	Montmorillonite	Goethite
COOH tip	~11 nm	reference	~30 nm
CH ₃ tip	~9 nm	~15 nm	~23 nm
NH ₂ tip	reference	~13 nm	reference

tips, to ~30 nm for NH₂ tip as there is no prominent feature that can be used for alignment. For the other minerals, the images within each column in Fig. 6 match well among each other, nevertheless, slight variations were observed. Specifically, some surface features in the down-right images of Fig. 6b and d show some differences compared to the other images along the same column. We calculated a relocation error as listed in Table 1. From the table it appears that the relocation accuracy depends on both, the probe as well as the sample shape. The best accuracy was obtained for kaolinite followed by the one of montmorillonite. For goethite with its needle-like structure the lowest accuracy was reached.

The case study of the clay minerals covered a significant diversity of forms, sizes and nano-structures. The capability to scan the same particle surface repetitively by tips with various chemical functionalizations is crucial, as this eliminates topographical interferences in the experiments. Thus, differences between the functionalized tips in adhesion towards exact the same particle surface can be attributed to different chemical-bonding affinities between the functionalized tips and the particle surface while a deviation of adhesion forces caused by different contact geometries of different kaolinite particles can be

excluded.

The relocation time for each particle of Fig. 6 varied. In air, a relocation-cycle required 10–15 min. This involves changing the sample, moving the probe to a new target grid-square, adjusting the scan parameters, engaging, doing a fast scan and performing offsets to relocate the ROI at the center of the image. Since changing the sample lasts longer in liquid-based experiments, a relocation cycle required ~20 min. However, if there is no need to change the sample, i.e. if several replicate measurements on the same grid are obtained, a relocation process lasts less than 5–7 min.

4.3. AFM/ESEM correlative microscopy

As another application example (beside the repeated measurement with differently functionalized tips) we used AFM/ESEM correlative microscopy at the "ε" shaped goethite cluster. The result of the AFM scan presented by the peakforce channel (Fig. 7a) is superimposed by a white color ESEM image (Fig. 7b). This superimposition shows a general match between both images. However, it is evident that the ESEM image reveals typical AFM dilation artifacts indicated by the size enlargement of the goethite clusters at the underlying AFM image. An example is indicated by the blue arrows in Fig. 7. In Fig. 7b, the maximum dilation length (values beside the arrows) as well as the respective cluster height (values in brackets) is given. It is evident that the higher the cluster height, the larger the dilation length. This is probably due to the side interaction between the canonical tip and the particle edge.

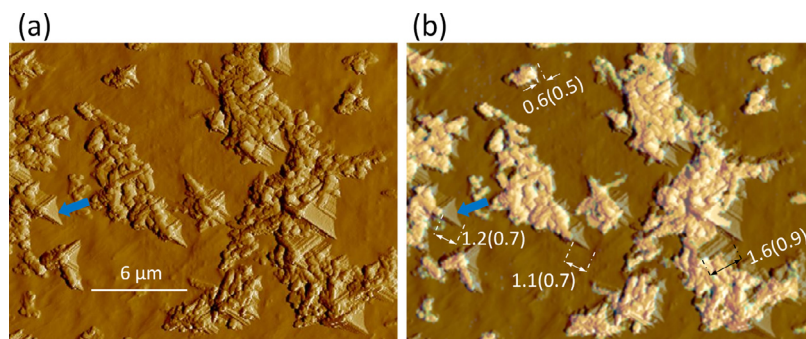


Fig. 7. Correlative AFM/ESEM microscopy: (a) peakforce AFM image and (b) an overlay of (a) and a white ESEM image of the "ε" goethite cluster that was investigated in Fig. 6c. The blue arrow indicates a dilation artifact. Double arrows and white values nearby in (b) indicate the dilation length (μm) of some clusters with the corresponding cluster height in brackets (μm).

4.4. General applicability of the relocation approach

The glue firmly holds particles and cells by its excellent sticking ability which avoids the use of additional adhesion agents and their potential negative effects on the natural state of the samples. The glue is inert and long-term stable under ambient conditions and remains solid up to a temperature as high as $\sim 40^\circ\text{C}$. The relocation time-per-cycle varies according to the experimental modification needed between the cycles. However, the time needed to fulfill the relocation steps is with 5–7 min in many cases equal or lower than the time required to find an appropriate region of interest on natural often quite heterogeneous samples.

With these characteristics, the presented relocation method offers a simple and robust tool for the physicochemical evaluation of nano and micro sized objects in which variations of environmental or physiological conditions are required. Thus, it has a great potential for applications in diverse fields of life sciences. The optimal size of the particles in our method is less than 100 μm , whereas, larger opaque particles or flat samples hide the grid and rather need another principle of relocation e.g. front side markers or non-marker techniques (category i or vi, respectively, in Supplemental Information, Table SI-1).

The large variety of AFM modes also requires a variety of specific relocation methods. The best scan modes for our method are those associated with less frictional forces e.g. non-contact, tapping, or peak-force modes, rather than the contact mode which might remove the particles. Only in this case, an additional adhesion agent, e.g., Poly-L-Lysine, is needed.

As an example for correlative microscopy, we showed how the proposed method allows correlative AFM/ESEM imaging which is an essential tool for nano-biological investigations. Other combinations with optical imaging technologies are applicable provided low-power light is used (e.g., bright and dark field optical microscopy). However, the method cannot be applied in analysis techniques that require specific properties of the substrate not fulfilled by the resin, e.g. electrical conductivity for Conductive Atomic Force Microscopy (C-AFM), thermal stability for annealing studies or carbon free substrates (e.g., for AFM-Raman). But modern coupled microscopic imaging systems offer smart solutions for switching between multiple techniques (e.g., by simply rotating the microscope turret) without the need of a relocation method.

5. Conclusions

The overview over different existing methods for relocation of nROI together with their key information shows that a variety of methods with different approaches already exist, each of them highly adapted to specific applications. Our newly developed relocation method is essential for the study of nano and micro sized particles and cells in air as well as in aqueous solutions. The simple, fast and cost-effective approach can be applied to a number of materials and leads with a relocation accuracy between 10–40 nm to highly reproducible results. The multi-loaded relocation system reduces the number of images and of relocation and calibration processes needed, to compare different samples. Resulting reduced tip wear and a more stable tip radius as well as other calibrated cantilever properties improve the comparability of adhesion measurements of different samples. In addition, it enables the implementation of non-coupled AFM/ESEM correlative microscopy without any adaptation of the AFM or ESEM sample stages and can thus help to detect AFM artifacts. The method relies on the presence of easily recognizable sample features in micro and nanometer scale, e.g., particle clusters as well as arrangement of single particles. Thus, for larger samples with relatively homogeneous areas, e.g., for quartz particles, relocation in the nanometer scale is difficult. However, for larger homogeneous surfaces, relocation in a nanometer scale is in most cases not necessary but a larger scale is sufficient. Due to the temperature sensitivity of the glue, the method is restricted to measurement

temperatures below 40°C . Hence, we developed a new valuable relocation strategy for environmental samples, especially suitable for our future studies of bacterial-mineral interactions and their role for surface properties in soils.

Declaration of Competing Interest

The authors declare that they no known competing financial interests or personal relationships that could have appeared to influence the work reported in this paper.

Acknowledgments

This work was supported by the German Research Foundation / Deutsche Forschungsgemeinschaft [Grant no DI 1907-2-1]. We want to thank both unknown reviewers for their valuable input.

Supplementary materials

Supplementary material associated with this article can be found, in the online version, at doi:10.1016/j.ultramic.2020.112945.

References


- [1] D.J. Müller, J. Helenius, D. Alsteens, Y.F. Dufrene, Force probing surfaces of living cells to molecular resolution, *Nat. Chem. Biol.* 5 (2009) 383–390, <https://doi.org/10.1038/nchembio.181>.
- [2] P. Zhou, H. Yu, J. Shi, N. Jiao, Z. Wang, Y. Wang, L. Liu, A rapid and automated relocation method of an AFM probe for high-resolution imaging, *Nanotechnology* 27 (2016) 395705, <https://doi.org/10.1088/0957-4484/27/39/395705>.
- [3] Y. Cao, Y. Liang, S. Dong, Y. Wang, A multi-wall carbon nanotube (MWCNT) relocation technique for atomic force microscopy (AFM) samples, *Ultramicroscopy* 103 (2005) 103–108, <https://doi.org/10.1016/j.ultramic.2004.10.007>.
- [4] Y. Maeda, Y. Gao, M. Nagai, Y. Nakayama, T. Ichinose, R. Kuroda, K. Umehara, Study of the nanoscopic deformation of an annealed nafion film by using atomic force microscopy and a patterned substrate, *Ultramicroscopy* 108 (2008) 529–535, <https://doi.org/10.1016/j.ultramic.2007.08.005>.
- [5] D.B. Nowak, M.K. Vattipalli, J.J. Abramson, E.J. Sánchez, Fabrication of a versatile substrate for finding samples on the nanometer scale, *J. Microsc.* 230 (2008) 32–41, <https://doi.org/10.1111/j.1365-2818.2008.01952.x>.
- [6] P. Markiewicz, M.C. Goh, Identifying locations on a substrate for the repeated positioning of AFM samples, *Ultramicroscopy* 68 (1997) 215–221, [https://doi.org/10.1016/S0304-3991\(97\)00035-1](https://doi.org/10.1016/S0304-3991(97)00035-1).
- [7] A. Wu, Z. Li, L. Yu, H. Wang, E. Wang, A relocated technique of atomic force microscopy (AFM) samples and its application in molecular biology, *Ultramicroscopy* 92 (2002) 201–207, [https://doi.org/10.1016/S0304-3991\(02\)00133-X](https://doi.org/10.1016/S0304-3991(02)00133-X).
- [8] Z. Liu, Z. Li, H. Zhou, G. Wei, Y. Song, L. Wang, Mechanically engraved mica surface using the atomic force microscope tip facilitates return to a specific sample location, *Microsc. Res. Tech.* 66 (2005) 156–162, <https://doi.org/10.1002/jemt.20158>.
- [9] M. Su, Z. Pan, V.P. Dravid, A convenient and rapid sample repositioning approach for atomic force microscopy, *J. Microsc.* 216 (2004) 194–196, <https://doi.org/10.1111/j.0022-2720.2004.01406.x>.
- [10] D.C. Turner, C. Chang, S.L. Brandow, D.B. Murphy, B.P. Gaber, Use of a repositionable substrate to acquire and compare distinct atomic force microscope images of a field of microtubules, *Ultramicroscopy* 58 (1995) 425–434, [https://doi.org/10.1016/0304-3991\(95\)00009-P](https://doi.org/10.1016/0304-3991(95)00009-P).
- [11] A. Fejfar, M. Hývl, A. Vetushka, P. Pikna, Z. Hájková, M. Ledinský, J. Kočka, P. Klapetek, A. Marek, A. Mašková, J. Vyskočil, J. Merkel, C. Becker, T. Itoh, S. Misra, M. Foldyna, L. Yu, P. Roca i Cabarrocas, Correlative microscopy of radial junction nanowire solar cells using nanoindent position markers, *Solar Energy Mater. Solar Cells* 135 (2015) 106–112, <https://doi.org/10.1016/j.solmat.2014.10.027>.
- [12] S. Janel, E. Werkmeister, A. Bongiovanni, F. Lafont, N. Barois, CLAFEM: correlative light atomic force electron microscopy, *Methods Cell Biol.* 140 (2017) 165–185, <https://doi.org/10.1016/bs.mcb.2017.03.010>.
- [13] K.A. Jahn, D.A. Barton, K. Kobayashi, K.R. Ratinaç, R.L. Overall, F. Braet, Correlative microscopy: providing new understanding in the biomedical and plant sciences, *Micron* 43 (2012) 565–582, <https://doi.org/10.1016/j.micron.2011.12.004>.
- [14] H. Xie, D.S. Haliyo, S. Régnier, A versatile atomic force microscope for three-dimensional nanomanipulation and nanoassembly, *Nanotechnology* 20 (2009) 215301, <https://doi.org/10.1088/0957-4484/20/21/215301>.
- [15] W. Nogala, A. Celebanska, K. Szot, G. Wittstock, M. Opalio, Bioelectrocatalytic mediatorless dioxygen reduction at carbon ceramic electrodes modified with bilirubin oxidase, *Electrochim. Acta* 55 (2010) 5719–5724, <https://doi.org/10.1016/j.electacta.2010.05.007>.
- [16] A.P. Kao, J.T. Connelly, A.H. Barber, 3D nanomechanical evaluations of dermal structures in skin, *J. Mech. Behav. Biomed. Mater* 57 (2016) 14–23, <https://doi.org/10.1016/j.jmb.2016.01.001>.

- [org/10.1016/j.jmbbm.2015.11.017](https://doi.org/10.1016/j.jmbbm.2015.11.017).
- [17] J.I. Owen, J. Hüpkes, E. Bunte, Observation of the evolution of etch features on polycrystalline ZnO:Al thin-films, MRS Online Proceedings Library Archive, 2009, p. 1153, <https://doi.org/10.1557/PROC-1153-A07-08>.
- [18] B.M.G. O'Hagan, P. Doyle, J.M. Allen, K. Sutton, G. McKerr, The effects of atomic force microscopy upon nominated living cells, Ultramicroscopy 102 (2004) 1–5, <https://doi.org/10.1016/j.ultramic.2004.06.009>.
- [19] Q. Huang, H. Wu, P. Cai, J.B. Fein, W. Chen, Atomic force microscopy measurements of bacterial adhesion and biofilm formation onto clay-sized particles, Sci. Rep 5 (2015) 16857, <https://doi.org/10.1038/srep16857>.
- [20] S. Hartmans, J.P. Smits, M.J. van der Werf, F. Volkering, J.A.M. de Bont, Metabolism of styrene oxide and 2-Phenylethanol in the Styrene-degrading Xanthobacter strain 124X, Appl. Environ. Microbiol 55 (1989) 2850–2855.
- [21] Bruker, Load the sample and adjust the SPM scanner, (n.d.). <http://www.nanophys.kth.se/nanophys/facilities/nfl/afm/icon/bruker-help/Content/Fluid%20Imaging/Load%20Sample%20and%20Adjust%20the%20SPM%20Head.htm> (accessed October 24, 2018).
- [22] Y. Chao, T. Zhang, Optimization of fixation methods for observation of bacterial cell morphology and surface ultrastructures by atomic force microscopy, Appl. Microbiol. Biotechnol 92 (2011) 381–392, <https://doi.org/10.1007/s00253-011-3551-5>.

4 Quality control of direct cell–mineral adhesion measurements in air and liquid using inverse AFM imaging


 Cite this: *RSC Adv.*, 2021, **11**, 5384

Quality control of direct cell–mineral adhesion measurements in air and liquid using inverse AFM imaging†

 Abd Alaziz Abu Quba,^a Gabriele E. Schaumann,^a Mariam Karagulyan^b and Doerte Diehl *^a

The study of interaction forces between biological and non-living systems requires in-house production of probes modified with, e.g., bacterial cells or with minerals, in order to map irregularly shaped natural surfaces. In order to avoid artifacts, it is essential to control the functionality of the modified probes. Current methods for this purpose require removing the modified probe from the liquid-cell, inserting it into another device and/or have a too low resolution to detect local changes within the interacting areas. Therefore, we present a fast and cost-effective method that overcomes the above mentioned problems by the inverse AFM imaging principle. First, the 3-D shape of a fresh sharp AFM tip is modeled by measuring the shape of a standard rough pattern and post blind tip reconstruction analysis. The so calibrated characterizer tip was extracted and upside-down fixed rigidly on a disc together with the sample. Before and after the cell–mineral interaction, the modified probe is then inversely imaged by the fixed characterizer controlling changes in finest 3-D details of the modified probe. The characterization of probes modified with kaolinite and *P. fluorescens* cells and their interactions with *R. erythropolis* and montmorillonite samples show that the method allows a fast precise investigation of tip modifications before and after cell–mineral interactions in air and liquid such that artifacts in adhesion between cell and mineral at the single-cell level can be excluded.

 Received 6th January 2021
 Accepted 22nd January 2021

DOI: 10.1039/d1ra00110h

rsc.li/rsc-advances

1 Introduction

Organic coatings on mineral substances play a crucial role for wetting properties of soil particles¹ and thus for the ecological functions of soils.² Large part of the organic material in soil is represented by living and dead bacterial biomass.³ The role of bacterial biomass for soil wettability strongly depends on its ability to adsorb to mineral particles and thus to reduce hydrophilic surfaces for water adsorption.⁴

Atomic force microscopy (AFM) has an outstanding ability to study the interactions between biological systems and abiotic surfaces⁵ because it offers high resolution studies under environmental conditions with minimal sample preparation.⁶ However, a special tip-sample configuration is required for the direct measurement of interaction forces between natural abiotic and biological substances. These cell–mineral interactions can be achieved by scanning a respective substrate with

a probe modified with biological cells or *vice versa* by scanning biological cells with a probe modified by, e.g., mineral particles.⁷ Thereby, both, tip and sample are undefined and need to be characterized before their interaction. In addition, natural soft materials may be deformed or mineral particles may be contaminated with organic material after interactions. Only when they remain unchanged after interactions, artifacts due to contamination can be excluded.

Several methods to validate the functionality of biologically modified probes, like optical microscopy,⁸ fluorescence microscopy,^{5,9} scanning electron microscopy (SEM),^{10,11} or force–distance curves (FD curves) before and after the modification process as well as before and after interactions of a bacterium with hydrophobic or hydrophilic surfaces¹² have been reported. Also multiple quality control methods like a combination of both, SEM and FD curves,^{13,14} or other correlative setups to test viability of bacterial cells with FD curves¹⁵ or SEM¹⁶ have been applied.

However, these methods have certain limitations. Except for FD curves, all methods require moving the modified probe from the AFM (liquid) holder to another imaging technique with potentially different environmental conditions. This not only consumes time but also subjects the biological cells to unfavorable conditions risking dehydration, denaturation, and eventual death.⁵ Further, although SEM overcomes the low-resolution of light and fluorescence microscopy, it is not only

^aEnvironmental and Soil Chemistry Group, iES Institute for Environmental Sciences, University of Koblenz-Landau, Fortstr. 7, 76829 Landau, Germany. E-mail: diehl@uni-landau.de

^bDepartment of Environmental Biotechnology, Helmholtz Centre for Environmental Research – UFZ, Leipzig, Germany

† Electronic supplementary information (ESI) available. See DOI: 10.1039/d1ra00110h



time consuming¹⁷ but also destructive for biological material by its electron beam and vacuum.^{18–20} FD curves of bacterial coated probes are characterized by randomness even on smooth surfaces²¹ and can, thus, only be used as a reference for the quality of modified probes when the average of a large number of curves is considered. Finally, natural surfaces are mostly rough and exhibit a certain tilt. Therefore, the contact area of a tip with a calibration sample might be different from the one with the real cell or mineral surface at which the interaction takes place. Thus, a method is needed by which the quality of the whole modified tip area that is potentially in contact with the sample can be tested between several applications in order to ensure that form and material of the modified probe remained the same.

Blind tip reconstruction permits the geometry of a tip to be accurately 3-D modeled by scanning over a reference sample, e.g., made of a grating of sharp spikes which allows to calculate the tip radius and thus to get a detailed estimation of the dilation effect.²² Inverse AFM imaging allows imaging the surface of the modified AFM probe by scanning it against a rigid sharp tip fixed upside-down at the AFM sample stage.^{23,24} In this work, we developed a method that combines blind tip reconstruction and inverse imaging with the fabrication of a sample disc on which beside the sample also a sharp characterizer is inversely fixed. By this, scanning the sample with the modified probe as well as repeated inverse images of the modified probe before and after cell–mineral interaction under exactly the same environmental conditions without changing the modified probe is possible. By fixing the sample and the characterizer on the same sample holder, no interruption is needed between the modified tip characterization and the cell–mineral interaction.

2 Methods

2.1 Blind tip reconstruction of potential built-in characterizers

Before a relocation system with a built-in characterizer could be prepared, the potential characterizers had to be characterized themselves. A detailed description is given in ESI (SI-1, step 1).[†] Briefly, a sharp nitride lever tip ($k = 0.12 \text{ N m}^{-1}$, SNL-10, Bruker, USA) was characterized by scanning a titanium roughness sample (RS-12M, Bruker, USA, ESI-Fig. 1a[†]) in Peak Force Quantitative Nanomechanical Mapping (PFQNM) mode in air with an atomic force microscope (AFM, Dimension Icon, Bruker Corporation, USA) and further used as built-in characterizer for the kaolinite modified probe. The titanium roughness sample allows the characterization of the very end of the AFM tip²⁵ which was needed to precisely define the dilation length of the $\sim 40 \text{ nm}$ thick kaolinite sheets. As a characterizer for the bacterial modified tipless probe, the more elongated Tap150A probe ($k = 5 \text{ N m}^{-1}$, Bruker, USA) was characterized by tapping mode using a test grating TGT1 (NT-MDT Spectrum Instruments, USA). The TGT1 characterizes the overall tip shape at a sub-micron scale, which was essential for the morphology imaging of the bacteria in μm scale. We always used the frame down command, i.e., a horizontal fast scan direction. The resultant images were flattened by first order and subjected to blind tip reconstruction analysis using NanoScope Analysis software (version 8.15, Bruker).

2.2 Fabrication of relocation systems with samples and built-in characterizers

Two relocation systems were produced by submerging a TEM grid (TEM-SG-CU, 3.3 mm diameter, 400 mesh, 47 μm holes, NanoAndMore GmbH, Germany) into resin glue (tempfix, PLANO GmbH, Wetzlar, Germany) melted for 2 minutes at 130 °C covering each of two sample discs (Stainless Steel Metal Specimen Support Disc, 16207-M, NanoAndMore GmbH, Wetzlar, Germany) and subsequent 2 minutes cooling at room temperature. More details about the fabrication of a relocation system are described in SI-9.[†] An extracted and blind tip reconstructed SNL tip was set directly beside each relocation grid fixed by another heating for 30 minutes at 38 °C (as described in detail in SI-1, step 2[†]). Then, a droplet of montmorillonite suspension (2 g L^{-1}) or of *R. erythropolis* cells (tenfold diluted suspension in ultrapure water with an original optical density of 0.9) was pipetted on the disc at an area above the grid and dried in air for 15 min in a laminar flow box.²⁶ Thereby, care was taken not to wet the built-in characterizer in order to avoid its contamination. Other fixation methods might allow adding the characterizer tip after the sample preparation. In order to prevent loosely bound or freely moving particles during measurement that might cause contamination of tips and surfaces, a reliable sample fixation is one of the most crucial steps and a basic requirement for the whole method. Fixation of montmorillonite was improved by subsequent heating of the sample disc at 38 °C for 30 minutes using a heater (MH 15, Roth, Germany), while this could not be applied to the bacterial sample. Finally, both samples were intensively rinsed by water (for montmorillonite) or by a 10 mM KNO_3 solution (for *R. erythropolis*) to remove loosely attached particles or cells. For more details, please refer to Abu Quba *et al.* (2020)²⁶ and to ESI-Fig. 7a.[†] In the present study, the *R. erythropolis* cells adhered well to the resin, however, in other cases an additional surface preparation (e.g. with poly-L-lysine²⁷) might be required to improve the fixation of the bacterial cells.

For preliminary studies, for which the fixation strategy still has to be developed, we propose a system with removable built-in characterizer which allows checking quality control of the characterizer after the imaging process (SI-9[†]).

2.3 Characterization of the samples in the relocation system

The grid index of a single montmorillonite particle, which was later used for cell–mineral interaction against the bacterial coated probe, was recorded using the light microscope integrated in the AFM. Then, the structure of the respective particle was studied in PFQNM mode at 5 nN in air using a new SNL probe ($k = 0.12 \text{ N m}^{-1}$, SNL-10, Bruker, USA). The same process was applied to a single *R. erythropolis* cell before its interaction with the kaolinite probe.

2.4 Preparation of the modified probes

For the cell–mineral interaction between montmorillonite and *P. fluorescens*, we attached the bacterial cells on a tipless cantilever ($k = 0.1 \text{ N m}^{-1}$, MLCT-O10, Bruker, USA). Therefore, the tipless



cantilever was cleaned by immersing it several times in ethanol and then in Milli-Q water, three times immersed in a *P. fluorescens* suspension with an optical density (OD) of 0.9 and shortly air dried to form a bacterial film. Finally, it was rinsed with 10 mM KNO_3 to remove loosely attached cells (SI-4†).

For the cell–mineral interaction between kaolinite and *R. erythropolis*, a little amount of resin glue (tempfix) was placed on a steel disc and heated up to 130 °C melting the glue. The substrate of an SNL probe ($k = 0.12 \text{ N m}^{-1}$, SNL-10, Bruker, USA) was fixed at a custom made XYZ navigation system which is driven manually by micrometer screws and has a stage that links the substrate by an X type tweezer. Visually controlled using a binocular, the SNL probe was driven towards the melted glue (Fig. 1a). Thereby, the cantilever was hold with a horizontal inclination of $\sim 30^\circ$ in order to get minimal contact between glue and the end of the probe. The cantilever–glue contact was indicated by visible changes in the light reflection. After this, the probe was driven back away to cool down and let the attached glue solidify again. Afterward, the substrate of the glue tip was fixed by a double-sided adhesive tape on a steel disk on its backside (Fig. 1b). Kaolinite was sprinkled over the substrate and distributed evenly by a spatula forming a pile which fully covers the probe (Fig. 1c). By heating for 30 min at 38 °C in an oven, the kaolinite–resin contact was strengthened. Then, the probe was cleaned by rinsing with Milli-Q water in order to remove displaceable particles (Fig. 1d). After drying, the probe was carefully detached from the adhesive tape using a tweezer and mounted to AFM.

2.5 Calibration and characterization of the modified probes by inverse imaging

For calibration, the bacterial coated tipless probe was used to obtain FD curves at its built-in characterizer in air using 600 nm ramp size and 1.03 Hz ramp rate. The FD curves were analyzed as described in our work²⁶ in order to get the deflection

sensitivity which allows calculation of the spring constant k by the thermal noise method using the NanoScope software. The calibration of the spring constant could be also done in fluid.²⁸ Then, the bacterial probe was introduced to the liquid environment by forming a meniscus of 10 mM KNO_3 solution between the AFM liquid holder and the relocation sample. Every time before the ramp mode was applied, once again some FD curves were obtained in KNO_3 solution in order to get the deflection sensitivity in the new environment. Therefore, a small inverse map ($2 \times 2 \mu\text{m}$) of the modified probe was imaged at a local area free of microbial modification. Then FD curves with nano offsets between them were obtained at this area. It is essential to find an area which is free from any microbial modification to ensure a rigid contact between the characterizer tip and the original tipless surface which leads to a pure deflection of the modified probe with increasing load. Then a $26 \times 30 \mu\text{m}$ map of the end of the modified part of the probe was obtained by inverse imaging in KNO_3 solution using PFQNM mode at 5 nN. Afterwards, fine tunes were made to image a local area within the large map. Using the grid, the modified probe relocated and interacted with the montmorillonite particle studied in Section 2.3. The modified probe was moved back to the built-in characterizer in order to make a subsequent scan of the same local area and check if the cells remained intact.

To calibrate the kaolinite probe, however, FD curves were obtained by the kaolinite cluster at the top of the glue tip on the built-in characterizer using the same ramp parameters mentioned above. A detailed description of the alignment process of the glue tip apex over the characterizer is given in SI-7.† By analyzing the FD curves as done in our previous work,²⁶ we obtained the deflection sensitivity which the NanoScope software used to calculate the spring constant k . The modified probe was characterized by an inverse image ($2 \times 2 \mu\text{m}$) of the glue tip apex and the geometry, deformation and adhesion of the kaolinite cluster trapped at the top of the glue were studied using cross-sectional analysis.

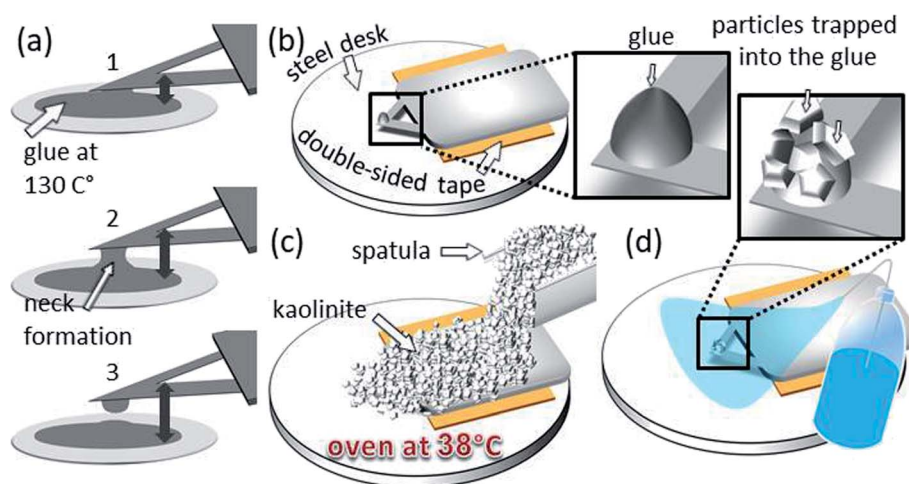


Fig. 1 Preparation steps for the kaolinite probe: (a) in the order from 1 to 3 a glue-tip formation by withdrawal process from the molten glue stain is demonstrated, (b) the substrate of the same probe glued to a double-sided adhesive tape onto a steel disc, (c) coverage of the whole probe with kaolinite particles using a spatula and post heating of the system at 38 °C for 30 minutes so the glue becomes more adhesive and (d) the probe and the tip after cleaning with Milli-Q water.



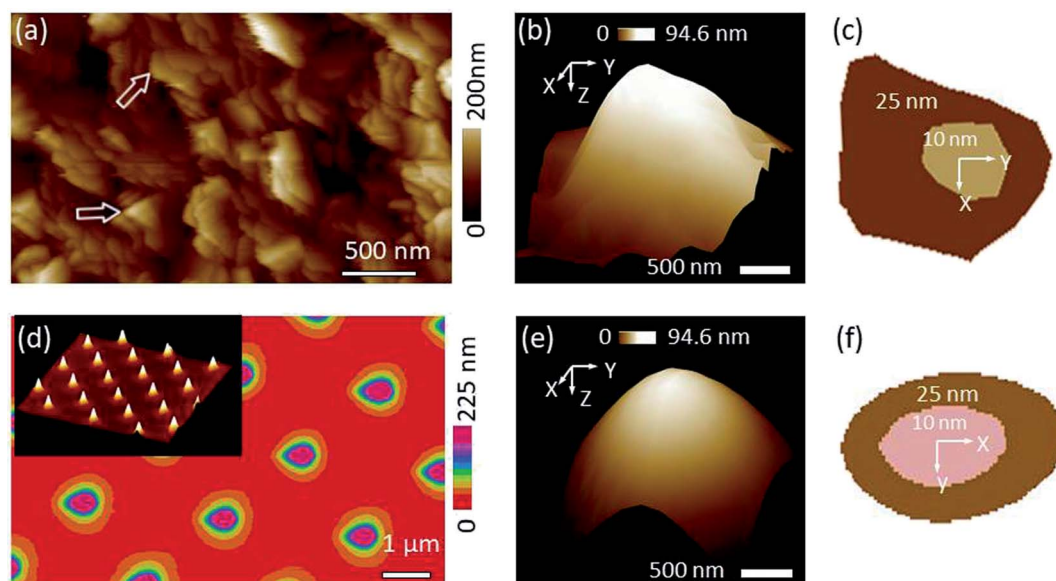


Fig. 2 (a) Roughness image obtained by scanning a sharp SNL probe against titanium sample, (b) 3-D view of the tip that was blind tip reconstructed based on the rough pattern in (a), (c) 2-D sections of the tip at (b) at two Z levels (inner at $Z = 10$ nm and outer at $Z = 25$ nm starting from the tip apex as an origin), (d) roughness image obtained by scanning a Tap150A probe against TGT1 grating sample. The inset shows 3-D view of the TGT1 spikes, (e) and (f) are the same as (b) and (c) by analyzing (d) image. Using the grating yields better tip reconstruction in terms of the smoothness of the tip shape (e), however, leads to more elongated profile (f) compared to tip obtained at the titanium sample (b) and (c), respectively.

2.6 Measurement of the cell–mineral interaction

The cell–mineral interaction between *P. fluorescens* and montmorillonite was exerted in 10 mM KNO_3 using PFQNM mode at 5 nN following the same steps as described in the third paragraph of SI-4.[†] For a detailed investigation of the cell–mineral adhesion, 45 force–distance (FD) curves (1.03 Hz ramp rate) were recorded at the cell center and 30 FD curves at the left and right cell edges of a single cell with nano offsets between them to avoid repetitive sweeps at the same point. The ramp size of 600 nm was determined in preliminary measurements with 2 μm ramp size as sufficient to break free from the sample surface. The cell–mineral interaction between the kaolinite probe and the single *R. erythropolis* cell was exerted in air and adhesion was measured using PFQNM mode at 5 nN.

3 Results and discussion

3.1 Quality of the characterizers

The titanium roughness sample that was used to qualify the SNL tip which was later used as built-in characterizer for the kaolinite probe is dominated by jagged sharp peaks (Fig. 2a). In order to deduce the tip shape, the NanoScope software identified a number of peaks with the sharpest characters (examples indicated by arrows in Fig. 2a). Based on the identified peaks, the blind tip reconstruction calculations result in a 3-D model of the tip (Fig. 2b). Considering the tip apex to be the coordinate origin in Z direction, the cross-section at $Z = 10$ nm corresponds to a cut face area of 189 nm^2 (inner section in Fig. 2c) and a tip surface area of 280 nm^2 while at $Z = 25$ nm these two values increase to 1037 nm^2 (outer section) and 1429 nm^2 , respectively.

Inspection of the tip morphology showed that the shape of the cross-section at $Z = 25$ nm resemble a kite with one sharp and 3 more rounded corners which is in line with a pyramidal tip shape with lower front and higher back angle of the edges as specified from the producer. However, at $Z = 10$ nm, the cross-section was fairly approximated to a circle with the same 2-D area yielding a radius of 8.14 nm. In fact, we found that above $Z \approx 15$ nm, the sections tend to be elongated. The low PeakForce value of 5 nN used in this work ensured a maximum deformation depth of ~ 10 nm. Thus, the very sharp and more symmetric part of the characterizer is the one which engaged all surface interactions ensuring a high precision of dimensional and other measurements.

The TGT1 grating used to study the Tap150A probe as a characterizer for the bacterial probe revealed very regularly distributed sharp spikes (2-D view in Fig. 2d with an inset of a 3-D view). The result of the blind tip reconstruction of the Tap150A tip represented by the 3-D model in Fig. 2e appears smoother compared to that of the SNL tip studied at the titanium sample in Fig. 2b. The 2-D sections reveal a rotated tip shape in line with specifications from the producer (Fig. 2f). Other 2-D sections at various Z levels (results not shown) exhibited that the rotated shape of the tip is sustained up to $Z \approx 40$ nm which suggests that this characterizer is especially suitable for applications with larger deformation or for objects with higher elevations like the bacterial cells. Nevertheless, the model generated at the grating is elongated in the fast scan direction as shown by the 2-D sections in Fig. 2f. The high aspect ratio of the spikes probably caused a poor sample tracking in this direction and lead to the apparent elongation.



3.2 Characterization of the bacterial coated probes before and after the cell–mineral interaction

Inverse images of the bacterial coated probes show that their interaction areas were fully and evenly covered with bacterial films before their first use for cell–mineral interaction (Fig. 3a and ESI-Fig. 8a†). When the distribution of bacterial cells was uneven the respective probe was not used for cell–mineral interaction (ESI-Fig. 8c†). This shows that inverse imaging using a build-in characterizer enables a fast check of the functionality of the modified probes avoiding artifacts due to uneven tip functionalization. The inverse image of the bacterial probe after cell–mineral interaction with a montmorillonite particle under the same environmental conditions shows that the microbial coverage was removed from the tip apex (ESI-Fig. 8b†). Therefore, the use of alternative fixation method is recommended. The attachment of *P. fluorescens* cells on the tipless cantilever

seems to be more stable than on the colloidal tip because the inverse images before and after cell–mineral interaction are identical (Fig. 3g and j, respectively).

3.3 Cell–mineral interaction between *P. fluorescens* and montmorillonite

The cell–mineral interaction image of the bacterial coated tipless probe by the montmorillonite particle (Fig. 3a and b) compared with the inverse image of the probe at the built-in characterizer (Fig. 3g and h) generally reveal similar features, although the bacterial cells and their sub-micron fragments appear larger in the cell–mineral interaction image (Fig. 3a). The montmorillonite particle characterized by a sharp SNL probe (Fig. 3c) exhibits nano-shaped features that probably played the tip role of the cell–mineral interaction and imaged the bacterial cells although the size of the montmorillonite

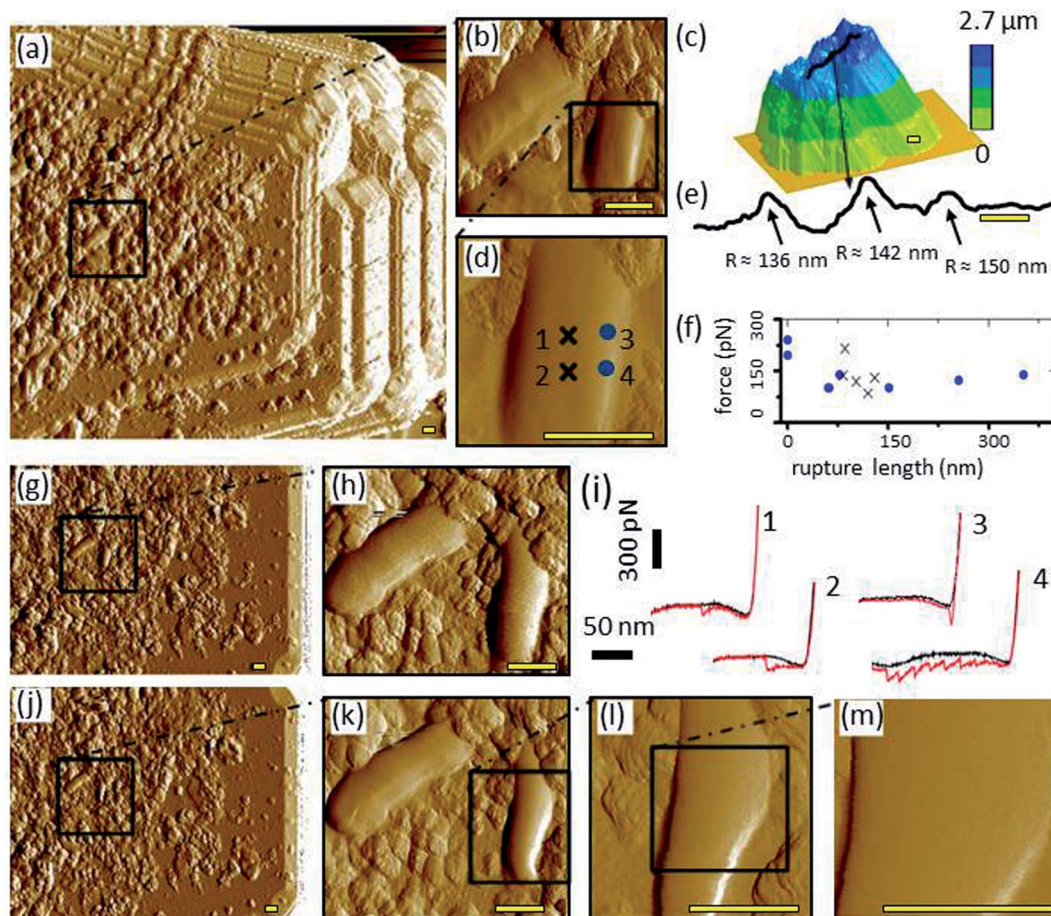


Fig. 3 (a) Image of cell–mineral interactions between a bacteria (*P. fluorescens*) coated tip and a montmorillonite particle, (b) inset inside (a) of two bacteria cells, (d) inset inside (b), (c) height image of the respective montmorillonite particle made by a sharp probe in air, (e) line-scan as shown in (c), (i) cell–mineral FD curves at the locations indicated by the corresponding numbers in (d), (f) distribution of the minimum-adhesion-force-jump-magnitude in a relation to the rupture length of 45 FD curves from the cell center (x) and 30 FD curves from the cell edge (circles), (g) inverse image of the bacterial probe over the Tap150A characterizer before the cell–mineral interaction, with the inset (h) at the same location of (b), (j) inverse image with the insets (k and l) at the same locations of (b) and (d) after the cell–mineral interaction, (m) high resolution inset made to check the local structure of the investigated cell after the cell–mineral interaction. It is clear that the right-low edge of the cell (right cell in (h)) rearranges after the repetitive FD curves during the cell–mineral interaction as shown in (k and l). However, the cell center remains pure after the cell–mineral interaction (m) which indicates a valid adhesion experiments at the center. Scale bar 400 nm. If not stated otherwise, images were made in 10 mM KNO_3 and images show the PeakForce error channel.



particle is much larger than that of a single bacterium. A transect line over the particle surface (Fig. 3e, see black line in Fig. 3c) is characterized by sharp peaks which supports our interpretation.

Single FD curves between the montmorillonite particle and the bacterial coated probe at the cell center and cell edge (Fig. 3i for 4 exemplary locations indicated in Fig. 3d) show that the cell center retraction curves 1 and 2 look quite similar and show a delayed adhesion peak, whereas the retraction curves 3 and 4 at the cell edge exhibit adhesion peaks at various positions. Such delayed adhesion peaks at the cell center may be caused by a stretch of the cell^{29,30} or may indicate the presence of extracellular polymeric (EPS) layers on the cell surface.³¹ The average adhesion of ~ 130 pN at the center is in the same range with values reported for single detachment events from the cell wall.^{32–35} The jumps in adhesion force, *i.e.*, local force minima in the detachment peaks, plotted *versus* the rapture length show that most peaks of both positions, cell center and cell edge, are in the same range between 75 and 225 pN (Fig. 3f). This suggests that these values represent single unbinding events between tip and molecules at the cell surface¹⁶ which are independent from the contact geometry. The rapture length, however, distributes quite differently. At the cell center, data is restricted to a narrow range at ~ 100 nm, whereas, the edge data are scattered between 0–300 nm. Obviously, the reproducibility of the rapture length arises from geometrical aspects. In the center, the

montmorillonite tip faces almost a flat cell surface leading to the same interaction area at each point, whereas for the edge-edge contact between montmorillonite tip and cell wall the interaction area depends on, *e.g.*, slope and form of the respective contacting edges. Edge effects on adhesion measurements were also reported elsewhere.³⁶ Thus, Méndez-Vilas *et al.*, recommended avoiding force measurements on the edges of microbial organisms in order to prevent a significant underestimation of adhesion forces.³⁷

After cell–mineral interaction, the cell on which FD curves were obtained slightly changed its morphology (compare right cell in Fig. 3h with *k* and the corresponding height images in ESI-Fig. 11a with *c*,† respectively), whereas the left cell and the sub-micron fragments appear similar before and after the cell–mineral interaction which confirms that the detected change of the morphology of the investigated cell on the right side is not an artifact due to contamination of the built-in characterizer. Closer images (Fig. 3l, m, and ESI-Fig. 11d†) revealed the purity of the investigated cell center which indicates that adhesion measurements at the cell center cause no or only negligible changes whereas the edges should be avoided as they are very likely subjected to structural changes by these measurements. This case study highlights the importance of inverse imaging before and after cell–mineral interaction measurements under the same environmental conditions because it enables an easy quality control and prevents undetected artifacts.

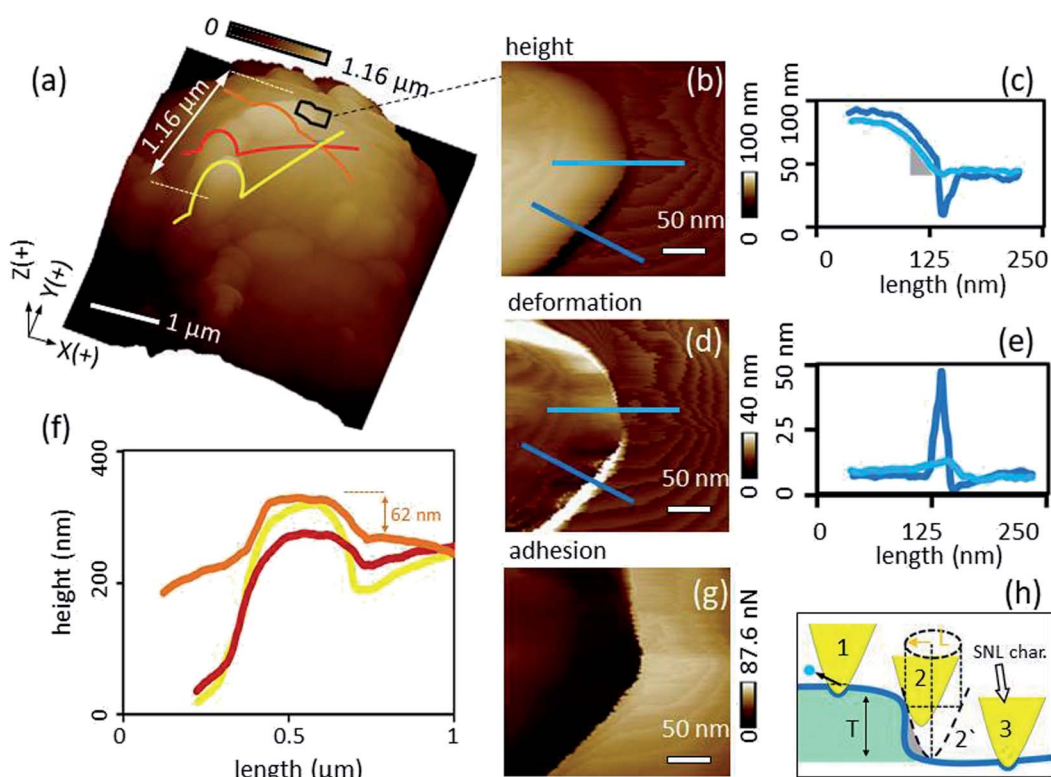


Fig. 4 (a) 3-D view of the glue tip showing fine kaolinite clusters trapped at and around the tip apex, (b, d and g), inset from (a) showing height, deformation and adhesion channels, respectively, of an area at the kaolinite–glue interface, (c and e) sections of height, deformation channels, respectively, (f) Z extension of kaolinite cluster (yellow, red and orange lines in (a)) at the top of the glue, and (h) an imaginary series showing the influence of the kaolinite edge on the spatial resolution of the SNL characterizer (the dilation *L* is indicated by the golden arrow).



Table 1 Distribution of kaolinite particles and clusters in Fig. 4a

Cluster or particle index	1	2	3	4	5	6	7	8	9	10	11	12	13	14
# particles in the cluster	3	4	2	9	1	1	6	5	10	2	5	15	3	2
Cluster-area/total-area (%)	2.8	3.3	1.4	10.9	0.4	0.1	0.9	1.4	4.6	0.6	3.6	6.1	1.7	0.5

3.4 Characterization of the kaolinite modified probe

Kaolinite aggregates were attached at and in the vicinity of the apex of the glue tip (Fig. 4a). Evaluation of the surface ratio revealed that $\sim 38\%$ of the glue tip surface was covered by kaolinite particles and clusters. Thereby, a cluster refers to a group of particles having at least one boundary in common. A counted number of 12 clusters and only 2 individual particles (Table 1) indicate that the kaolinite particles tend to be trapped in clusters which leads to a quite inhomogeneous distribution.

Height comparison of transect lines over the most extended kaolinite cluster (consisting of three particles) at the tip apex (Fig. 4f) show that the most extended part of the kaolinite probe was reached by the particle of the representative cluster crossed by the orange line in Fig. 4a. Further, the extension of the three particles forming the cluster on the top are all larger than the adjacent glue which is essential for the intended cell–mineral interaction experiment.

A more detailed image of the edge of the most extended cluster (black frame in Fig. 4a) including height, deformation and adhesion channels are shown in Fig. 4b, d and g respectively. Inspection of transects of height and deformation channels (Fig. 4c and e) crossing the cluster edges at different points (blue lines in Fig. 4b and d) highlight edge effects in dependence of the characterizer tip shape. The resolution at the edge of the kaolinite cluster decreases due to dilation. Fig. 4h at position 2' illustrates the maximum dilation situation where the dashed profile of the characterizer is captured instead of the actual blue profile of the kaolinite edge. In order to calculate the dilation, the cross-section of the characterizer at a Z level equal to the height of the kaolinite cluster of ~ 40 nm, has to be considered. As the cross-section of the characterizer is more elongated at a Z level >15 nm and was approximated to a kite (Section 3.1), its long diagonal (L) at $Z = 40$ nm well coincides with the dilation length of 36 nm (demonstrated by the gold line

in Fig. 4h). The deformation levels were comparable for the kaolinite and the glue background except at the edge of the cluster, where it increased dramatically for the dark blue line section (Fig. 4d and e). Since the PeakForce was constant during the scan, an explanation could be that the probe became less constrained at the steeper edge (position 2 in Fig. 4h) and slid off the sharp characterizer causing seemingly additional deformation as an artifact. The average adhesion of kaolinite (Fig. 4g) was in good agreement with a value obtained by a “normal setup” in which an SNL probe scanned a kaolinite particle fixed at the AFM stage (SI-6†). Thus, it can be concluded that the interaction was independent from the set-up. This shows that the proposed inverse imaging method is essential to check the reliability of the modification process.

3.5 Cell–mineral interaction between kaolinite and *R. erythropolis*

In order to determine the adhesion between kaolinite and *R. erythropolis*, we scanned a single cell by the kaolinite probe (Fig. 5a). Comparison of the cell–mineral interaction image with an image produced by a sharp probe of the same cell (Fig. 5c) shows that the kaolinite probe produced a triplicate image of the cell as a consequence of the interaction of the cluster consisting of the three kaolinite particles with the respective cell. This highlights that inverse images of modified probes are mandatory for an understanding of the results obtained by probes modified with natural material. That the kaolinite cluster interacted with the cell is also supported by the dimension of the imaged cell after correction for the dilation. The width of the triplicated cell image of $2.113 \mu\text{m}$ (Fig. 5a) is close to the sum of the dilation corrected width of the cluster at the tip apex (Fig. 4a) and the dilation corrected width of the single cell measured by the sharp probe (Fig. 5c): $(1.16 \mu\text{m} \text{ to } 2 \times 36 \text{ nm}) + (0.959 \mu\text{m} \text{ to } 2 \times 30 \text{ nm})$ resulting in $1.088 + 0.899 \mu\text{m} = 1.987 \mu\text{m}$.

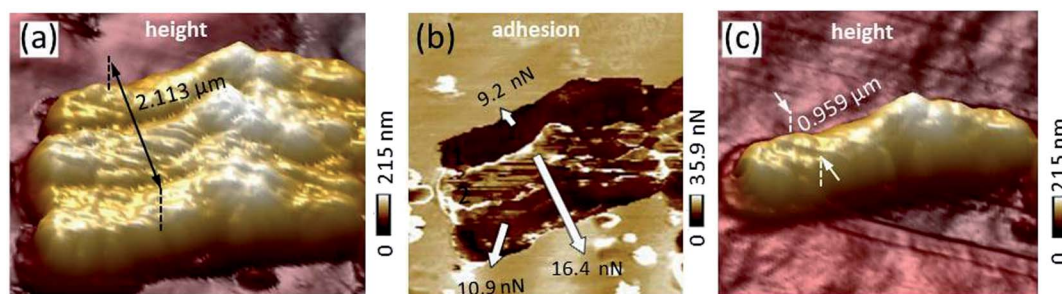


Fig. 5 (a) Height image of cell–mineral interactions produced by scanning the kaolinite modified probe against a single *R. erythropolis* cell fixed at the AFM stage, (b) adhesion channel of the cell–mineral interaction addressed in (a), and (c) the respective *R. erythropolis* cell scanned by a sharp SNL probe. The finite details of the cell morphology in (c) appear triplicated in (a) which originates from the interaction between the kaolinite cluster at the top of the glue tip and the respective cell.



The small deviation is probably caused by errors in positioning and analyzing the cross-sections. For the first and the third triplicated cells, adhesion of the cell–mineral interaction (Fig. 5b) measured at the cell center showed with 9.2 and 10.9 nN, respectively, comparable values. The second triplicated cell, nevertheless, exhibited a higher value. Since the second middle kaolinite particle (red line in Fig. 4f) is not as extended as the yellow and orange ones, it is very likely that its interaction with the cell was affected by the glue or the edges of adjacent kaolinite clusters and thus exhibited higher adhesion values. We thus excluded the second triplicated cell from our adhesion calculation.

4 Conclusions

In this work, inverse AFM imaging was applied in order to test the functionality of modified AFM probes. Our method proved an excellent ability to track the topography of inorganically and biologically modified tips with low and high aspect ratio and to quantitatively investigate parameters, like distribution, dimensions, adhesion, and deformation of the modifying substances. In addition, the method allowed detecting the cell–mineral adhesion at the single-cell level avoiding artifacts such as edge–edge contact between the cell wall and montmorillonite particle. Main advantages over current validation methods of modified probes are that it is fast, it can be done directly before and after the cell–mineral interaction under exact the same environmental conditions, and it enables detection of smallest local changes in the tip modification due to a high resolution.

Our future research aims at applying this method in the direct determination of cell–mineral interaction.

Conflicts of interest

There are no conflicts of interest to declare.

Acknowledgements

This work was supported by the German Research Foundation/Deutsche Forschungsgemeinschaft [grant number DI 1907-2-1].

References

- M. Ma'shum, M. E. Tate, G. P. Jones and J. M. Oades, *J. Soil Sci.*, 1988, **39**, 99–110.
- S. H. Doerr, R. A. Shakesby and R. P. D. Walsh, *Earth-Sci. Rev.*, 2000, **51**, 33–65.
- A. Miltner, P. Bombach, B. Schmidt-Brücken and M. Kästner, *Biogeochemistry*, 2012, **111**, 41–55.
- J. Achtenhagen, M.-O. Goebel, A. Miltner, S. Woche and M. Kästner, *Biogeochemistry*, 2015, **122**, 269–280.
- A. Beaussart, S. El-Kirat-Chatel, P. Herman, D. Alsteens, J. Mahillon, P. Hols and Y. F. Dufrêne, *Biophys. J.*, 2013, **104**, 1886–1892.
- J. A. Last, P. Russell, P. F. Nealey and C. J. Murphy, *Invest. Ophthalmol. Visual Sci.*, 2010, **51**, 6083–6094.
- H. J. Busscher, R. J. B. Dijkstra, D. E. Langworthy, D. I. Collias, D. W. Bjorkquist, M. D. Mitchell and H. C. Van der Mei, *J. Colloid Interface Sci.*, 2008, **322**, 351–357.
- F. Zuttion, C. Ligeour, O. Vidal, M. Wälte, F. Morvan, S. Vidal, J.-J. Vasseur, Y. Chevolut, M. Phaner-Goutorbe and H. Schillers, *Nanoscale*, 2018, **10**, 12771–12778.
- C. Rodriguez-Emmenegger, S. Janel, A. d. I. S. Pereira, M. Bruns and F. Lafont, *Polym. Chem.*, 2015, **6**, 5740–5751.
- M. Gultekinoglu, Y. Jin Oh, P. Hinterdorfer, M. Duman, D. Çatçat and K. Ulubayram, *RSC Adv.*, 2016, **6**, 17092–17099.
- Q. Huang, H. Wu, P. Cai, J. B. Fein and W. Chen, *Sci. Rep.*, 2015, **5**, 16857.
- N. Thewes, P. Loskill, P. Jung, H. Peisker, M. Bischoff, M. Herrmann and K. Jacobs, *Beilstein J. Nanotechnol.*, 2014, **5**, 1501–1512.
- M. Diao, E. Taran, S. M. Mahler and A. V. Nguyen, *J. Microbiol. Methods*, 2014, **102**, 12–14.
- X. Sheng, Y. P. Ting and S. O. Pehkonen, *J. Colloid Interface Sci.*, 2007, **310**, 661–669.
- G. Zeng, T. Müller and R. L. Meyer, *Langmuir*, 2014, **30**, 4019–4025.
- S. Kang and M. Elimelech, *Langmuir*, 2013, **25**, 9656–9659.
- T. Ogura, *Biochem. Biophys. Res. Commun.*, 2014, **450**, 1684–1689.
- L. Muscariello, F. Rosso, G. Marino, A. Giordano, M. Barbarisi, G. Cafiero and A. Barbarisi, *J. Cell. Physiol.*, 2005, **205**, 328–334.
- D. J. Stokes, *Microsc. Anal.*, 2013, **25**, 67–71.
- A. K. Fritzsche, A. R. Arevalo, A. F. Connolly, M. D. Moore, V. Elings and C. M. Wu, *J. Appl. Polym. Sci.*, 1992, **45**, 1945–1956.
- P. E. Marszalek and Y. F. Dufrêne, *Chem. Soc. Rev.*, 2012, **41**, 3523–3534.
- G. Jozwiak, A. Henrykowski, A. Masalska, T. Gotszalk, I. Ritz and H. Steigmann, 2011, arXiv:1105.1472 [physics].
- L. Montelius, J. O. Tegenfeldt and P. van Heeren, *J. Vac. Sci. Technol., B: Microelectron. Nanometer Struct.–Process., Meas., Phenom.*, 1994, **12**, 2222–2226.
- C. J. Cattin, M. Düggelin, D. Martinez-Martin, C. Gerber, D. J. Müller and M. P. Stewart, *Proc. Natl. Acad. Sci. U. S. A.*, 2015, **112**, 11258–11263.
- D. Vorselen, E. S. Kooreman, G. J. L. Wuite and W. H. Roos, *Sci. Rep.*, 2016, **6**, 36972.
- A. A. Abu Quba, G. E. Schaumann, M. Karagulyan and D. Diehl, *Ultramicroscopy*, 2020, **211**, 112945.
- M. J. Doktycz, C. J. Sullivan, P. R. Hoyt, D. A. Pelletier, S. Wu and D. P. Allison, *Ultramicroscopy*, 2003, **97**, 209–216.
- F. Sumbul, N. Hassanpour, J. Rodriguez-Ramos and F. Rico, *Front. Physiol.*, 2020, **8**, 301.
- H. C. van der Mei, H. J. Busscher, R. Bos, J. de Vries, C. J. P. Boonaert and Y. F. Dufrêne, *Biophys. J.*, 2000, **78**, 2668–2674.
- R. Yongsunthorn, V. G. Fowler, B. H. Lower, F. P. Vellano, E. Alexander, L. B. Reller, G. R. Corey and S. K. Lower, *Langmuir*, 2007, **23**, 2289–2292.
- J. Friedrichs, K. R. Legate, R. Schubert, M. Bharadwaj, C. Werner, D. J. Müller and M. Benoit, *Methods*, 2013, **60**, 169–178.



- 32 A. Taubenberger, D. A. Cisneros, J. Friedrichs, P.-H. Puech, D. J. Muller and C. M. Franz, *Mol. Biol. Cell*, 2007, **18**, 1634–1644.
- 33 D. T. L. Le, T.-L. Tran, M.-P. Duviau, M. Meyrand, Y. Guérardel, M. Castelain, P. Loubière, M.-P. Chapot-Chartier, E. Dague and M. Mercier-Bonin, *PLoS One*, 2013, **8**, e79850.
- 34 C. Formosa-Dague, M. Castelain, H. Martin-Yken, K. Dunker, E. Dague and M. Sletmoen, *Microorganisms*, 2018, **6**, 39.
- 35 V. Sundar Rajan, V. M. Laurent, C. Verdier and A. Duperray, *Biophys. J.*, 2017, **112**, 1246–1257.
- 36 H. H. P. Fang, K.-Y. Chan and L.-C. Xu, *J. Microbiol. Methods*, 2000, **40**, 89–97.
- 37 A. Méndez-Vilas, M. L. González-Martín, L. Labajos-Broncano and M. J. Nuevo, *J. Adhes. Sci. Technol.*, 2002, **16**, 1737–1747.



5 Changes in cell surface properties of *Pseudomonas fluorescens* by adaptation to NaCl induced hypertonic stress

Changes in cell surface properties of *Pseudomonas fluorescens* by adaptation to NaCl induced hypertonic stress

Abd Alaziz Abu Quba¹, Marc-Oliver Goebel², Mariam Karagulyan³, Anja Miltner³, Matthias Kästner³, Jörg Bachmann², Gabriele E. Schaumann¹, Doerte Diehl^{1,*}

¹Institute of Environmental Sciences, Rheinland-pfälzische Technische Universität Kaiserslautern-Landau, RPTU in Landau, Fortstrasse 7, 76829 Landau, Germany

²Institute of Soil Science, Leibniz Universität Hannover, Herrenhäuser Straße 2, 30419 Hannover, Germany

³Helmholtz Centre for Environmental Research - UFZ, Department of Environmental Biotechnology, Permoserstraße 15, 04318 Leipzig, Germany

*Corresponding author. Institute of Environmental Sciences, Environmental and Soil Chemistry Group, Rheinland-pfälzische Technische Universität Kaiserslautern-Landau, RPTU in Landau, Fortstrasse 7, 76829 Landau, Germany. E-mail: d.diehl@rptu.de

Editor: [Jana Jass]

Abstract

Determination of the effect of water stress on the surface properties of bacteria is crucial to study bacterial induced soil water repellency. Changes in the environmental conditions may affect several properties of bacteria such as the cell hydrophobicity and morphology. Here, we study the influence of adaptation to hypertonic stress on cell wettability, shape, adhesion, and surface chemical composition of *Pseudomonas fluorescens*. From this we aim to discover possible relations between the changes in wettability of bacterial films studied by contact angle and single cells studied by atomic and chemical force microscopy (AFM, CFM), which is still lacking. We show that by stress the adhesion forces of the cell surfaces towards hydrophobic functionalized probes increase while they decrease towards hydrophilic functionalized tips. This is consistent with the contact angle results. Further, cell size shrunk and protein content increased upon stress. The results suggest two possible mechanisms: Cell shrinkage is accompanied by the release of outer membrane vesicles by which the protein to lipid ratio increases. The higher protein content increases the rigidity and the number of hydrophobic nano-domains per surface area.

Keywords: hypertonic osmotic stress, hydrophobicity, chemical force microscopy, cell surface, *Pseudomonas fluorescens*, X-ray photoelectron spectroscopy

Highlight: Changes in chemical composition and nanomechanical properties of cell surfaces due to adaptation to hypertonic NaCl stress explain the increase in hydrophobicity measured at nano- and microscale.

Introduction

Soil water repellency (SWR), defined as a property which limits or completely prevents water infiltration into the soil (Diehl 2013), attracts a lot of attention as it may essentially change soil properties and functions (Doerr et al. 2000). A microbial cover, often in combination with biofilm formation, can change the surface properties of pure mineral interfaces (Schneider et al. 1997, Berquand 2011). Especially in soil ecosystems, bacteria have a great influence on the physicochemical properties of solid surfaces. The bacterial biomass residues and in particular cell envelope fragments form a significant part of the soil organic matter (SOM) (Miltner et al. 2012) and, thus, contribute to the lipid pool causing water repellency (Schurig et al. 2013). For example, it was detected for a soil chronosequence that even a low biological cover of ca. 10% of *P. putida* cells on quartz grains significantly increases the contact angle of the resultant cell-mineral association compared to the uncovered quartz particles (Achtenhagen et al. 2015). Therefore,

bacterial wetting properties are of major concern in soil ecosystems (Cao et al. 2006).

Bacteria adapt to stress inducing surroundings by several mechanisms by which they undergo a rapid or gradual change of several physicochemical properties (Baumgarten et al. 2012b). Thereby, the outer membrane of Gram negative bacteria plays an essential role in the cellular response to changes in the environmental conditions (Inoue and Horikoshi 1989). Adaptation mechanisms may include an increase in cell hydrophobicity (Baumgarten et al. 2012a), a reduction in negative cell surface charge (Baumgarten et al. 2012b), a change in membrane fatty acid composition (Heipieper et al. 2007), a change of cell morphological characteristics like a reduction in size and cell wall rigidity upon a decrease in cell turgor pressure (Deng et al. 2011), and finally a release of outer membrane vesicles as a first step of biofilm formation (Baumgarten et al. 2012a). Furthermore, it is well accepted that osmotic stress can lead to conformational changes of the proteins embedded in the bilayer of Gram negative bacteria (Bremer and Krämer 2019). The regulation of the cell volume due to stress by shrinking reduces the stretch of the cell wall and decreases the lateral membrane tension (Spagnoli et al. 2008, Francius et al. 2011), thus reducing the cell stiffness. However, changes in cell volume may also be associated with a modification of the protein content. More specific, the swelling of bacteria leads to

Received 5 January 2022; revised 26 October 2022; accepted 5 December 2022

© The Author(s) 2022. Published by Oxford University Press on behalf of FEMS. This is an Open Access article distributed under the terms of the Creative Commons Attribution-NonCommercial License (<https://creativecommons.org/licenses/by-nc/4.0/>), which permits non-commercial re-use, distribution, and reproduction in any medium, provided the original work is properly cited. For commercial re-use, please contact journals.permissions@oup.com

a higher protein synthesis to maintain the same density at the cell surface (Lang 2007, Wood 2015), whereas, cell shrinkage stimulates the degradation of proteins to amino acids (Botsford et al. 1994, Lang 2007). Thereby, due to its incompressible structure (Weber and de Bont 1996, Hwang et al. 2018), the protein density at the cell surface has an influence on the cell rigidity. An enrichment of the proteins content has a stiffening effect on the cell outer membrane as they reduce the fluidity of surrounding lipids (Dombek and Ingram 1984, Weber and de Bont 1996, Hwang et al. 2018).

However, previous research on the impact of osmotic stress on cell envelopes and on the effect of drought on cell fragments in soil lacks a comprehensive relation between the resulting modifications in morphology, elasticity, chemical composition and hydrophobicity of bacterial cell surfaces which is needed for understanding the mechanisms involved.

A promising tool to analyze nanoscale surface properties of cells under environmental conditions is atomic force microscopy (AFM). Especially chemical force microscopy (CFM) allows to measure specific chemical interactions, i.e. the adhesion of AFM tips modified by different specific chemical groups towards the cell surface molecules. Thus, CFM has been widely applied to study the properties of microbial surfaces because it is the only technique that offers high resolution investigation of chemical interactions under environmental conditions (Beaussart et al. 2020). For example, an increasing gradient along the cell in adhesion forces between $-CH_3$ probes and the cell surface of *R. erythropolis* could be attributed to a gradient in the distribution of the chemical composition along the cell length which is essential for cell division process (Dorobantu et al. 2008). CFM could also be performed by attaching a single cell or a cell film to an AFM probe and scanning functionalized surfaces with this probe as, e.g. done by El-Kirat-Chatel et al. (2014) with a single *Pseudomonas fluorescens* cell. The force spectroscopy analysis towards hydrophobic ($-CH_3$) or hydrophilic ($-OH$) substrates revealed that a sequential unfolding of the large adhesin protein LapA+ only occurred during interaction with the hydrophilic substrate (El-Kirat-Chatel et al. 2014).

Our research project aims at a more comprehensive view on the relation between adaptation to hypertonic stress, cell surface properties of soil bacteria and their effect on soil water repellency. Repellent properties in soil appear when soil dries out, but often persist even after the following rewetting event and thus result in persistent irregular wetting patterns with wet and dry soil domains (Täumer et al. 2005). Our interest is therefore focused on the long-term effects of drying stress on surfaces of soil bacteria, e.g. in the range of days to weeks. Hence, in the present study we asked the question: Which mechanisms lead to a long-term increased cell surface hydrophobicity of the Gram negative soil bacterium *P. fluorescens* upon growth under hypertonic stress?

To answer this question, *P. fluorescens* cells grown under NaCl induced hypertonic stress and under optimum ionic strength conditions for bacterial growth (unstressed) were investigated under similar condition excluding osmotic stress at the time of analyses. A hypothesized stress dependent higher hydrophobicity of cell surfaces (hypothesis H1) was tested by the macroscopic contact angle (CA) obtained from sessile drop measurements on dried cells and by the adhesion of cells towards hydrophobic ($-CH_3$) and hydrophilic ($-COOH$, $-NH_2$) functionalized tips both in an aqueous medium with low ionic strength using CFM. We choose these two hydrophilic groups for CFM because they are present in proteins and lipids as two main cell wall constituents and are typical abundant functional groups in SOM. Furthermore, the use of these tips allows to identify the effect of surface charges. Both functional

groups have a different pH dependent charge. While $-NH_2$ groups ($pK_a \sim 9-10$) are uncharged at the experimental pH of ~ 6 , $-COOH$ groups ($pK_a \sim 2-4$) are usually deprotonated and thus negatively charged (Vezenov et al. 1997). Thus, a hypothesized lower surface charge of stressed cells (H2) can be detected by a higher adhesion towards $-COOH$ tips. Differences in size and in nanomechanical properties of the stressed and unstressed cells, like a hypothesized smaller size and softer cell surface of the stressed cells (H3), were obtained from height images and the DMT Modulus (Derjaguin-Müller-Toporov model of the Young's Modulus) using AFM. To detect the hypothesized reduced protein and increased lipid content in the cell surface composition of the stressed cells (H4), the AFM results are related to the proportion of surface carbon associated with proteins (C_{Pr}/C), polysaccharides (C_{PS}/C) and hydrocarbon-like compounds (C_{HC}/C) as well as to the surface elemental O/C, C/N and N/P ratios obtained by X-ray photoelectron spectroscopy (XPS).

Methods

Bacterial Strain and Growth Conditions

Pseudomonas fluorescens (DSM 50090) was obtained from DSMZ/UMB strain collection and grown in 250 ml of sterile mineral salt media, consisting of 7 g Na_2HPO_4 , 2.8 g KH_2PO_4 , 0.5 g NaCl, 1 g NH_4Cl , 0.1 g of $MgSO_4 \cdot 7H_2O$, 0.01 g of $FeSO_4 \cdot 7H_2O$, 5 mg of $MnSO_4 \cdot H_2O$, 6.4 mg of $ZnCl_2$, 1 mg of $CaCl_2 \cdot 6H_2O$, 0.6 mg of $BaCl_2$, 0.36 mg of $CuSO_4 \cdot 7H_2O$, 0.36 mg of $CuSO_4 \cdot 5H_2O$, 6.5 mg of H_3BO_3 , 0.01 g of EDTA, 146 μ l of HCl 37% per liter of distilled water with supplementation of 1 g/l of yeast extract and 4 g/l sodium succinate as carbon source (Hartmans et al. 1989). Osmotic potential of the media was reduced by addition of 0.5 M NaCl by -2.5 MPa to induce osmotic (hypertonic) stress. Control and NaCl amended media were inoculated with freshly grown overnight cultures, to obtain initial optical densities (OD_{560}) of 0.05 in 250 ml glass vials. The vials were incubated at $30^\circ C$ on an orbital shaker (160 rpm). Cell growth was monitored by optical density measurement (OD_{560}) using a Perkin Elmer UV/VIS Spectrophotometer (UV-Vis Spektrometer: Lambda2S, Perkin/Elmer, Waltham, USA). Cells were harvested after 6 hours by centrifugation at 11 000 g for 15 min (Hermle Z383K), resuspended in 2 ml KNO_3 (10 mM, pH 7.0) and transferred to 2 ml reaction tubes. Each sample was washed twice with 2 ml KNO_3 followed by 1 min centrifugation at 10 000 g. The washed biomass was resuspended in 1 ml KNO_3 and stored at $5^\circ C$ until further analysis. Thus, we tested long-term differences of cells grown under stress in a hypertonic medium as compared to cells grown in a control medium that persist even when the cells were immersed in low ionic strength solution or shortly air dried for sample preparation.

Contact Angle

Contact angles of *P. fluorescens* cells were determined with the sessile drop method (Baumgarten et al. 2012a, van Loosdrecht et al. 1987) using a CCD-equipped contact angle microscope (OCA 15, DataPhysics, Filderstadt, Germany). Bacterial samples were prepared by filtering *P. fluorescens* cell suspension through cellulose acetate filters (0.45 μ m pore size). The filters with a dense multi-layer of bacterial cells were air-dried for two hours and the central part of the air-dried filters was fixed on microscopy glass slides using double-sided adhesive tape. Directly after preparation, a 1- μ l drop of deionized water was placed on the sample surface and the initial solid-water contact angle was evaluated at the intersections of the drop contour line with the solid

surface by automatic drop shape analysis using the software SCA20 (DataPhysics, Filderstadt, Germany). Contact angles are given as arithmetic means of nine independent measurements.

X-ray Photoelectron Spectroscopy

Part of the results of the X-ray measurements have been recently published and the method described in detail (Karagulyan et al. 2022). Briefly, surface elemental composition of *P. fluorescens* cells was analyzed by XPS using an Axis Ultra DLD (Kratos Analytical, Manchester, UK) with monochromatic AlK α radiation (1486.6 eV; emission current: 20 mA, voltage: 6 kV). For the measurement, the central point of an air-dried filter, prepared the same way as for the contact angle analysis, was fixed on a bar using conductive carbon tape (Agar Scientific Elektron Technology UK Ltd., Stansted, UK).

Bacterial cell envelopes can be considered to consist of three major classes of constituents, namely proteins (Pr), polysaccharides (PS), and hydrocarbon-like compounds (HC). By combining information on the chemical composition of these model constituents with the surface elemental composition measured by XPS it is possible to estimate the molecular composition of the cell surface (Genet et al. 2008). The proportion of surface carbon associated with proteins (C_{Pr}/C), polysaccharides (C_{PS}/C) and hydrocarbon-like compounds (C_{HC}/C) was estimated from the observed elemental concentration ratios $[N/C]_{obs}$ and $[O/C]_{obs}$ with the following set of equations (Equ. 1–4). The coefficients in Equ. 1 and 2 are based on data computed for the major outer membrane protein of *P. fluorescens* and the general chemical formula of proteins and polysaccharides ($[C_6H_{10}O_5]_n$) (Genet et al. 2008):

$$[N/C]_{obs} = 0.279 (C_{Pr}/C) \quad (1)$$

$$[O/C]_{obs} = 0.325 (C_{Pr}/C) + 0.833 (C_{PS}/C) \quad (2)$$

$$[C/C]_{obs} = (C_{Pr}/C) + (C_{PS}/C) + (C_{HC}/C) = 1 \quad (3)$$

The mass percentage of the respective constituent *i* (i.e. Pr, PS, HC) is then calculated as

$$\text{Constituent } i \text{ (mass \%)} = \frac{(C_i/C)}{M_i} \cdot \frac{1}{\frac{(C_{PS}/C)}{M_{PS}} + \frac{(C_{Pr}/C)}{M_{Pr}} + \frac{(C_{HC}/C)}{M_{HC}}} \quad (4)$$

where M_i is the carbon concentration in the constituent (43.5, 37.0, and 71.4 mmol C g⁻¹ for Pr, PS and HC, respectively) (Genet et al. 2008). Statistical significance of differences in contact angle and surface chemical composition between control and stressed cells was tested by paired t-tests when normality was met (tested by Shapiro–Wilk test) or by Wilcoxon signed-rank test, using SigmaPlot 13.0 (Systat Software, Inc., San Jose, USA).

Atomic and Chemical Force Microscopy

The cells were fixed on poly-L-lysine coated coverslips. The coverslips were cleaned first with acetone (ROTISOLV® Pestilyse® plus $\geq 99.9\%$, ROTH, Germany) and immediately, before drying, left for 30 minutes in a conventional ultrasonic bath containing $\sim 70\%$ ethanol (ROTIPURAN® $\geq 99.8\%$, p.a, ROTH, Germany) and $\sim 30\%$ ultrapure water. After air drying, a drop of poly-L-lysine (P8920, Sigma-Aldrich, Germany) was pipetted near the center of the coverslips and air dried again. Finally, a drop of the bacterial suspension (tenfold diluted suspension in 10 mM KNO₃ with an original

optical density of 0.9) was pipetted on the top of the poly-L-lysine spot (located by the ring effect), air dried and intensively rinsed by a 10 mM KNO₃ solution to remove loosely attached cells. The air drying step was important to ensure good fixation of the cells at the glass surface but was kept as short as possible to avoid drought stress (i.e. < 1 minute).

AFM maps were executed by atomic force microscope (AFM, Dimension Icon, Bruker Corporation, USA) operated in the Peak Force Quantitative Nanomechanical Mapping (PFQNM) mode in 10 mM KNO₃ solution at a force setpoint of 5 nN. In order to maintain the same concentration of 10 mM KNO₃ over time, we compensated for the loss of water via evaporation by a custom built pump (SI-1). We used OLTESPA-R3 probes (ASYLUMRESEARCH, USA), calibrated their deflection sensitivity (Sv) on mica and estimated their spring constant (*k*) by the thermal noise method. The tip geometries were obtained by imaging the topography of a titanium roughness sample and post blind tip reconstruction analysis as done in our previous work (Abu Quba et al. 2020). To compensate for that fewer cells were found in the stressed compared to control cultures, a higher number of regions of interest (ROIs) of the stressed (25 ROIs) than of the control cells (16 ROIs) was imaged by height and DMT Modulus channel.

CFM experiments were performed using chemically modified AFM probes. The probes (SmartTips®) were chemically functionalized by the producer (NanoAndMore GmbH, Wetzlar, Germany) as follows: The gold surface of the probes were cleaned (UV-Ozone), before being submerged in a 1 mmol thiol solution overnight. Afterwards, the probes were cleaned with ethanol and stored in solution in individual containers. The specific thiols used are 1-octadecanethiol, 11-mercaptoundecanoic acid, and 11-amino-1-undecanethiol for –CH₃, –COOH and –NH₂, respectively. The deflection sensitivity (Sv), the spring constant (*k*) and the tip radii were obtained as mentioned above. A 3 μm ramp size and 1.03 Hz ramp rate were sufficient to break free from the surface. In order to enhance the chemical interaction, the tip-sample contact time was set to one second using the surface delay function.

We aimed to protect the CFM probes from damage or contamination by ensuring minimal use of the probes. Thus we applied a low force setpoint and obtained a quality control (adhesion tests) on freshly cleaved mica (Mica Sheet, V5 Quality, Science Services, München, Germany). As long as quality control on mica revealed no changes before and after the CFM experiments, we considered the measurements as reliable, i.e. without damages in the organic layer of the CFM probes. To locate cells, low resolution maps (32 to 64 lines) were captured using the point and shoot function at a force setpoint < 3 nN. Then, several force-distance (FD) curves were obtained at a force setpoint of 5 nN on the center of the cells found in the image.

In total, we used eight –CH₃ probes (4 for control and 4 for stressed cells), six –COOH probes (3 for control and 3 for stressed cells) and four –NH₂ probes (2 for control and 2 for stressed cells).

Processing of AFM Data and Statistical Analysis of Data

To get the cell height and length, sectional analyses of the NanoScope Analysis software (version 2.0, Bruker) were applied in the height maps (Fig. 1e). The shape of the cells was approximated to cylinders with diameter and length equal to the cell height and length, respectively. This allowed estimating their total surface area and volume. For more details, see (SI-2) and (SI-3). The roughness (R_q) was evaluated using the roughness function of the NanoScope Analysis software in the height maps. To avoid

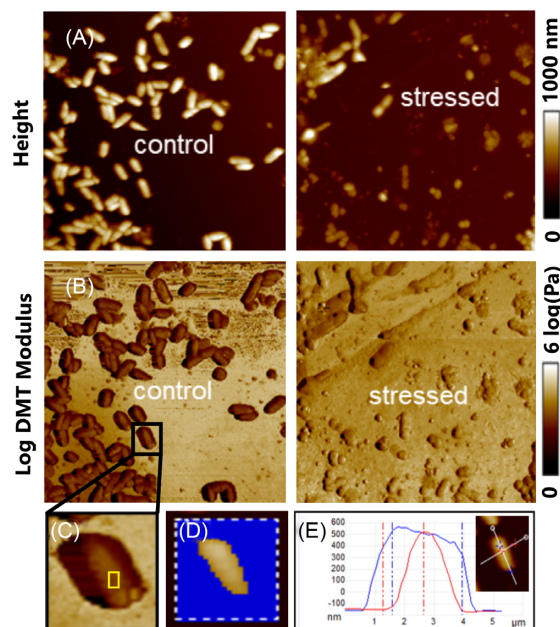


Figure 1. AFM maps of (A) height and (B) log DMT Modulus of control (left) and stressed (right) *P. fluorescens* cells, (C) digital zoom into a single cell with a marker on the area considered for measuring the stiffness, (D) the same cell as in (C) in Height Sensor channel with a threshold of 200 nm to measure R_q , (E) two sections along the cell length and width made to measure the cell length and height, respectively.

the dilation effect recently shown in Abu Quba et al. (2021) on biological ‘irregular’ samples we considered only the top of the cell for R_q estimation using a threshold of $Z = 200$ nm (Fig. 1D). The elastic Modulus described by the Derjaguin-Muller-Toporov (DMT) Modulus was estimated using the roughness function at the logDMT Modulus channel (Fig. 1C). The adhesion force in the FD curves was determined as the minimum force in the baseline corrected retraction curve using R (R Core Team 2020) and the R-package {afmToolkit} (Benítez et al. 2017). Each adhesion force was normalized by the radius of the respective tip in order to account for the different contact areas achieved by the tips with various tip curvatures (e.g. Vezenov et al. 1997, Poggi et al. 2004, Vadillo-Rodríguez et al. 2004, Gourianova et al. 2005, Uner et al. 2006, Jiang and Turner 2016). The ‘jump to contact’ events were searched in the approach curves to check if there are attractive interactions between the functionalized probes and the cell surfaces.

Data of height, length, R_q , and Log DMT Modulus revealed unequal variances (Levene’s test, R package {car}; Fox and Weisberg 2011) and were not normally distributed (Shapiro-Wilk test, R package {stat}). Thus Wilcoxon rank sum tests (R-package {stat}) were applied to detect significant differences in these parameters between control and stressed cells. The differences in cell height, cell R_q and Log DMT Modulus were expressed in percentage of the control values.

Linear mixed effect models (R packages {lme4} (Bates et al. 2015) and {lmerTest} (Kuznetsova et al. 2017)) were applied to test the effect of stress on the adhesion force of FD curves with different individual tips or different individual cells as random effect: $\text{force} \sim \text{stress} + (1|\text{tip}) / \text{force} \sim \text{stress} + (1|\text{cell})$ for the eight $-\text{CH}_3$, the six $-\text{COOH}$ or the four $-\text{NH}_2$ tips which were used for FD curves on randomly selected control and stressed cells. In order to ensure validity of the models (Levene’s and Shapiro-Wilk test of the residuals), adhesion forces were Box-Cox transformed (R package {caret}; Kuhn et al. 2016).

Results

Wettability and Surface Chemical Composition (XPS)

The hypertonic stress resulted in a lower cell surface wettability as the contact angle of the dried stressed cells ($93^\circ \pm 2^\circ$) was by $\sim 24^\circ$ significantly larger than the one of the dried control cells ($69^\circ \pm 5^\circ$; Table 1).

The XPS measurements (partly already published in Karagulyan et al. (2022)) revealed some pronounced differences in the surface elemental composition of *P. fluorescens* as a result of adaptation to hypertonic stress. As shown in Fig. 2, we found a significantly lower surface K content as well as a significantly higher surface Fe, S, Na, and N content for the stressed cells as compared to the control cells. In contrast, surface P, O, and C tended (not significant) to be lower for the stressed cells than for the control, which was reflected by significant differences in the C/N and N/P ratios.

Estimation of the mass percentage of main cell surface compounds revealed a stress induced higher amount of surface carbon associated with proteins and a lower amount of surface carbon associated with the polysaccharides and hydrocarbon-like compounds (Table 1). In a study of bacterial biofilm, *P. fluorescens* contains up to 50% of proteins (Baum et al. 2009) which is in accordance with our results from XPS measurements on the stressed bacteria.

Atomic and Chemical Force Microscopy

The height of the control cells scatters with a symmetric distribution around ~ 620 nm (Fig. 3a). In contrast, the heights of the cells grown under hypertonic stress were significantly ($P < 0.001$) shifted to smaller values scattering around ~ 360 nm, however with a strongly right-skewed distribution (Fig. 3a). The length of the cells grown under stress was with ~ 1.9 nm only slightly but significantly ($P < 0.001$) shifted by ~ 0.2 nm to lower values compared to the length of the control cells with ~ 2.1 nm (Fig. 3b). Thus, the stress more strongly reduced the cell height of *P. fluorescens* by 42% than the cell length by 12% leading to a 50% lower surface area and a 70% lower volume (Table 1). Line scans across height maps (Fig. 4a and b) show that the stressed cells besides having lower heights also tend more strongly to form clusters. This clustering made the height determination more difficult and might have led to an overestimation of the heights of individual cells and thus to the right-skewed height distribution of the stressed cells.

The log DMT Modulus values of the control cells was confined within 6–8 log(Pa) with a monomodal distribution and a maximum around 7 log(Pa), whereas the values of the stressed cells ranged from 3 up to 9 log(Pa) with a trimodal distribution around density peaks at 8.5, 7.5, and 5.5 log(Pa) with decreasing density (Fig. 3C). Obviously, the stress resulted in different effects ranging from a rather strong decrease of the DMT modulus (7.5–5) to a pronounced increase (7–8.5), whereas a third group of cells remained almost unchanged (7.5–7). The surface roughness R_q of the stressed cells was symmetrically distributed (Fig. 3D) and with ~ 53 nm by ~ 3 nm slightly but significantly ($P < 0.001$) higher than of the control cells with ~ 50 nm (Table 1). Thus, the stress application had less effect on cell R_q and log DMT Modulus than on the cell size with an increase by only 6% and 5%, respectively. The log DMT Modulus values of the control cells was confined within 6–8 log(Pa) with a monomodal distribution and a maximum around 7 log(Pa), whereas the values of the stressed cells ranged from 3 up to 9 log(Pa) with a trimodal distribution around density peaks at 8.5, 7.5, and 5.5 log(Pa) with decreasing density (Fig. 3C).

Table 1. Medians, standard deviations and differences of chemical cell surface composition, cell shape, and physical cell parameters studied by sessile drop method, XPS and AFM (errors of differences reflect the 95 percentile, asterisks indicate significance with * $P < 0.05$, ** $P < 0.01$, *** $P < 0.001$).

	Control cells			Stressed cells			Difference		
Contact angle (°)	69	±	5	93	±	2	24	±	13***
Hydrocabons (%) ^a	18.6			12.6			6		
Proteins (%) ^a	37.8			51.6			13.8		
Polysaccharides (%) ^a	43.7			35.8			7.9		
Height (nm)	616	±	100	358	±	161	235.00	±	21.50***
Length (μm)	2.11	±	0.68	1.85	±	0.64	0.23	±	0.11***
Volume (μm ³)	0.63	±	0.33	0.19	±	0.15	0.44		
Surface area (μm ²)	4.68	±	1.94	2.28	±	1.47	2.4		
R _q (nm)	50.50	±	7.43	53.50	±	6.07	3.00	±	1.10***
log DMT Modulus (log Pa)	7.17	±	0.38	7.54	±	1.10	0.28	±	0.15***

^aData published in Karagulyan et al. (2022)

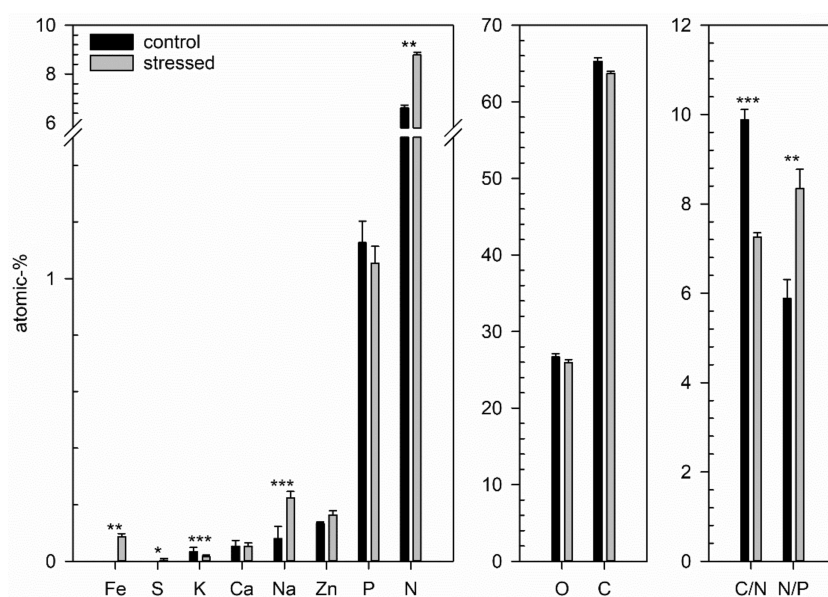


Figure 2. Surface chemical composition of control and stressed cells of *P. fluorescens*. Error bars indicate the standard deviation ($n = 3$). Asterisks indicate significant difference between control and stressed cells (significance levels: * $P < 0.05$, ** $P < 0.01$, *** $P < 0.001$). Data are partly already published in Karagulyan et al. (2022).

In all force-distance curves of the present study, ‘jump to contact’ events as well as repulsive barriers could not be detected. Thus, long-range repulsive or attractive electrostatic interactions were virtually absent or smaller than the detection limit. After contacting the cell surface for one second, all CFM tips adhered to control and stressed cells in different strengths (Fig. 5). The stress induced an increase in the adhesion forces of $-CH_3$ tips from 12.5 ± 1.3 pN nm⁻¹ towards control cells to 16.4 ± 1.3 pN nm⁻¹ towards stressed cells, and thus results in a difference of 4.0 ± 1.8 pN nm⁻¹ ($P < 0.05$). In contrast, the stress induced a decrease in the adhesion forces of the $-COOH$ from 13.9 ± 1.2 towards control to 10.2 ± 1.2 towards stressed cells with a difference of 3.7 ± 1.7 pN nm⁻¹ ($P < 0.001$). While the adhesion forces of the $-NH_2$ tips decreased from 24.6 ± 1.9 pN nm⁻¹ to 15.5 ± 1.9 pN nm⁻¹ resulting in a difference of 9.0 ± 2.7 pN nm⁻¹ ($P < 0.01$) between stressed and control cells.

In Fig. 5, it is remarkable that the $-NH_2$ group adheres stronger than the other chemical groups towards either control or stressed cells, and also stress seems to have a stronger impact on the adhesion forces towards the $-NH_2$ group than the other two tip types.

Although there is a common trend of the distribution of the violins with a maximum density around the mean and elongated extension upward, i.e. a right-skewed distribution, the distribution differed for a given tip and does not always look like the violins in Fig. 5. We refer to (SI-4) for more details.

Discussion

Effect of Hypertonic Stress on Cell Surface Hydrophobicity

We studied the changes in elasticity, surface chemistry and wettability of *P. fluorescens* cells upon adaptation to hypertonic stress. The enhanced tendency for hydrophobic interactions detected by the adhesion of $-CH_3$ group and the reduced tendency for hydrophilic interactions detected by the adhesion of $-NH_2$ and $-COOH$ groups towards the NaCl stressed *P. fluorescens* cells compared to control cells is in good agreement with their reduced macroscopic wettability and supports our hypothesis (H1) that cells grown under hypertonic NaCl stress increased their cell

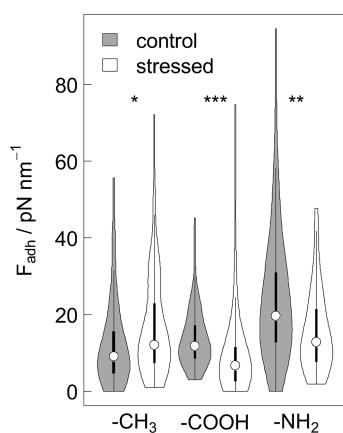


Figure 5. Violin plots of adhesion forces of CFM probes functionalized with $-\text{CH}_3$, $-\text{COOH}$, and $-\text{NH}_2$ groups towards *P. fluorescens* grown under control conditions and under osmotic stress (0.45 M NaCl).

this might be that at the low ionic strength of 10 mM KNO_3 , the increase of the repulsive forces in the FD curve was very flat and the jump-in due to the van der Waals interactions occurred very close to the surface and both were thus barely visible (Butt 1991).

Effect of Hypertonic Stress on Cell Wall Composition and Morphology

The higher protein content, the smaller size and the higher stiffness of the cells grown under stress than of the control cells are in contrast to our expectations. Thus, we have to reject our hypotheses H 3 and 4 that adaptation to hypertonic stress results in smaller and softer cells due to the degradation of proteins (Botsford et al. 1994, Lang 2007). The cell volume reduction upon adaptation to hypertonic stress of $\sim 70\%$ agrees well with those reported for various *Escherichia coli* strains of 63%, 65%, and 73% (Francius et al. 2011) but is higher than the 40% addressed in another work also on *E. coli* (Pilizota and Shaevitz 2013). The regulation of the cells to lower volumes by stress could be related to water loss from the cell interior to the surrounding solution (Pilizota and Shaevitz 2012). The outer membranes of Gram negative bacteria are composed of lipopolysaccharides (LPS) that are anchored with their lipid parts in a phospholipid bilayer and extend their core- and outer-polysaccharide chains into the surrounding solution. Embedded in the fluid phospholipid bilayer are proteins like porins. A pure physical effect would be that the reduced cell size caused a decrease of the distances between the proteins as hydrophobic binding sites in the lipid bilayer and thus a relative increase of the protein coverage on the cell surface at the expense of lipopolysaccharides (LPS) and lipids that might have been partly released as outer membrane vesicles (Baumgarten et al. 2012a, Eberlein et al. 2018). The resultant closer vicinity of the proteins reduces the fluidity of the lipids between them increasing the ordering of the lipid alkyl chains and thus the rigidity of the outer membrane (Shinitzky 1984). Thereby, the surface C/N ratio increases and a relatively higher protein and lower polysaccharide content become detectable by XPS.

Both explanations are in good agreement with the higher stiffness of the stressed than the control cells. Such stiffening effects with increasing protein content have been already reported for inner membranes of Gram negative bacteria upon organic solvent or mechanical stress (Dombek and Ingram 1984, Weber and de Bont 1996, Hwang et al. 2018). However, the trimodal distribution of the stiffness suggests a heterogeneous stress effect. A

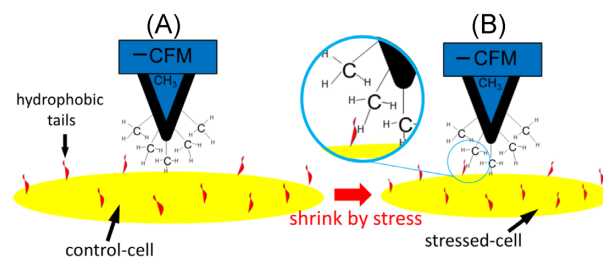


Figure 6. Sketch of the proposed interaction between a $-\text{CH}_3$ tip and (A) control and (B) stressed planar cell surface. As the stress reduced the cell size (or surface area), the hydrophobic components accumulate on the surface which allow the $-\text{CH}_3$ tip to interact with more protein segments as illustrated in the inset (B).

possible explanation could be that some cells died resulting in lower stiffness, while others react by stiffening to the stress situation and some cells already recovered from the stress and turned to the unstressed cell physiology. Also the observed small but significantly higher roughness of the stressed cells support our explanation that the stress induced hydrophobization is caused by modifications of the cell wall ultrastructure. However, it remains speculative by which processes structure and composition of the outer cell wall components were affected upon stress.

Effect of Protein Content on Hydrophobicity

Single molecule force spectroscopy (SMFS) maps within single cells revealed that the adhesion is restricted to concentrated nano-domains (Dorobantu and Gray 2010) which supports our explanation that the hydrophobic sites on the cellular surface are localized in concentrated nanodomains.

Both, the polysaccharides (Cunha and Gandini 2010) and the headgroup components of lipids exposed to the outer membrane (Nagle and Tristram-Nagle 2000) are of hydrophilic nature while the partially nonpolar (Giovambattista et al. 2008) or highly hydrophobic (Whited and Park 2014) protein structures present hydrophobic domains. It is thus likely that the increase of protein coverage of the membrane as a response to stress reduced the hydrophilic space available for the water drop to spread leading to lower wettability. Furthermore, this also reduced the interactions with the hydrophilic CFM tips leading to a reduction of adhesion forces towards the $-\text{NH}_2$ and $-\text{COOH}$ probes. Owing to an enhanced exposition of hydrophobic binding sites of stressed compared to control cells, the probability of the $-\text{CH}_3$ tip to interact with such a hydrophobic molecule or molecule part increases for the stressed cells (compare the proposed tip-sample interaction sketch in Fig 6A for the control cell with Fig 6B for the stressed cell). By unloading the cantilever, it would be energetically more favorable to hold the contact between the $-\text{CH}_3$ tip and the hydrophobic stressed cell surface than being wetted by the polar medium up to the point when the restoring force of the cantilever overcomes the adhesion force between tip and sample.

Conclusions

Combination of nanoscale physical properties like size, roughness and stiffness with nanoscale interfacial properties like adhesion to hydrophobic and hydrophilic functionalized AFM tips together with microscale surface chemical composition and macroscale wettability of stressed and unstressed cells of *Pseudomonas fluorescens* increased our understanding of the processes that promote bacterial induced SWR. Adaptation to hypertonic stress reduced

the cell size probably due to release of water under the turgor pressure but increased stiffness due to structural changes at the outer cell layer of *Pseudomonas fluorescens*. The marked increase in surface protein content suggests two possible mechanisms for the structural changes that probably complement each other. The destabilization of the outer membrane upon cell shrinkage is probably compensated for by the release of outer membrane vesicles by which the protein content increases. The higher protein content increases the rigidity of the cell wall and the number of hydrophobic nano-domains per surface area. In addition, an electrostatic collapse of outer- and core-polysaccharide chains may have led to a vertical contraction of the outermost layer thus exposing the proteins embedded in the outer membrane more to the outside. We could show that by adaptation to osmotic stress *Pseudomonas fluorescens* reduces the wettability of colonized surfaces and thus may contribute to the dynamic of water repellency in the complex soil systems.

To unravel details on the interplay of different cell adaptation mechanisms to hypertonic stress further investigations are required by which the influence of each mechanism could be tested separately. This does not only involve studying the role of the release of the outer membrane vesicles and the contraction of surface polymers for changes of the cell surface properties, but should also include dynamic changes of the cell morphology, elasticity and adhesion by in situ AFM technology (Mularski et al. 2016). Finally, the validity of the results for *P. fluorescens* has to be tested for a wider range of soil bacteria from different taxonomic groups.

Acknowledgements

We want to thank Susanne K. Woche for the XPS measurements and the unknown reviewers for their valuable input.

Supplementary data

Supplementary data are available at [FEMSMC](https://femsmicrobes.com) online.

Conflicts of interest. None declared.

Funding

We are grateful for the funding of the present study by the German Research Foundation (DFG) as part of the project 'Impact of bacterial biomass on the surface wettability of soil particles under varying moisture conditions' (GO 2329/2-1/MI 598/4-1/DI 1907/2-1).

References

- Abu Quba AA, Schaumann GE, Karagulyan M et al. A new approach for repeated tip-sample relocation for AFM imaging of nano and micro sized particles and cells in liquid environment. *Ultramicroscopy* 2020;**211**:112945.
- Abu Quba AA, Schaumann GE, Karagulyan M et al. Quality control of direct cell-mineral adhesion measurements in air and liquid using inverse AFM imaging. *RSC Adv* 2021;**11**:5384-92.
- Achtenhagen J, Goebel M-O, Miltner A et al. Bacterial impact on the wetting properties of soil minerals. *Biogeochemistry* 2015;**122**:269-80.
- Ahimou F, Denis FA, Touhami A et al. Probing microbial cell surface charges by atomic force microscopy. *Langmuir* 2002;**18**:9937-41.
- Bates D, Mächler M, Bolker B et al. Fitting linear mixed-Effects models using lme4. *J Statist Soft* 2015;**67**:48.
- Baum MM, Kainović A, O'Keeffe T et al. Characterization of structures in biofilms formed by a *Pseudomonas fluorescens* isolated from soil. *BMC Microbiol* 2009;**9**:103.
- Baumgarten T, Sperling S, Seifert J et al. Membrane vesicle formation as a multiple-stress response mechanism enhances *Pseudomonas putida* DOT-T1E cell surface hydrophobicity and biofilm formation. *Appl Environ Microbiol* 2012;**78**:6217-24.
- Baumgarten T, Vazquez J, Bastisch C et al. Alkanols and chlorophenols cause different physiological adaptive responses on the level of cell surface properties and membrane vesicle formation in *Pseudomonas putida* DOT-T1E. *Appl Microbiol Biotechnol* 2012;**93**:837-45.
- Beaussart A, Feuillie C, El-Kirat-Chatel S. The microbial adhesive arsenal deciphered by atomic force microscopy. *Nanoscale* 2020;**12**:23885-96.
- Benítez R, Bolós VJ, Toca-Herrera J. afmToolkit: an R package for automated AFM force-Distance curves analysis. *R J* 2017;**9**:291, DOI: 10.32614/RJ-2017-045.
- Berquand A. Quantitative imaging of living biological samples by PeakForce QNM Atomic Force microscopy. *Application Note* 2011;**135**:1-10.
- Botsford JL, Alvarez M, Hernandez R et al. Accumulation of glutamate by *Salmonella typhimurium* in response to osmotic stress. *Appl Environ Microbiol* 1994;**60**:2568-74.
- Bremer E, Krämer R. Responses of microorganisms to osmotic stress. *Annu Rev Microbiol* 2019;**73**:313-34.
- Butt H-J. Measuring electrostatic, van der Waals, and hydration forces in electrolyte solutions with an atomic force microscope. *Biophys J* 1991;**60**:1438-44.
- Cao T, Tang H, Liang X et al. Nanoscale investigation on adhesion of *E. coli* to surface modified silicone using atomic force microscopy. *Biotechnol Bioeng* 2006;**94**:167-76.
- Cunha AG, Gandini A. Turning polysaccharides into hydrophobic materials: a critical review. Part 1. Cellulose. *Cellulose* 2010;**17**:875-89.
- Deng Y, Sun M, Shaevitz JW. Direct measurement of cell wall stress stiffening and turgor pressure in live bacterial cells. *Phys Rev Lett* 2011;**107**:158101.
- Diehl D. Soil water repellency: dynamics of heterogeneous surfaces. *Colloids Surf A* 2013;**432**:8-18.
- Doerr SH, Shakesby RA, Walsh RPD. Soil water repellency: its causes, characteristics and hydro-geomorphological significance. *Earth Sci Rev* 2000;**51**:33-65.
- Dombek KM, Ingram LO. Effects of ethanol on the *Escherichia coli* plasma membrane. *J Bacteriol* 1984;**157**:233-9.
- Dorobantu LS, Bhattacharjee S, Foght JM et al. Atomic force microscopy measurement of heterogeneity in bacterial surface hydrophobicity. *Langmuir* 2008;**24**:4944-51.
- Dorobantu LS, Gray MR. Application of atomic force microscopy in bacterial research. *Scanning* 2010;**32**:74-96.
- Eberlein C, Baumgarten T, Starke S et al. Immediate response mechanisms of gram-negative solvent-tolerant bacteria to cope with environmental stress: cis-trans isomerization of unsaturated fatty acids and outer membrane vesicle secretion. *Appl Microbiol Biotechnol* 2018;**102**:2583-93.
- El-Kirat-Chatel S, Beaussart A, Boyd CD et al. Single-Cell and Single-Molecule analysis deciphers the localization, adhesion, and mechanics of the biofilm adhesin LapA. *ACS Chem Biol* 2014;**9**:485-94.
- Fox J, Weisberg S. *An R Companion to Applied Regression*. 2nd ed. Thousand Oaks, Calif: SAGE Publications, 2011.
- Francius G, Polyakov P, Merlin J et al. Bacterial surface appendages strongly impact nanomechanical and electrokinetic properties of *Escherichia coli* cells subjected to osmotic stress. *PLoS One* 2011;**6**:e20066.

6 Hypertonic stress induced changes of *Pseudomonas fluorescens* adhesion towards soil minerals studied by AFM



OPEN

Hypertonic stress induced changes of *Pseudomonas fluorescens* adhesion towards soil minerals studied by AFM

Abd Alaziz Abu Quba¹, Marc-Oliver Goebel², Mariam Karagulyan³, Anja Miltner³, Matthias Kästner³, Jörg Bachmann², Gabriele E. Schaumann¹ & Doerte Diehl¹✉

Studying bacterial adhesion to mineral surfaces is crucial for understanding soil properties. Recent research suggests that minimal coverage of sand particles with cell fragments significantly reduces soil wettability. Using atomic force microscopy (AFM), we investigated the influence of hypertonic stress on *Pseudomonas fluorescens* adhesion to four different minerals in water. These findings were compared with theoretical XDLVO predictions. To make adhesion force measurements comparable for irregularly shaped particles, we normalized adhesion forces by the respective cell-mineral contact area. Our study revealed an inverse relationship between wettability and the surface-organic carbon content of the minerals. This relationship was evident in the increased adhesion of cells to minerals with decreasing wettability. This phenomenon was attributed to hydrophobic interactions, which appeared to be predominant in all cell–mineral interaction scenarios alongside with hydrogen bonding. Moreover, while montmorillonite and goethite exhibited stronger adhesion to stressed cells, presumably due to enhanced hydrophobic interactions, kaolinite showed an unexpected trend of weaker adhesion to stressed cells. Surprisingly, the adhesion of quartz remained independent of cell stress level. Discrepancies between measured cell–mineral interactions and those calculated by XDLVO, assuming an idealized sphere-plane geometry, helped us interpret the chemical heterogeneity arising from differently exposed edges and planes of minerals. Our results suggest that bacteria may have a significant impact on soil wettability under changing moisture condition.

Adhesion to solid surfaces plays a crucial role for bacteria¹, resulting from a complex interplay of physicochemical interactions including electrostatic, van der Waals and Lewis acid–base (AB) forces^{2,3}. In soil ecosystems, bacteria exert a significant influence on various soil properties and soil functions. For instance, their capacity to colonize surfaces contributes to soil aggregate formation and mineral weathering⁴. Even a slight increase in microbial biomass or its residues at mineral surfaces can lead to substantial changes in surface characteristics, such as surface roughness, surface charge, adsorption affinities and wettability⁵. Consequently, bacterial adhesion is of major importance regarding soil functions in soil ecosystems^{6,7}.

The majority of soil bacteria regularly experience suboptimal growth conditions due to competition for resources, or changing environmental factors, putting them nearly constantly under stress. With climate change, particularly drought stress will become increasingly important for the soil microbial community⁸. Surprisingly, there are currently no studies available that have analyzed the impact of drought stress on the adhesion of bacterial cells to minerals. Hence, our goal is to investigate the role of bacterial cells and their cell wall remnants in shaping the dynamics of mineral surface properties in soil under changing moisture conditions. In a recent study, we demonstrated that subjecting *Pseudomonas fluorescens* cells to hypertonic stress induced by NaCl reduces their wettability⁹. We now seek to explore whether soil bacteria and their cell envelopes not only decrease the wettability of soil particles after dry periods but also exhibit stronger adhesion to surfaces, making them less susceptible to degradation, ultimately leading to an increased persistence of soil water repellency.

In liquid media, the aggregation or dispersion behavior of cell–mineral associations can be described using the extended Derjaguin–Landau–Verwey–Overbeek (XDLVO) theory^{2,4,10}. However, XDLVO calculations necessitate

¹Institute for Environmental Sciences, University of Kaiserslautern-Landau (RPTU), Landau, Germany. ²Institute of Soil Science, Leibniz Universität Hannover, Hannover, Germany. ³Department of Environmental Biotechnology, Helmholtz Centre for Environmental Research – UFZ, Leipzig, Germany. ✉email: d.diehl@rptu.de

geometrically well-defined interfaces with uniform surface charge density, whereas real colloidal systems in soil display morphological and chemical variations that can lead to significant deviations from theoretical models with simplified geometrical shapes (e.g., spherical and planar approximation)^{11–13}. Numerical methods such as surface element integration (SEI) can determine the precise interaction forces between different any shapes and a flat surface^{14,15}. However, considering chemical heterogeneity arising from structural edge effects of minerals demands substantial computational power¹⁵ and, to our knowledge, has not been applied yet. Consequently, it is imperative to directly measure adhesion forces under the most realistic conditions.

Atomic force microscopy (AFM) serves as a powerful tool for investigating cell-mineral interactions (CMI)^{4,16} and is the only technique with nano-resolution applicable to living cells in aqueous solutions¹⁷. In examining the interaction between *E. coli* and “flat” single crystals of muscovite, goethite and graphite, it was revealed that electrostatic forces predominantly dictate the adhesion forces’ polarity. Simultaneously, both the surface hydrophobicity and roughness of the minerals exert a direct influence on the absolute force magnitude within the attractive force regimes¹⁸. When dealing with irregularly shaped natural substances, tip-sample interactions become increasingly complex due to the effect of contact area, and the potential for contact at multiple sites. Adhesion measurements involving *E. coli*-coated tipless probes interacting with hematite or corundum nanoparticles have demonstrated that smaller-radius particles adhere more strongly to the cells due to a greater number of tip-sample contact sites compared to larger particles¹⁹. Consistently, *E. coli* cells displayed stronger adhesion to needle-like goethite particles than to flat goethite surfaces⁴.

Hence, adhesion values without information on the contact area pose interpretation challenges, rendering quantitative comparison of interaction forces between various strains and substrates unfeasible^{20–22}. Consequently, the adhesion pressure, defined as the normalized adhesion force over the corresponding tip-sample contact area, was introduced¹⁶. This parameter facilitates a quantitative comparison of interaction data¹⁶. A novel protocol for characterizing irregular interface geometries formed by natural mineral particles and cells enables the measurement of CMI in a liquid medium²³.

In addition to the contact area, the orientation at which a mineral particle contacts the cell surface likely influences adhesion. Some minerals exhibit anisotropic crystallographic structure^{24–28}, such as goethite which comprises double chains of Fe-octahedra connected via hydrogen bonds across the long axis of the particle²⁵. The edges, despite representing only 2–5% of the particle surface, contain a higher density of potential hydrogen bonding sites per unit area compared to the particle planes^{24,25}. Similarly, montmorillonite and kaolinite possess additional polar sites along their edges with octahedral Al–OH and tetrahedral Si–OH groups located at the edges of the particle rather than on the basal planes which are terminated by either one of these groups for kaolinite and by Si–OH for montmorillonite, respectively^{26,27}. Larger quartz grains have irregularly shaped surfaces that become hydroxylated in water facilitating hydrogen bonding with lipopolysaccharides of Gram-negative bacteria²⁸.

To investigate the effect of growth under drought stress on bacterial cell adhesion to minerals, we tested four hypotheses:

- H1 Since cells are likely slightly negatively charged at the experimental pH of 5.9, we anticipate jump-to-contact events in force spectroscopy for positively charged minerals indicating an attractive force⁴ and repulsive electrostatic forces when negatively charged mineral tips approach cell surfaces.
- H2 Mineral wettability influences adhesion pressures towards cells. More wettable minerals adhere to bacteria to a lesser extent as a polar aqueous medium readily wet hydrophilic surfaces during cell-mineral separation.
- H3 The increased protein content (hydrophobic surface domains) on stressed cell surfaces compared to unstressed cells⁹ makes adhesion to mineral surfaces in a polar aqueous medium more energetically favorable for stressed cells resulting in an increased adhesion pressure.
- H4 The non-uniform distribution of functional groups and charge on kaolinite surfaces⁴ generally leads to less agreement between AFM spectroscopy results and XDLVO theory for the interaction with stressed and unstressed bacteria compared to quartz, montmorillonite and goethite.

To assess these hypotheses, we conducted direct single cell-mineral interaction studies using AFM. Specifically, we measured force-distance (FD) curves towards *P. fluorescens* cells grown under hypertonic stress or under unstressed conditions using probes modified with kaolinite, montmorillonite, goethite or quartz particles. The minerals used represent a diverse range of particle shapes and physicochemical properties. Our experiments thus encompass the complexity of interactions with the typical Gram-negative soil bacterium *P. fluorescens*. Adhesion forces were normalized to the real 3D contact area. Surface roughness extends the range and depth of the secondary minimum while decreasing the energy barrier’s magnitude²⁹. Furthermore, morphological heterogeneity increases attractive interactions in the primary minimum compared to XDLVO calculations using simplified geometrical models¹⁵. Hence, we only qualitatively compared the measured adhesion pressures with theoretical XDLVO energy profiles. In these models, minerals and cells were approximated as spheres and planes, respectively, using macroscopic parameters like contact angle and zeta potential. Any deviations were attributed to mineral shapes and potential chemical heterogeneity resulting from differently exposed clay edges and planes when interacting with bacterial cells. This approach enabled the discussion of potential relationships between surface charge, crystal structure, wettability, and chemical composition of minerals with the adhesion pressure of specific cell-mineral pairs.

Results

Characteristics of the minerals and their aggregates

To provide an overview of the size, shape and aggregation behavior of the minerals used, Fig. 1a–c present Height and Peak Force Error images of goethite, kaolinite and montmorillonite, respectively. Figure 1d displays an image

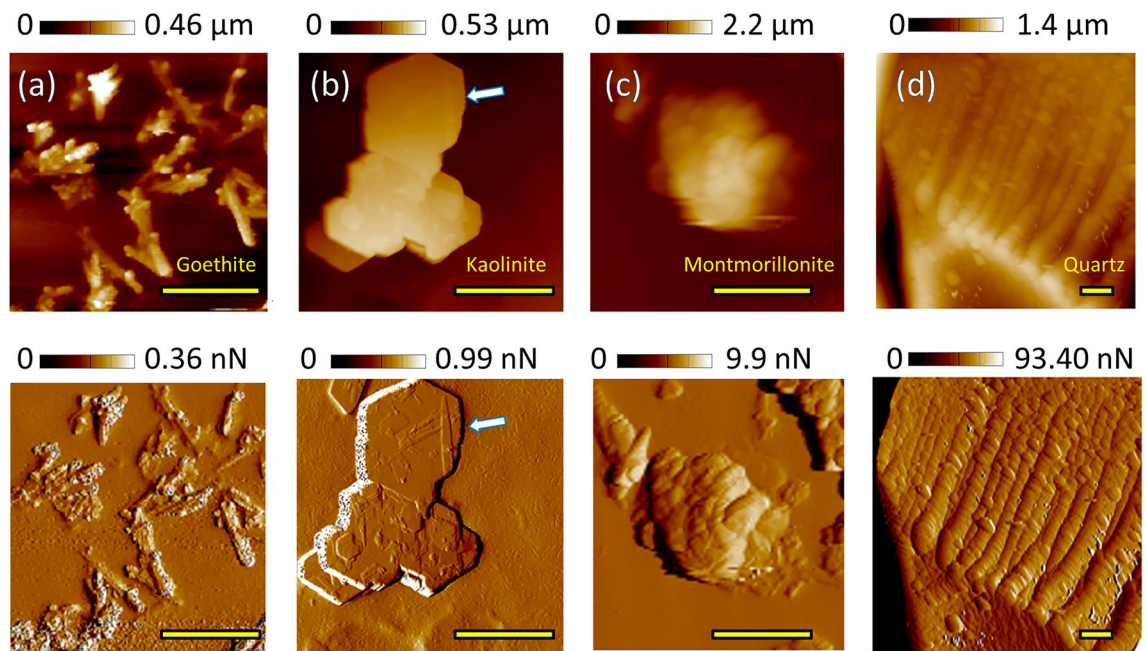


Figure 1. AFM Height (top) and Peak Force Error (bottom) maps of (a) goethite, (b) kaolinite, (c) montmorillonite and (d) quartz, obtained in KNO_3 solution with sharp tips. The scale bar is $1.5 \mu\text{m}$ for all images.

of the edge of a quartz particle. More detailed images can be found in Supplementary Fig. S-I 1. The appearance of goethite and kaolinite notably reflect their crystal structures (Fig. 1a,b). While many kaolinite particles exhibit a flat shape with a nominal average size of $\sim 500 \text{ nm}$ and aggregate in form of smooth plates with sharp edges, others exhibit the typical pseudo-hexagonal shape²⁶ (indicated by arrows in Fig. 1b and Supplementary Fig. S-I 1). Goethite crystals with a nominal size of $100 \times 800 \text{ nm}$ can be identified by their needle-like shape in individual particles or within aggregated structures where some needles protrude from goethite clusters. Montmorillonite particles averaging around 400 nm in size formed the largest and highest aggregates with an exfoliated morphology (Fig. 1c and Supplementary Fig. S-I 2). Conversely, larger quartz grains exhibit irregular shapes (Fig. 1d). Consequently, the small and relatively smooth goethite particles and the smoothest kaolinite aggregates possess smaller and less variable roughness R_q values of $18 \pm 9 \text{ nm}$ ($n = 150$) and $11 \pm 9 \text{ nm}$ ($n = 80$), respectively. In contrast, montmorillonite aggregates and quartz particles have higher roughness values of $141 \pm 88 \text{ nm}$ ($n = 100$) and $119 \pm 126 \text{ nm}$ ($n = 60$), respectively.

Characteristics of the modified tips

In Fig. 2a, the mineral clusters and quartz particles adhering to the glue of the tipless probe, as imaged by ESEM and AFM, exhibit comparable structures to those presented in Fig. 1. The region of the probes extending most into the z direction (height) as shown in Fig. 2b,c offers a closer look at the “potential” mineral tip when the probe is used to scan bacterial cells. The 3D tip area represented as a function of height for each mineral tip (area-height function) corresponds to the contact area as a function of deformation depth during specific cell-mineral interactions (Fig. 2d and Supplementary chapter S-I.2 with Supplementary Fig. S-I 3 and Supplementary Fig. S-I 4). For the average deformation observed during the cell-mineral interactions, the 3D areas tend to decrease in the order of quartz > kaolinite > montmorillonite > goethite (Supplementary Fig. S-I 5). Both, roughness and 3D area of the particles attached to the probes increase with height, albeit with a narrower range of variation for the 3D area (Fig. 2d). However, although kaolinite and goethite surfaces were expected to be smoother, they did not exhibit lower roughness compared to montmorillonite and quartz surfaces (Fig. 2d). Nevertheless, the tip area-height functions vary considerably among individual modified tips of the same mineral (Fig. 2d). This variation reflects topographical irregularities including orientation, flatness, or aggregated structure of the particles. Despite the fact that the size of the mineral particles or aggregates at the end of the AFM probe is larger than that of a single bacterium, their irregular shapes locally provide nanoscale “tips” for AFM force measurements under low loading forces, and, consequently, low deformation.

Effects of cell-mineral interactions on cell morphology

To assess the impact of cell-mineral interactions (CMI) on cell integrity, Fig. 3 provides a comparative analysis of height images of the same unstressed *P. fluorescens* cells scanned by (a) standard sharp tip before CMI, (b) a mineral modified tip during CMI and (c) a standard sharp tip after CMI. Generally, for goethite, kaolinite and montmorillonite, similar cell structures are evident in the images obtained before, during and after CMI, underscoring the ability to detect single cells through the proposed modification process. However, in the case of the quartz tip, the interaction does not precisely replicate the shape of the corresponding cells measured by a sharp

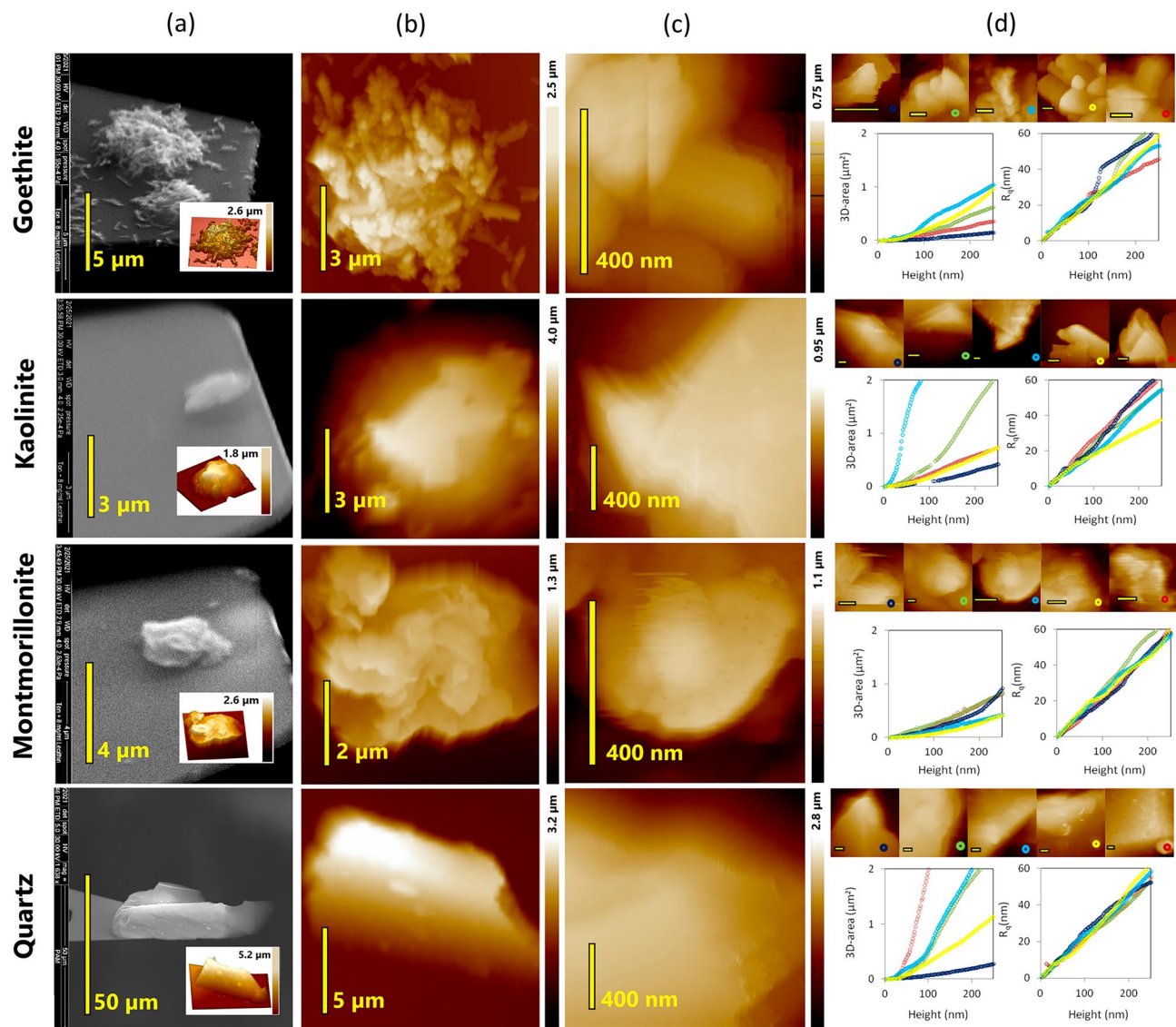


Figure 2. Correlative AFM/ESEM characterizations of tips modified with four different minerals shown for each mineral in one row: (a) ESEM pictures of the cantilevers modified with the minerals with insets showing 3D inverse AFM images of the respective modifying mineral, (b) closer AFM images of the mineral clusters at the top of the glue spot, (c) insets of local areas inside (b) with the highest z extension, and (d) local AFM maps (scale bar of 200 nm) of the set of 5 probes later used for the cell-mineral interactions and graphs presenting their tip area (left) and R_q (right) as a function of height (or deformation depth).

tip (Supplementary Figs. S-I 7 and 6). It is probable that the large quartz particle made contact with the same cell at different positions acting as multiple tips and producing replicated images of the same cell. Additional images illustrating interactions between both stressed and unstressed cells and several tips for each mineral are provided in Supplementary Fig. S-I 8. These images demonstrate that goethite and in some cases kaolinite tips yielded the best resolution, followed by montmorillonite, while quartz tips occasionally revealed repetitive cell structures. Most importantly, it can be observed that the cell structures remain consistent throughout the cell-mineral interaction, indicating that cell integrity is preserved (Fig. 3a,c).

A more comprehensive interpretation of the measured CMI and the effect of loading force, contact time, and contact area on adhesion forces, adhesion pressure, adhesion efficiency and rupture and adhesion events, is presented in Supplementary Figs. S-I 9 to 13 in chapter S-I.6 and S-I. 7.

Effect of hypertonic growth conditions of cells for their interactions with minerals

To quantitatively compare cell-mineral interactions, the adhesion pressure (P_{ad}) obtained from force-distance (FD) curves using five modified tips for each mineral at a fixed loading force (5 nN) on stressed and unstressed cells is presented in Fig. 4. Notably, a considerable variability in the data was observed among tips made from the same interacting materials (Supplementary Fig. S-I 14). The hypertonic stress experienced during the growth phase led to a substantial increase in P_{ad} for *P. fluorescens* cells interacting with montmorillonite rising from

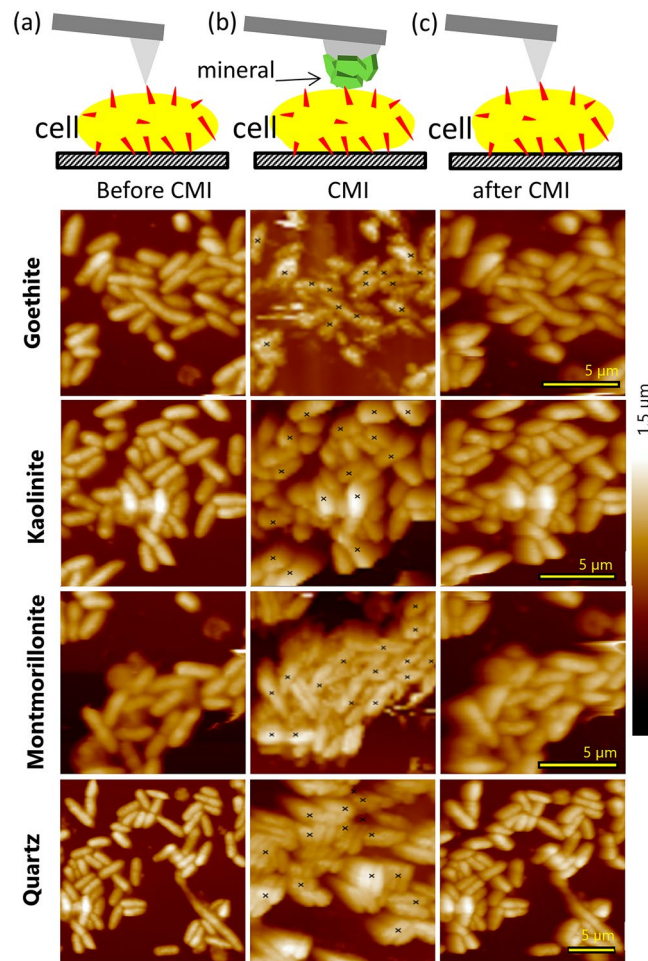


Figure 3. Exemplary images of the same unstressed bacterial cultures in 10 mM KNO_3 solution for one mineral with the same scale in each row made by (a) a sharp tip before the cell-mineral interactions, CMI, (b) a mineral modified tip during the CMI with the marks indicating the positions of FD curve acquisition, and (c) a sharp tip after the CMI.

7.4 to 21.1 kPa and with goethite increasing from 30.3 to 94.0 kPa, while P_{ad} decreased when interacting with kaolinite from 24.6 to 7.7 kPa. Conversely, P_{ad} values for *P. fluorescens* cells interacting with quartz were 6.3 kPa and 8.3 kPa for unstressed and stressed cells, respectively, and thus remained relatively unaffected by the growth conditions (Fig. 4). Among the minerals, *P. fluorescens* cells exerted the highest P_{ad} with goethite, followed by kaolinite, and the lowest P_{ad} with montmorillonite and quartz (Fig. 4). These differences in P_{ad} between the minerals were significant, with two exceptions: the difference in P_{ad} between kaolinite and quartz on unstressed cells was offset by the stress-dependent decrease in P_{ad} towards kaolinite. In contrast, P_{ad} values for unstressed cells were similar when interacting with montmorillonite and quartz, whereas stress significantly increased P_{ad} when interacting with montmorillonite.

Physicochemical properties and surface chemical composition (XPS) of cells and minerals

Table 1 provides physicochemical properties of the minerals and bacteria. Goethite exhibited a positive zeta potential at pH 5.9, while the zeta potentials of the other minerals and the bacteria were negative, with the stressed cells showing slightly more negative potentials than the unstressed cells. The contact angles of the minerals were generally below 45° , indicating complete wettability for quartz and slight water repellency for the other minerals, with goethite having the largest contact angle. The wettability of the minerals was also reflected by the large values ($> 37 \text{ mJ m}^{-2}$, cf.³⁰) of the electron-donor component (γ_s^-), which exhibited an inverse relationship with the contact angle. In contrast, the non-polar Lifshitz–van der Waals component (γ_s^{LW}) was similar for all mineral types. The contact angles of the bacteria were considerably larger than those of the minerals, with a noticeable increase for the cells cultivated under hypertonic stress. Similar to the minerals, γ^- exhibited an inverse relationship to the contact angle, while γ_s^{LW} remained similar for both stressed and unstressed cells. Both γ^- and γ_s^{LW} were significantly smaller for bacteria than for the minerals.

The surface chemical composition of the minerals corresponded to their general chemical composition (Supplementary Fig. S-I 15). Oxygen (O) and silicon (Si) dominated the surface chemical composition of phyllosilicates and quartz, with a notable contribution of carbon (C) at ~4–5 at.%. Kaolinite and montmorillonite exhibited

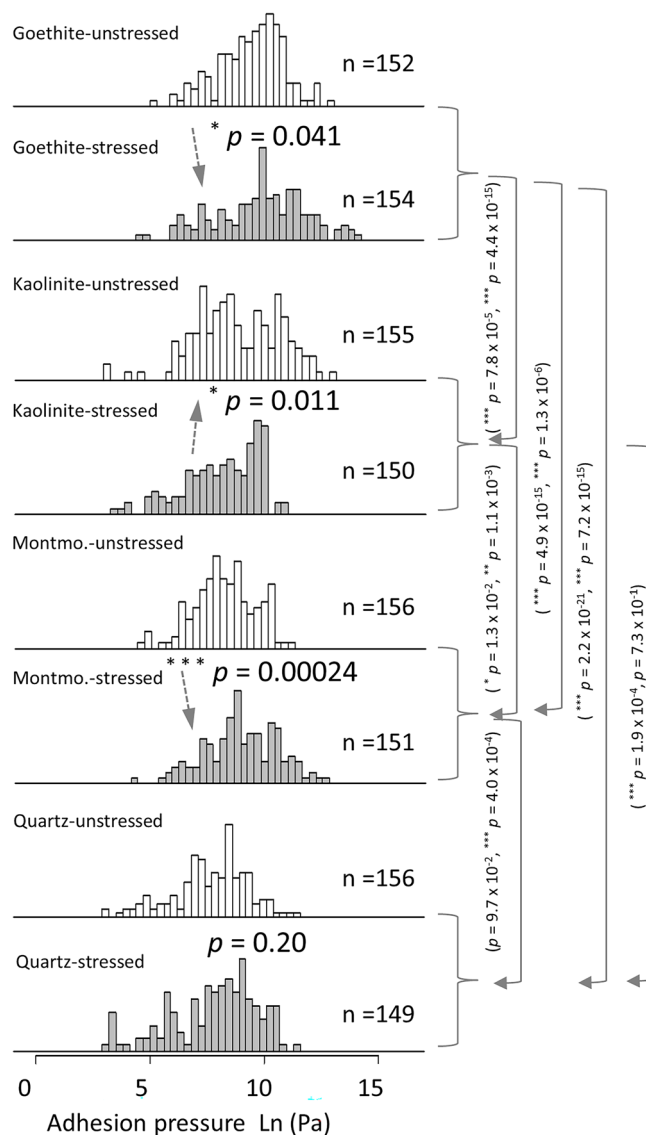


Figure 4. Frequency distributions of adhesion pressures of cell-mineral interactions between cells of two independent unstressed and three independent stressed *P. fluorescens* cultures and five individual functionalized tips for each mineral (Fig. 2d) in 10 mM KNO₃ solution. A set of ~30 FD curves for each tip with 1 s contact time and 5 nN applied force was made. The solid arrows highlight significant differences in adhesion pressures between the minerals (with p values for unstressed and stressed separated by “;”) while the dashed arrows show the effect of stress on adhesion pressure.

larger proportions of aluminum (Al) and traces of iron (Fe), potassium (K), calcium (Ca) and magnesium (Mg), each accounting for less than 1 at.%. For quartz, traces of sodium (Na) and zinc (Zn), each below 0.3 at.%, were detectable. The surface chemical composition of goethite was primarily characterized by O and Fe, but it also featured a substantial amount of C at 14.4 at.% along with traces of chromium (Cr) and sulfur (S) at less than 0.7 at.%. The elevated proportion of surface C can be attributed to C components adsorbed from the gas phase, commonly referred to as ‘adventitious carbon’³¹.

Comparison between AFM measurements, XDLVO calculations and work of adhesion

Theoretical energy profiles illustrating the interaction between bacterial cells and mineral modified tips, calculated using the XDLVO theory based on the values provided in Table 1, are presented in Supplementary Fig. S-I 16 and Supplementary Fig. S-I 17. Notably, for kaolinite, montmorillonite and quartz, the impact of stress on cell-mineral interaction was evident. While the energy profiles for unstressed cells indicate strong repulsive interactions with these minerals, the profiles for stressed cells featured energy barriers and the presence of primary minima at short separation distances, signifying attractive interactions. In the case of goethite, exclusively attractive interactions were indicated for both unstressed and stressed cells, but with deeper primary minima (indicating stronger attractive interactions) observed for stressed cells. The generally attractive interactions

	ζ	ψ	θ	γ_s^{LW}	γ_s^+	γ_s^-
	(mV)	(mV)	(°)	(mJ m ⁻²)		
Goethite	24.2 ± 4.0	28.6	44 ± 8	43.9	1.3 × 10 ⁻²	37.3
Kaolinite	-45.3 ± 1.8	-53.5	24 ± 2	43.1	2.3 × 10 ⁻³	58.8
Montmorillonite	-35.5 ± 2.1	-41.9	18 ± 3	43.7	5.2 × 10 ⁻⁴	63.3
Quartz	-36.7 ± 4.5	-43.3	0 ± 0	44.4	1.5 × 10 ⁻²	66.1
<i>P. fluorescens</i> (unstressed) ^a	-10.6 ± 2.4	-12.5	67 ± 5	35.8	1.7 × 10 ⁻¹	17.0
<i>P. fluorescens</i> (stressed) ^a	-12.3 ± 1.4	-14.5	93 ± 2	35.0	2.7 × 10 ⁻¹	3.4

Table 1. Physicochemical properties of minerals and bacteria: Zeta potential (ζ), surface potential (ψ), contact angle (CA), and the calculated electron-donor (γ_s^-), -acceptor (γ_s^+) and non-polar Lifshitz-van der Waals component of surface free energy (γ_s^{LW}). Error margins indicate one standard deviation (zeta potential: $n = 10$; contact angle: $n = 9$). ζ : zeta potential, ψ : surface potential, θ : solid–water contact angle, γ_s^- : solid surface free energy. Meaning of superscripts: ‘LW’: Lifshitz–van der Waals, ‘+’: electron acceptor, ‘-’: electron donor component of surface free energy, respectively. ^aData from Karagulyan et al.³³

between the cells and goethite can be primarily attributed to the positive surface charge of goethite (Table 1), leading to electrostatic attraction with the negatively charged cells.

Table 2 provides a qualitative comparison of the effect of growth under hypertonic stress on cell–mineral adhesion pressures (P_{ad}) measured by AFM and interaction forces calculated based on the XDLVO. The most favorable qualitative agreement between AFM measurements and the predictions based on the XDLVO theory was observed for the goethite-modified tips, with only one out of five tips displaying a trend opposite to what was expected from the XDLVO theory. This was followed by montmorillonite and quartz where two tips exhibited

		Goethite					Kaolinite					Montmorillonite					Quartz				
Probe		1	2	3	4	5	1	2	3	4	5	1	2	3	4	5	1	2	3	4	5
AFM	(a) Effect of stress on P_{ad}																				
	(b) Force regime towards unstressed cells																				
	(c) Force regime towards stressed cells																				
XDLVO	(d) Energy barrier towards unstressed cells																				
	(e) Energy barrier towards stressed cells																				
	(f) Effect of stress on force regime?																				
	(g) P_{ad} vs. XDLVO	✓	✗	✓	✓	✓	✓	○	✗	✗	○	✓	✓	✓	○	○	✓	✓	✓	○	✗

Table 2. Qualitative comparison of the effect of stress on the cell–mineral interactions between energy profiles calculated by the XDLVO theory from values presented in Table 1 and FD curves obtained by AFM using 5 mineral modified probes for each mineral: (a) Increased (green) or decreased (red) mean adhesion pressures (P_{ad}) upon stress, XDLVO based calculated repulsive (red) and attractive (green) forces towards (b) unstressed and (c) stressed cells, XDLVO based calculated energy barriers towards (d) unstressed and (e) stressed cells, (f) absolute shift of the attractive forces (goethite) or repulsive forces (other minerals) of unstressed cells towards more attractive (negative) forces on stressed cells, and (g) agreement (✓), disagreement (i.e., $p > 0.1$, ○), or contradiction (✗) of the response to stress between measured and calculated values. More fields indicate higher effects or size of the respective values and darker colors in (a) indicate $p < 0.05$, lighter $0.5 < p < 0.1$ and no color $p > 0.1$.

deviating interactions. However, for kaolinite, only one tip displayed agreement with the XDLVO theoretical energy profiles while the other four demonstrated no agreement or even contradictory interactions. Notably, with an aspect ratio of approximately 2.3, the kaolinite tips were on average 1.7, 1.6 and 1.4 times more elongated than montmorillonite, goethite and quartz tips, respectively (Supplementary Fig. S-I 18). This implies that the underlying assumption of our XDLVO calculations, which consider a spherical tip facing a planar cell surface, is best satisfied for montmorillonite and least satisfied for kaolinite.

Finally, the work of adhesion (W_{ad}) between stressed and unstressed cells and the four minerals calculated from their contact angles exhibits a linear increase with rising P_{ad} for goethite, montmorillonite and quartz. Generally, the values are higher and the slopes are steeper for stressed cells compared to unstressed cells (Fig. 5). Notably, for kaolinite P_{ad} was lower while W_{ad} was higher when interacting with stressed cells compared to unstressed cells. The calculated W_{ad} values were positive for the interactions of stressed cells with all of the minerals under study, suggesting attraction in all cases, although to different extents depending on the mineral. In contrast, the calculated W_{ad} values for unstressed cells in interactions with kaolinite, montmorillonite and quartz are negative, indicating repulsive interactions. Conversely, interactions with goethite were attractive for unstressed cells, yielding positive W_{ad} values.

Discussion

Contrary to the often reported jump-to-contact events⁴ and the prominent role of electrostatic forces in cell-mineral adhesion^{33–35}, we did neither detect attractive nor repulsive **forces during single cell-mineral interactions (CMI)**. This finding does not support our hypothesis H1 and suggests that almost no long-range electrostatic forces are involved in the single cell-mineral interactions. This is also in contrast to the calculated energy profiles of goethite, which indicate attractive electrostatic interactions with both unstressed and stressed cell types due to opposite surface charges. One possible explanation could be that repulsive interactions stemming from the positive charges of the poly-L-lysine coating underneath and between the cells may have compensated for the attractive interactions towards the cells. However, since we observed no differences in long-range electrostatic forces for positively or negatively charged minerals, we suggest that the charge of the poly-L-lysine coating has only a negligible effect. Probably, the single cell resolution and the small cell-mineral interaction area in our study rendered the magnitude of the electrostatic forces much smaller than in other studies where a higher number of cells attached to a tipless probe approached a flat goethite surface⁴. Approach FD curves measured by sharp functionalized AFM tips ($-\text{COOH}$, $-\text{NH}_2$, $-\text{CH}_3$) on *Pseudomonas fluorescens* displayed a very flat profile and did not show indications of long-range forces⁹. This leads to the conclusion that bacterial adhesion exhibited negligible charge effects, although some levels of repulsion in the form of an energy barrier or van der Waals jump-in interactions beyond the sensitivity of the cantilevers could not be excluded. This suggests that in our observation, it is not the long-range electrostatic interactions¹⁸ but rather specific short-range forces that play the predominant role in line with recent findings^{36–38}. Such specific interactions can be attributed to hydrophobic interactions and hydrogen bonds^{35,38,39}. This is further supported by the contact time dependence of the adhesion

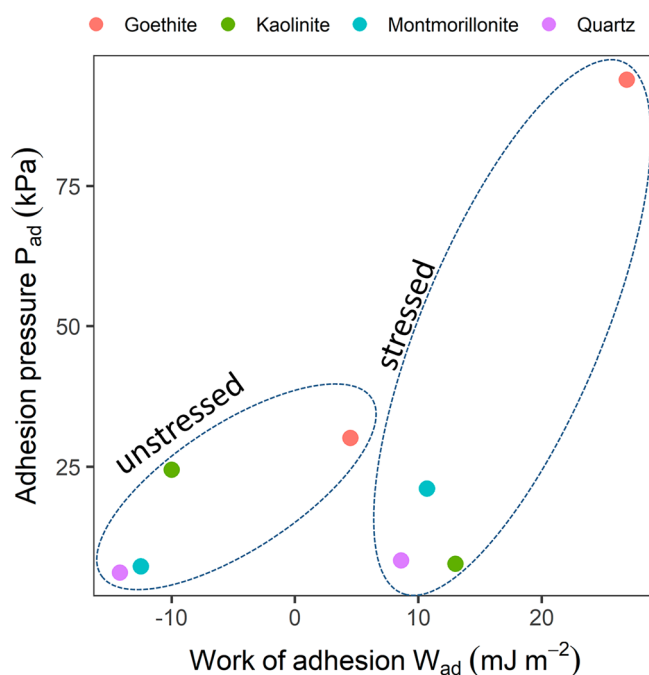


Figure 5. The work of adhesion was calculated from CA data as described in Traini et al.⁶³ (Eq. 8). Adhesion pressure values are the mean of the medians extracted from the boxplots (Supplementary Fig. S-I 14) and thus just approximate values to show the general relationship. In contrast to the energy profiles, the negative values found for the CMI with unstressed cells indicate repulsive interactions.

forces. Long-range nonspecific interactions act instantaneously during the approach to the sample surface and have little⁴⁰ or no³⁸ dependence on the contact time. In contrast, when the cell-mineral contact time is extended, more hydrogen bonds may form, leading to higher adhesion forces until saturation is reached after a few seconds (e.g., 4 s)⁴, when all potential bond partners have met. Additionally, or alternatively, bond strengthening during contact time could be due to a rearrangement of non-polar molecule moieties towards the mineral surfaces with low wettability, away from the water interface. The significant decrease in average adhesion and rupture forces, along with a decrease in the frequency of rupture events with decreasing tip-sample contact time, provides evidence that the adhesion forces predominantly originate from specific forces, especially hydrogen bonding³⁸. Our choice of a 1-s contact time followed by a 0-s contact is suitable for studying the mechanisms of bond strengthening and inferring the forces that drive initial cell attachment to the mineral phase. Nevertheless, for research purposes focused on studying the viscoelastic properties of cells¹⁶ or determining the time required for cell-mineral adhesion to fully strengthen⁴, an exploration of cell adhesion at incrementally increasing time intervals is required.

The occurrence of multiple rupture events can be attributed to the stretching of organic molecules (e.g., membrane molecules or extracellular polymeric substances) that adsorb to the mineral tips during single CMI and gradually desorb during tip retraction⁴ (Supplementary Fig. S-I 19). The unbinding forces, observed in the range of ~200–700 pN for the various CMI scenarios in this study, suggest that several bonds were broken simultaneously, as a single hydrogen bond rupture force typically occurs at ~10 pN². The presence of 10 mM KNO₃ during the experiments may have amplified this effect by screening the charges and reducing the repulsive tip-sample steric forces. Consequently, this results in a more rigid and compacted polymer layer and higher adhesion forces compared to experiments with lower or no salt concentration⁴¹. It is plausible that during tip retraction the stretching of molecules is accompanied to some extent by the stretching of the cell membrane until the point when the restoring force of the cantilever exceeds the unbinding forces exerted by the group of molecules adsorbed to the mineral tip.

The positive correlation between contact areas and adhesion forces (Supplementary Fig. S-I 9) lends support to the validity of the approach of using adhesion pressure¹⁶ (adhesion force per contact area) for comparing measurements obtained with different mineral probes of varying contact areas. Data on adhesion pressure¹⁶ are not yet commonly reported but significantly enhance the comparability of single CMI results among minerals with different properties, although it is worth noting that the influence of the irregular shapes of the mineral tips on single CMI cannot be entirely ruled out. Nonetheless, the intertwined effects of chemical and morphological heterogeneity are inherent in nature and thus constitute a part of real CMI scenarios, such as those encountered in soil. Our findings concerning the **impact of mineral properties** on adhesion pressures align with a study on Gram-negative *Pseudomonas putida* adsorption onto clay minerals³³, where the quantity of adsorbed cells decreased in the order of goethite > kaolinite > montmorillonite. This observation is further corroborated by an examination of bacterial-mineral suspensions which reveals a distinct pattern⁴. Goethite formed strong and closely bonded connections with bacterial surfaces, while kaolinite also exhibited good adhesion to these cells, although not as robust as goethite. On the other hand, there were hardly any aggregates of bacterial cells found with montmorillonite, indicating a relatively weaker adhesion of this mineral to the cells⁴. In the case of goethite, which had the highest contact angle, hydrophobic interactions, in addition to hydrogen bonds seemed to govern the CMI. This includes interactions between the mineral surface with adsorbed organic impurities and hydrophobic proteins on the cell surface⁹. The favorable adhesion of cells to goethite is consistent with the absence of an energy barrier in the interaction energy profiles. The hydrophilic nature of the quartz surfaces, characterized by the lowest contact angle, facilitates their rewetting during separation from the cell surface. This likely led to a lower single cell-mineral adhesion of quartz compared to kaolinite and montmorillonite which have higher contact angles. In line with other studies⁴², we found that a higher affinity to adsorb organic impurities from the air (adventitious carbon⁴³) correlated with a higher contact angle and a greater affinity for other less polar molecules on the cell surface, particularly in the presence of a polar aqueous medium. This may explain the positive correlation between the work of adhesion calculated based on the contact angle data and the adhesion pressure detected by AFM at the single cell level, supporting our hypothesis **H2**, which posits an increasing adhesion affinity with decreasing wettability.

In a previous study, it was found that the increase in the hydrophobicity of *P. fluorescens* due to hypertonic stress was mediated by chemical modifications that resulted in an increase in protein coverage (i.e., the number of hydrophobic domains) on the cell surface at the expense of lipopolysaccharides⁹. The **effect of cell growth conditions** on the adhesion pressure towards both goethite and montmorillonite as expressed by a stress-induced increase in P_{ad} of the cells, can be attributed to stronger hydrophobic interactions. These interactions occur due to the presence of more or larger hydrophobic domains on the cell surfaces, and this supports our hypothesis **H3**. This observation aligns with an increase in the contact angle of the surfaces of stressed cells³² and a significant increase in the γ_s^{LW}/γ_s^- ratio, which has been previously shown to be related with increasing cell adhesion⁴⁴. It is also consistent with the higher calculated work of adhesion between minerals and stressed cells compared to the unstressed cells. Furthermore, the lack of a significant stress-dependent difference in adhesion towards the hydrophilic quartz particles confirms the importance of hydrophobic interactions in adhesion within a polar aqueous medium during tip-sample detachment. However, the adhesion pressure of kaolinite towards stressed cells is unexpectedly lower than towards unstressed cells, contradicting **H3**. This difference may be attributed to the fact that the contact area between kaolinite and the single cells involves smooth and polar mineral surface structures. The relative reduction of hydrophilic zones on the surfaces of stressed cells may have led to a reduced number of hydrogen bonds, which is not compensated for by hydrophobic interactions with the cell proteins. It is possible that the cell proteins embedded within the outer membrane⁴⁵ are less accessible to the smoother kaolinite sheets compared to the rougher surface of the other minerals, resulting in an overall reduction in adhesion compared to unstressed cells. This phenomenon might also apply to quartz, however, due to the large

contact area and the potential contact with more than one cell, quartz may be less affected by the heterogeneity of the cell structure. The aggregation of single goethite needles on the glue tips likely results in a more complex contact area compared to the kaolinite sheets, despite the smooth structure of individual goethite needles.

Deviations from the measured CMI compared to the XDLVO theory can be best explained by differences in the geometrical orientation and, consequently, the tip shape of the more or less heterogeneous particle surfaces during single CMI and during physicochemical characterization. In the case of **kaolinite**, the best agreement of measured adhesion forces with the XDLVO-based predictions were found for the probe with a nearly flat orientation of the kaolinite basal planes, which are also the most exposed when fixed on a flat surface during the contact angle measurements (Fig. 6a). All probes with higher tilt angles of the kaolinite sheets disagreed with the expected theoretical trend, likely because the exposed edge planes form not only more but also stronger hydrogen bonds^{26,27,46} with hydrophilic molecules on the cell surface, resulting in locally higher adhesion forces than at the basal planes (Fig. 6b,c and Supplementary Fig. S-I 18). Although the elongated shape of kaolinite tips makes them unsuitable for directly comparing single CMI determined with AFM with XDLVO predictions, approximating the tip shape to an ideal sphere will only affect the strength of calculated interaction forces⁴⁷. The direction of the forces, i.e. attractive or repulsive, is not affected by an inappropriate geometrical approximation unless the backside of the particle is involved in long-range interactions with the sample surface⁴⁸, which is irrelevant for our study. Thus, the contradiction between single CMI and XDLVO results (Tips 3 and 4, Table 2) cannot be solely attributed to surface irregularities. Instead, it is a combination of both chemical heterogeneity and morphological irregularities that contributes to this disagreement which partially supports hypothesis **H4** that the chemical heterogeneity of kaolinite causes the lowest agreement between AFM measurements and predictions based on XDLVO theory. In this context, it is the different polar site density, rather than the surface charge across different particle planes^{4,12,47}, that is responsible for the large heterogeneity of CMI.

In contrast to kaolinite, **montmorillonite** possesses porous domains²⁷ and, on a small scale, exhibits more irregularities and a significantly higher R_q than kaolinite. However, the montmorillonite tips show the most confined and repeatable area-height functions among all studied minerals. This, along with a better agreement of single CMI of montmorillonite compared to kaolinite with XDLVO-based predictions, suggests that montmorillonite tips are more homogeneous over the entire contact area. This homogeneity likely results from the rounder shaped tips with an aspect ratio of 1.4 compared to 2.3 for the kaolinite tips. Probably, the contact area with montmorillonite contains repetitive overlapping textures with clearly visible basal/edge stacking units, leading to a homogeneous mixture of edge and basal planes exposed towards the outer surface²⁷. This results in a comparable polar site density of the tips and the layers for the contact angle measurements (Fig. 6d,e,f).

The generally good agreement of the measured adhesion pressure between **goethite** and single bacteria with the XDLVO calculations suggests that for goethite, the samples used for contact angle measurement have surfaces more similar to that of the modified tips than for kaolinite. Goethite tends to form aggregates with random particle orientation, exposing both sides and edges of the needles randomly upward. However, there is one exception among the goethite probes that appear to contact the cell surface uniformly across the elongated particle

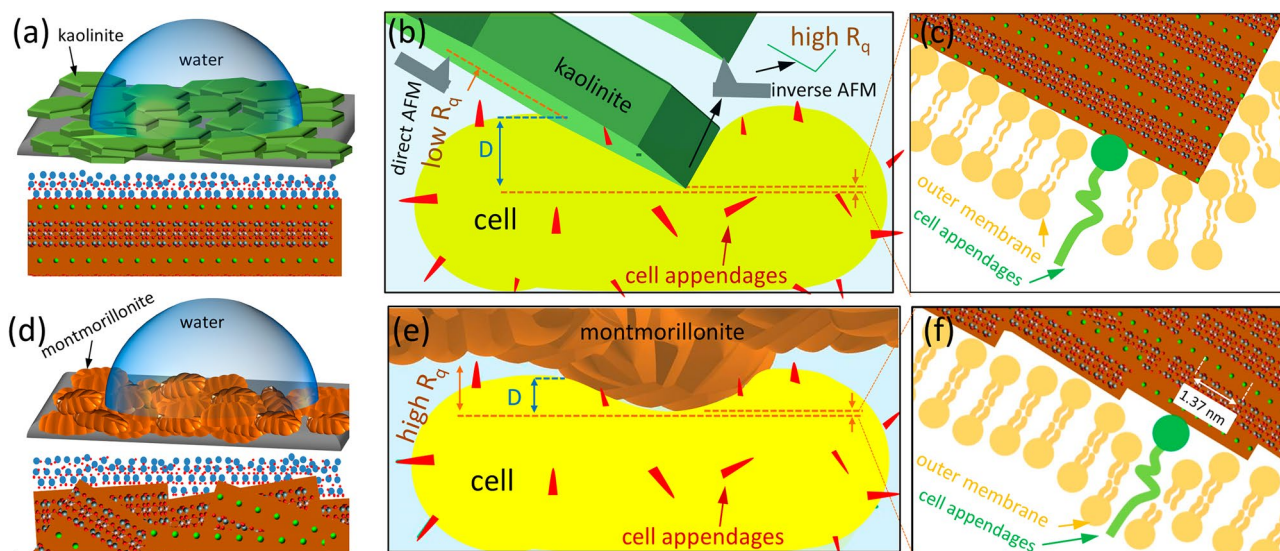


Figure 6. (a) sketch of a water drop on a kaolinite surface (top) demonstrating the preferential flat orientation of the particles on the glue surface with the magnification (bottom) showing the interaction between water molecules and the basal planes, (b) interaction between a flat kaolinite particle and a planar cell surface with the magnification (c) which illustrates how the basal plane with low atomic packing and edge plane with high atomic packing contact the cell surface, (d) same as (a) for montmorillonite, (e) interaction between a porous domain of a montmorillonite particle and a planar cell surface with the magnification (f) showing the basal/edge stacking units that get in contact with the cell surface. The crystal pattern is made by Avogadro free software (version 2.0) and it is general for clay minerals. The overlapping basal/edge stacking units of montmorillonite are pure imagination based on our AFM results and the literature^{10,27}.

side. For this tip, not only is the aspect ratio significantly larger than for the other tips, reducing the accuracy of the fit to the theoretical predictions, but also the chemistry is different from goethite aggregates, resulting in a contradiction between the measured single CMI and the XDLVO calculations (Supplementary Fig. S-1 18).

The increased adhesion of three **quartz** grains towards stressed cells compared to unstressed cells, in agreement with the XDLVO theory, can be explained by the homogeneous chemical structure of this mineral⁴⁹ as well as the sufficient roundness of the tips. However, even though the effect of stress on adhesion is expected to be reproducible among the different quartz tips, two did not follow the theoretical trends. The relatively flat contact region between the two largest quartz particles and cell surfaces may have resulted in multiple contact sites, perhaps even in domains far away from the area of maximum z-extension. This challenges the assumption of single-cell interaction and leads to contradictions with the XDLVO model and an overestimation of the adhesion pressures for quartz. These findings highlight the limitations of our approach for colloidal systems characterized by a significant difference in the size of the interacting materials. However, the underestimation of the contact area does not affect the order of CMI strength among the minerals because quartz exhibited the lowest adhesion and normalization by actual larger contact areas would shift adhesion pressures even lower. Therefore, it is recommended to use a low loading force such as our selected value (5 nN) to achieve single-cell resolution. Otherwise, there is a risk that not only quartz but also the small mineral particles forming clusters at the AFM probe may establish multiple contacts with the cells at higher loads.

Conclusions

By individually considering the 3D contact area for each cell-substrate pair, this study enabled a direct comparison of cell-mineral interactions through adhesion pressure. Our investigation sheds light on the role of Gram-negative bacterial cells and their cell wall debris in influencing the dynamics of mineral surface properties in soil under changing moisture conditions. From the results, we conclude that the increased hydrophobicity of cells due to hypertonic stress enhances their adhesion towards goethite and montmorillonite. This can lead to the formation of more stable bacterial layers on these minerals, consequently reducing the soil's surface free energy. Such changes have implications for soil biology and chemistry, as higher adhesion can result in more stable and less easily degradable hydrophobic bacterial layers and thus increase the persistence of soil water repellency. Increased soil water repellency, known to inhibit plant growth and increase bacterial stress, can feed back into the hydrophobizing effect of bacteria. The strong adhesion of bacterial cells to iron oxides underscores the potential role of these minerals in preserving organic matter against degradation and, therefore, long-term soil water repellency. Conversely, a reduced adhesion of stressed cells towards kaolinite may indicate that kaolinite-rich soils are less likely to exhibit long-term water repellency due to bacterial adhesion. However, these results should also be tested with other bacterial strains. The comparison between measured single CMI and XDLVO calculations, based on an idealized sphere-plane geometry, indicates that the interaction between soil matrix and cells is significantly determined by both the type and shape of minerals present. Contradictions in trends between measured and calculated interactions have helped interpret chemical heterogeneity due to differently exposed edges and planes of minerals.

Methods

Minerals used for cell–mineral interactions

We employed typical soil minerals, including montmorillonite (Sigma-Aldrich: montmorillonite K 10, no. 69866), kaolinite (Sigma-Aldrich: kaolinite natural, no. 03584), goethite (Bayferrox 920 Z, Lanxess) and quartz (Merck Millipore: quartz fine granular, washed and calcined, no. 1075361000) to investigate cell-mineral interactions. The reported mineral particle sizes for montmorillonite, kaolinite, and goethite were 412 nm⁵⁰, 447 nm⁵⁰, and 580 nm⁵¹, respectively. Quartz had a particle size of 0.2–0.8 mm according to the technical data sheet.

Preparation of bacterial cell suspensions

Pseudomonas fluorescens DSM 55,090, obtained from the Leibniz Institute DSMZ—German Collection of Microorganisms and Cell Cultures was cultured in 50 ml sterile mineral salt medium containing 7 g Na₂HPO₄, 2.8 g KH₂PO₄, 0.5 g NaCl, 1 g NH₄Cl, 0.1 g MgSO₄ · 7 H₂O, 0.01 g FeSO₄ · 7 H₂O, 5 mg MnSO₄ · H₂O, 6.4 mg ZnCl₂, 1 mg CaCl₂ · 6 H₂O, 0.6 mg BaCl₂, 0.36 mg CuSO₄ · 7 H₂O, 0.36 mg CuSO₄ · 5 H₂O, 6.5 mg H₃BO₃, 0.01 g EDTA and 146 µl HCl (37%) per liter of distilled water⁵². Additionally, 4 g L⁻¹ sodium succinate and 1 g L⁻¹ yeast extract were added as carbon sources. Bacterial cells were subjected to osmotic stress by adding 0.5 M NaCl, reducing the water potential of the growth media to – 2.5 MPa. Cell growth was monitored by measuring optical density at 560 nm using a UV/VIS spectrophotometer (Lambda2S, PerkinElmer, Waltham, USA). Cells were harvested during the late exponential growth phase by centrifugation at 11,000g for 15 min (Hermle Z383K). They were then resuspended in 2 ml KNO₃ (10 mM, pH 7.0) and transferred to 2 ml reaction tubes. Each sample was washed twice with 2 ml KNO₃ followed by 1 min centrifugation at 10,000g. The washed biomass was resuspended in 1 ml KNO₃ and stored at 5 °C until further use.

Characterization of minerals by AFM

To ensure that the shapes of the mineral particles used as tip modifications were representative, we scanned all minerals in 10 mM KNO₃ with an AFM system (AFM, Dimension Icon, Bruker Corporation, USA). We used sharp SNL tips ($k = 0.12 \text{ N m}^{-1}$, SNL-10, Bruker, USA) on flat multi-loaded systems⁵³ considering 60–150 particles in a total of 55 regions of interest (ROIs). We present an individual image for each mineral to enhance visualization. The root mean roughness ($R_q = \sqrt{\sum (Z_i)^2 / N}$, where Z_i is the current Z value, and N is the number of points) was calculated using the roughness function of the NanoScope Analysis software (version 2.0, Bruker) in the Height Sensor channel. For goethite, we estimated the roughness of individual needles or small clusters

with clear flat particle orientation by applying a threshold to exclude background data (Supplementary Fig. S-I 1). For the other minerals, we considered only the central areas of the particles for R_q estimation to avoid the dilation effect (Supplementary Fig. S-I 6).

Preparation of cell samples on relocation systems with built-in characterizers

We fixed minerals to the AFM probes and bacterial cells to a flat sample holder and not the other way around⁴. This approach allowed for single cell resolution and eliminated the challenges of attaching single bacterial cells to AFM cantilevers, reducing the risk of potential damage during probe calibration¹⁸.

Preparation of the sample holders in the form of relocation systems followed a modified protocol of *Abu Quba et al.*²³. First, cover glasses (hydrolytic class 1, $50 \times 24 \times 0.13$ – 0.16 mm, VWR, Germany) were cleaned first with acetone (ROTISOLV® Pestilyse® plus $\geq 99.9\%$, R T, Germany) and immediately before drying with $\sim 70\%$ ethanol (ROTIPURAN® $\geq 99.8\%$, p.a, R T, Germany) for 30 min in a conventional ultrasonic bath. Each cover glass with a small piece of resin (Tempfix, PLANO GmbH, Wetzlar, Germany) was heated up to 130°C for 30 s to melt the resin and create a flat surface. Then, a piece of freshly cleaved mica was fixed at the resin spot at 80°C and an extracted and blind tip reconstructed SNL tip was fixed at the resin near the mica sheet at 38°C . On the back side of the glass slide, a finder grid was fixed with transparent adhesive tape near the glue spot (Supplementary Fig. S-I 20). The shape, size and stiffness of stressed and unstressed *P. fluorescens* cells were found to be comparable when fixed at chemically inactive glue³² or poly-L-lysine⁹ surfaces. Therefore, poly-L-lysine (P8920, 166 Sigma-Aldrich, Germany) was used to improve cell fixation in this work. A drop of the latter was pipetted onto the front side exactly over the grid and air dried. The cells were attached by pipetting 1 – $2\ \mu\text{L}$ of cell suspensions onto the poly-L-lysine spot, air dried for 1 min and rinsed before being covered with a drop of $10\ \text{mM}$ KNO_3 solution in which the AFM measurement was performed. To maintain a constant concentration of $10\ \text{mM}$ KNO_3 during the scanning, we pumped water to the liquid meniscus at a rate equal to the evaporation rate using a custom-built pump which was used in our previous work⁹. The mica surface allowed direct calibration of the deflection sensitivity of the probe in liquid without changing the samples, while the blind tip reconstructed SNL tip served for quality control of the functionalized tips before and after the cell-mineral interactions by repeated inverse imaging²³.

Functionalization of tipless cantilevers with minerals

To functionalize the tips, we started by attaching a small amount of Tempfix resin to the end of an SNL probe ($k=0.12\ \text{N m}^{-1}$, SNL-10, Bruker, USA) following the detailed procedure outlined by *Abu Quba et al.*²³. Using the AFM XYZ navigation system, we gradually reduced the size of the resin at the tip of the SNL probe by making repeated contacts with a chip (visible as glue spots on the chip in Supplementary Fig. S-I 21) securely fixed to the AFM stage. This chip was heated to $\sim 100^\circ\text{C}$ allowing us to transfer tiny resin spots from the SNL tip to a set of tipless probes ($k=0.1\ \text{N m}^{-1}$, MLCT-O10, Bruker, USA), also fixed to the heated AFM stage. For the attachment of smaller particles, such as montmorillonite, kaolinite, or goethite to the resin coated tipless cantilevers, we sprinkled these particles over the resin spot and then subjected them to a 30 min heating at 38°C in an oven to enhance the adhesion between the minerals and the resin. Afterwards, the modified probe underwent a thorough rinse with Milli-Q water to remove any loosely bound particles followed by air drying.

In the case of quartz particles, epoxy glue (Pattex Kraft Mix, Henkel AG, Germany) was employed instead of resin. Here, a tipless probe was guided by the AFM navigation system, first into a glue spot at room temperature and then onto a quartz particle. It was allowed to sit for 3 min to ensure secure fixation. Subsequently, the modified probe underwent the same cleaning as described above.

To ensure the integrity of our probes, we conducted checks, both before and after cell-mineral interaction measurements. We utilized AFM inverse imaging and environmental scanning electron microscopy (FEI Quanta 250 ESEM, FEI Company, Hillsboro, United States). Only the results obtained from mineral tips that showed no changes in the modifying minerals after cell-mineral interaction measurements were considered for our analysis.

Direct cell–mineral interactions

Before commencing the cell-mineral interaction experiments, we determined the spring constant through a thermal tune, and calibrated the deflection sensitivity of each modified probe using force distance curves on integrated mica sheets. We conducted direct cell-mineral interactions using the “Point and Shoot” function in peak force quantitative nanomechanical mapping (PFQNM) mode employing conditions of $10\ \text{mM}$ KNO_3 , a $1.03\ \text{Hz}$ ramp rate (with forward and reverse velocity of $6\ \mu\text{m s}^{-1}$), a $5\ \text{nN}$ force set point, $3\ \mu\text{m}$ ramp size and contact times of 1 and 0 s after reaching the force set point (illustrated in Supplementary Fig. S-I 12). In relocation systems involving stressed and unstressed cells, we selected 5 to 8 ROIs. Within all ROIs we acquired ~ 150 force-distance (FD) curves on the highest points of the cells. To better capture the response of the cell communities, we distributed the FD curves across as many cells as possible in the scanned images, rather than conducting numerous replicates on the same cell. In instances where rupture events occurred, we measured the magnitude and distance of the last event when the tip fully separated from the surface using the markers function of NanoScope software. To assess the effect of enlarging the contact area on adhesion forces, we recorded 10 pull-off curves with one selected probe for each mineral. These curves were measured against both unstressed and stressed cells, as well as against double-sided adhesive tape (Tesa, Hamburg, Germany) with incremental loading forces ranging from 2 to $30\ \text{nN}$ (as shown in Supplementary Fig. S-I 13). The contact area and the number of contact points between tip and sample depend on the shape of the modified probe and the applied loading force. While flat⁴ or semi flat¹⁶ surfaces (e.g., those with a round shape and a large radius) can establish multiple contact points with the sample even with low loading forces like $1\ \text{nN}$ ⁴ or $10\ \text{nN}$ ¹⁶, our specific design involved the introduction of

a glue drop at the end of the cantilever, allowing the minerals attached to the glue to provide sharp features. In most cases, a loading force of 5 nN proved sufficient to achieve single cell resolution.

Quality control of direct cell–mineral adhesion

To avoid artifacts, we rigorously validated the stability of selected bacteria and minerals during cell–mineral interaction. This involved several steps: (1) We examined all mineral-modified tips using ESEM and some were further analyzed using correlative ESEM/AFM method prior to cell–mineral interaction. (2) After cell–mineral interactions, we checked all mineral modified tips with AFM at the built-in characterizer to obtain the tip–area–function. (3) We also inspected all cells with AFM using a sharp tip or the respective mineral tip (if sufficiently sharp), both before and after cell–mineral interaction. For more details please refer to Abu Quba et al.²³.

The FD curves were recorded with 1-s contact time followed by another curve with 0-s contact time. A decrease in adhesion forces with decreasing contact time served as a direct evidence that no irreversible modifications of the cell ultrastructure had occurred, as described in previous studies^{16,39}.

Evaluation of the FD curves

We determined the adhesion force using R (R Core Team, 2020)^(9,54). The FD curve data were exported from the NanoScope software as csv files, and the adhesion force was determined as the minimum force of the baseline corrected retraction curve. Each adhesion force was normalized by the 3D area of the respective tip that interacted with the cell surface at the specific deformation depth, yielding the adhesion pressure¹⁶ P_{ad} (Supplementary Fig. S-I 4). We also generated 2D sections of the mineral tips at two deformation levels (20 nm and 50 nm) to compare the ratio of the shortest and longest elongation, which helped to describe the shape deviation from the spherical shapes in our XDLVO calculations. We investigated the impact of loading force on adhesion force by calculating the adhesion efficiency η (%) defined as the ratio of the measured adhesion force to the applied loading force¹⁶.

To identify attractive interactions between the mineral modified-tips and the cell surfaces, we screened the FD curves for jump-to-contact events using the NanoScope Analysis software. In contrast, repulsive forces were identified as a gradual increase in the force curve as the distance to the surface decreased, before reaching the “linear” contact regime.

Zeta potential measurement and estimation of surface potential

Zeta potential measurements on bacteria and minerals were conducted to estimate their surface potential as a basis for calculating electrostatic interaction free energy. Zeta potential was calculated using Smoluchowski's equation⁵⁵ based on electrophoretic mobility which was measured through phase analysis light scattering (Zeta-PALS, Brookhaven Instruments Corp., Holtsville, USA). Bacterial cells were suspended in a 10 mM KNO_3 solution, adjusted to pH 6 using 1 M HNO_3 , in a concentration of $\sim 10^9$ cells L^{-1} . Mineral particles were suspended in a 10 mM KNO_3 solution adjusted to pH 6 at concentrations ranging from 23 to 40 mg L^{-1} (equivalent to $\sim 0.001\%$ by volume). Before measurement, the quartz particles were ground to an appropriate size for zeta potential measurements using an agate mortar, resulting in a mean particle size of ~ 1350 nm based on dynamic light scattering (ZetaPALS). The mean zeta potential was determined from 10 consecutive runs, each comprising 10 cycles.

Surface potential (ψ) was estimated from the zeta potential (ζ) using Eq. (1)⁵⁶:

$$\psi = \zeta \left(1 + \frac{z}{R} \right) \exp(\kappa z) \quad (1)$$

where z is the distance from the surface to the slipping plane, assumed as 0.5 nm⁵⁶, R represents the respective radius of the cells or the mineral particles, and κ is the inverse of the double layer thickness (m^{-1}). The value of κ was calculated using Eq. (2)⁵⁷:

$$\kappa^{-1} = \sqrt{\frac{\epsilon_r \epsilon_0 k_B T}{2N_A e^2 I}} \quad (2)$$

where ϵ_r is the relative dielectric permittivity of water (80.1 at 20 °C), ϵ_0 is the vacuum permittivity [8.854×10^{-12} C/(Vm)], k_B is the Boltzmann constant (1.38×10^{-23} J K^{-1}), T is the absolute temperature (K), N_A is the Avogadro number (6.02×10^{23} mol⁻¹), e is the charge of the electron (1.6×10^{-19} C), and I is the ionic strength of the KNO_3 solution (10 mol m^{-3}).

Contact angle measurement and calculation of surface free energy

Contact angles of bacteria and minerals were determined with a contact angle microscope equipped with a video camera (OCA 15, DataPhysics, Filderstadt, Germany). Bacterial cell samples were prepared by filtering cell suspension through cellulose acetate filters (pore size 0.45 μm , NC 45; Whatman) and fixing the air-dried filters on microscopy glass slides. Mineral samples were prepared by gently pressing air-dried mineral particles onto double-sided adhesive tape covering a microscopy glass. Non-adherent particles were removed by tapping the slide until no further material loss was observed. A drop of deionized water (1 μl) was placed on the sample surface immediately after preparation, and the initial water contact angle was measured at both intersections of the drop contour line with the sample surface using automated drop shape analysis with software SCA20 (DataPhysics, Filderstadt, Germany). Mean contact angles were calculated from ten independent measurements. Further details on the method and sample preparation can be found in Bachmann et al.⁵⁸ and Goebel et al.⁵⁹.

Additional contact angle measurements were performed using ethylene glycol and α -bromonaphthalene as testing liquids to calculate the surface free energy components of bacteria and minerals, forming the basis for

determining cell–mineral interaction energy. Solid and liquid interfacial properties were linked through the solid–liquid contact angle (θ) as expressed by Eq. (3)⁶⁰:

$$(1 + \cos\theta)\gamma_l = 2\left(\sqrt{\gamma_s^{LW}\gamma_1^{LW}} + \sqrt{\gamma_s^+\gamma_1^-} + \sqrt{\gamma_s^-\gamma_1^+}\right) \quad (3)$$

where γ_l is the liquid surface free energy (J m^{-2}), and γ_s is the solid surface free energy (J m^{-2}). Superscripts ‘LW’, ‘-’, and ‘+’ represent the non-polar Lifshitz–van der Waals component, the electron-donor (base) component, and the electron-acceptor (acid) component, respectively. The three unknown variables in Eq. (3), γ_s^{LW} , γ_s^- , γ_s^+ , were determined by solving a system of three independent linear equations, using the mean contact angles obtained with deionized water, ethylene glycol, and α -bromonaphthalene along with the respective surface free energy components of the liquids⁶⁰.

Calculation of the cell–mineral interaction energy profiles

Energy profiles of the interaction between bacterial cells and AFM tips functionalized with mineral particles were determined by calculating the total interaction free energy, $\Delta G_{132}^{\text{TOT}}$, between the mineral (1), and the bacterial cell (2) in aqueous solution (3). This calculation considered electrostatic, $\Delta G_{132}^{\text{EL}}$, Lifshitz–van der Waals, $\Delta G_{132}^{\text{LW}}$, and Lewis acid–base, $\Delta G_{132}^{\text{AB}}$, interaction free energies as a function of separation distance, as described by Eq. (4).

$$\Delta G(h)_{132}^{\text{TOT}} = \Delta G(h)_{132}^{\text{EL}} + \Delta G(h)_{132}^{\text{LW}} + \Delta G(h)_{132}^{\text{AB}} \quad (4)$$

Mineral functionalized tips used for measuring adhesion forces on bacterial cells were small compared to the cells. Therefore, we approximated the cell surface as planar geometry, and the mineral functionalized tip as a sphere with a diameter estimated from the contact radius individually determined for each tip. Energy profiles were determined for each combination of minerals and cells by explicitly considering the specific contact radius of each functionalized tip.

The electrostatic interaction free energy, $\Delta G_{132}^{\text{EL}}$ (J), was calculated using Eq. (5)⁶¹:

$$\Delta G(h)_{132}^{\text{EL}} = \pi R_m \epsilon_r \epsilon_0 (\psi_1^2 + \psi_2^2) \left\{ \frac{2\psi_1\psi_2}{\psi_1^2 + \psi_2^2} \ln \left[\frac{1 + \exp(-\kappa h)}{1 - \exp(-\kappa h)} \right] + \ln[1 - \exp(-2\kappa h)] \right\} \quad (5)$$

where R_m is the contact radius of the mineral tip (m), h is the separation distance between the mineral tip and the cell (m), and ψ_1 and ψ_2 are the surface potentials of the minerals and cells (V), respectively. R_m was determined for each functionalized tip based on the average deformation of the bacterial cell surface.

The Lifshitz–van der Waals interaction free energy component, $\Delta G_{132}^{\text{LW}}$ (J), was calculated by Eq. (6)⁶²:

$$\Delta G(h)_{132}^{\text{LW}} = -4\pi R_m \frac{h_0^2}{h} \left(\sqrt{\gamma_3^{LW}} - \sqrt{\gamma_2^{LW}} \right) \left(\sqrt{\gamma_3^{LW}} - \sqrt{\gamma_1^{LW}} \right) \quad (6)$$

where h_0 is the minimum equilibrium distance of 0.157 nm where physical contact occurs.

The Lewis acid–base interaction free energy component $\Delta G_{132}^{\text{AB}}$ (J) was calculated by Eq. (7)⁶²:

$$\Delta G(h)_{132}^{\text{AB}} = 4\pi R_c \lambda \exp\left(\frac{h_0 - h}{\lambda}\right) \left[\sqrt{\gamma_3^+} \left(\sqrt{\gamma_1^-} + \sqrt{\gamma_2^-} - \sqrt{\gamma_3^-} \right) + \sqrt{\gamma_3^-} \left(\sqrt{\gamma_1^+} + \sqrt{\gamma_2^+} - \sqrt{\gamma_3^+} \right) - \sqrt{\gamma_1^+ \gamma_2^-} - \sqrt{\gamma_1^- \gamma_2^+} \right] \quad (7)$$

where λ is the decay length of water (0.6 nm⁶²).

The work of adhesion (W_{ad}) between minerals and bacterial cells was calculated using Eq. (8)^{62,63}:

$$W_{\text{ad}} = -\Delta G_{132} = -2 \left[\begin{aligned} &\sqrt{\gamma_1^{LW}\gamma_3^{LW}} + \sqrt{\gamma_2^{LW}\gamma_3^{LW}} - \sqrt{\gamma_1^{LW}\gamma_2^{LW}} - \gamma_3^{LW} \\ &+ \sqrt{\gamma_3^+} \left(\sqrt{\gamma_1^-} + \sqrt{\gamma_2^-} - \sqrt{\gamma_3^-} \right) + \gamma_3^- \left(\sqrt{\gamma_1^+} + \sqrt{\gamma_2^+} - \sqrt{\gamma_3^+} \right) \\ &- \sqrt{\gamma_1^+ \gamma_2^-} - \sqrt{\gamma_1^- \gamma_2^+} \end{aligned} \right] \quad (8)$$

X-ray photoelectron spectroscopy

The surface elemental composition of mineral particles was analyzed using X-ray photoelectron spectroscopy (XPS) with an Axis Ultra DLD instrument (Kratos Analytical, Manchester, UK) equipped with monochromatic AlK α radiation (1486.6 eV; emission current: 20 mA, voltage: 6 kV). Samples were prepared by affixing air-dried minerals onto a bar (sample area: 50 mm²) using indium foil (Plano GmbH, Wetzlar, Germany). Survey spectra were obtained in the binding energy range of 1200–0 eV (with a 1 eV resolution) under a pressure of 4×10^7 Pa. The measurements utilized a pass energy of 160 eV, a dwell time of 500 ms, and comprised three sweeps per measurement cycle at a take-off angle of 0°. For each sample, three spectra were recorded at different locations (spot size: 300 \times 700 μm). After charge correction for the Si 2p peak of quartz (103 eV), the spectra were analyzed using Vision 2 software (Kratos Analytical, Manchester, UK). Surface elemental composition was quantified in

terms of atom percentage (at.-%) using the relative sensitivity factors incorporated in the software. For additional details regarding the fitting procedure, please refer to Woche et al.⁵⁸.

Statistics

Using R⁶⁴, we assessed the adhesion pressure for each mineral and stress level (N = 149–156) for normality through the Shapiro–Wilk-Test (shapiro.test) and checked for variance homogeneity using the Levene-Test (leveneTest). As the results did not indicate homogeneity, we conducted Wilcoxon-Rank-Sum tests (wilcox.test) to identify significant differences in adhesion pressure between stressed and unstressed bacterial cells when interacting with the four different minerals. To detect significant differences in adhesion pressure among different minerals when interacting with cells of the same stress level, we employed pairwise Wilcoxon-Rank-Sum tests (pairwise.wilcox.test). Specific results are presented in chapter S-I.15 and in Fig. 4.

Data availability

The datasets generated and/or analyzed during the current study are available in the OSF repository [<https://osf.io/6guwd>].

Received: 19 January 2023; Accepted: 5 October 2023

Published online: 10 October 2023

References

- Potthoff, E., Ossola, D., Zambelli, T. & Vorholt, J. A. Bacterial adhesion force quantification by fluidic force microscopy. *Nanoscale* **7**, 4070–4079 (2015).
- Chen, Y., Busscher, H. J., van der Mei, H. C. & Norde, W. Statistical analysis of long- and short-range forces involved in bacterial adhesion to substratum surfaces as measured using atomic force microscopy. *Appl. Environ. Microbiol.* **77**, 5065–5070 (2011).
- Marlière, C. & Dhahri, S. An in vivo study of electrical charge distribution on the bacterial cell wall by atomic force microscopy in vibrating force mode. *Nanoscale* **7**, 8843–8857 (2015).
- Huang, Q., Wu, H., Cai, P., Fein, J. B. & Chen, W. Atomic force microscopy measurements of bacterial adhesion and biofilm formation onto clay-sized particles. *Sci. Rep.* **5**, 16857 (2015).
- Achtenhagen, J., Goebel, M.-O., Miltner, A., Woche, S. K. & Kästner, M. Bacterial impact on the wetting properties of soil minerals. *Biogeochemistry* **122**, 269–280 (2015).
- Cao, T. et al. Nanoscale investigation on adhesion of *E. coli* to surface modified silicone using atomic force microscopy. *Biotechnol. Bioeng.* **94**, 167–176 (2006).
- Elbourne, A. et al. Bacterial-nanostructure interactions: The role of cell elasticity and adhesion forces. *J. Colloid Interface Sci.* **546**, 192–210 (2019).
- Maracchi, G., Sirotenko, O. & Bindi, M. Impacts of present and future climate variability on agriculture and forestry in the temperate regions: Europe. *Clim. Change* **70**, 117–135 (2005).
- Abu Quba, A. A. et al. Changes in cell surface properties of *Pseudomonas fluorescens* by adaptation to NaCl induced hypertonic stress. *FEMS Microbes* <https://doi.org/10.1093/femsmc/xtac028> (2022).
- Feng, B. et al. AFM measurements of Hofmeister effects on clay mineral particle interaction forces. *Appl. Clay Sci.* **186**, 105443 (2020).
- Van der Vold, M. J. Waals' attraction between anisometric particles. *J. Colloid Sci.* **9**, 451–459 (1954).
- Long, J., Xu, Z. & Masliyah, J. H. Role of illite–illite interactions in oil sands processing. *Colloids Surf. A Physicochem. Eng. Asp.* **281**, 202–214 (2006).
- Liu, J., Xu, Z. & Masliyah, J. Role of fine clays in bitumen extraction from oil sands. *AIChE J.* **50**, 1917–1927 (2004).
- Bhattacharjee, S., Ko, C. H. & Elimelech, M. DLVO interaction between rough surfaces. *Langmuir* **14**, 3365–3375 (1998).
- Shen, C., Jin, Y., Zhuang, J., Li, T. & King, B. Role and importance of surface heterogeneities in transport of particles in saturated porous media. *Crit. Rev. Environ. Sci. Technol.* **50**, 244–329 (2020).
- Lau, P. C. Y., Dutcher, J. R., Beveridge, T. J. & Lam, J. S. Absolute quantitation of bacterial biofilm adhesion and viscoelasticity by microbead force spectroscopy. *Biophys. J.* **96**, 2935–2948 (2009).
- Jaschke, M. et al. The atomic force microscope as a tool to study and manipulate local surface properties. *Biosens. Bioelectron.* **11**, 601–612 (1996).
- Lower, S. K., Tadanier, C. J. & Hochella, M. F. Measuring interfacial and adhesion forces between bacteria and mineral surfaces with biological force microscopy. *Geochim. Cosmochim. Acta* **64**, 3133–3139 (2000).
- Zhang, W., Stack, A. G. & Chen, Y. Interaction force measurement between *E. coli* cells and nanoparticles immobilized surfaces by using AFM. *Colloids Surf. B Biointerfaces* **82**, 316–324 (2011).
- Chen, Y., Harapanahalli, A. K., Busscher, H. J., Norde, W. & van der Mei, H. C. Nanoscale cell wall deformation impacts long-range bacterial adhesion forces on surfaces. *Appl. Environ. Microbiol.* **80**, 637–643 (2014).
- Spengler, C., Thewes, N., Jung, P., Bischoff, M. & Jacobs, K. Determination of the nano-scaled contact area of staphylococcal cells. *Nanoscale* **9**, 10084–10093 (2017).
- Carniello, V., Peterson, B. W., van der Mei, H. C. & Busscher, H. J. Physico-chemistry from initial bacterial adhesion to surface-programmed biofilm growth. *Adv. Colloid Interface Sci.* **261**, 1–14 (2018).
- Abu Quba, A. A., Schaumann, G. E., Karagulyan, M. & Diehl, D. Quality control of direct cell–mineral adhesion measurements in air and liquid using inverse AFM imaging. *RSC Adv.* <https://doi.org/10.1039/d1ra00110h> (2021).
- Ugwu, I. M. & Sherman, D. M. Irreversibility of sorption of cobalt to goethite (α -FeOOH) and disparities in dissolution of aged synthetic co-goethite. *Chem. Geol.* **467**, 168–176 (2017).
- Song, X. *Surface and Bulk Reactivity of Iron Oxyhydroxides: A Molecular Perspective* (Umeå University, 2013).
- Lázaro, B. Halloysite and kaolinite: Two clay minerals with geological and technological importance. *Rev. Real. Acad. Ciencias Zaragoza* **70**, 7–38 (2015).
- Shattar, S. F. A., Zakaria, N. A. & Foo, K. Y. Feasibility of montmorillonite-assisted adsorption process for the effective treatment of organo-pesticides. *Desalin. Water Treat.* **57**, 13645–13677 (2016).
- Zhuravlev, L. T. The surface chemistry of amorphous silica. Zhuravlev model. *Colloids Surf. A Physicochem. Eng. Asp.* **173**, 1–38 (2000).
- Suresh, L. & Walz, J. Y. Effect of surface roughness on the interaction energy between a colloidal sphere and a flat plate. *J. Colloid Interface Sci.* **183**, 199–213 (1996).
- van Oss, C. J. & Giese, R. F. The hydrophilicity and hydrophobicity of clay minerals. *Clays Clay Miner.* **43**, 474–477 (1995).
- Barr, T. L. & Seal, S. Nature of the use of adventitious carbon as a binding energy standard. *J. Vacuum Sci. Technol. A* **13**, 1239–1246 (1995).

32. Karagulyan, M. *et al.* Water stress-driven changes in bacterial cell surface properties. *Appl. Environ. Microbiol.* **88**, e00732–e822 (2022).
33. Jiang, D., Huang, Q., Cai, P., Rong, X. & Chen, W. Adsorption of *Pseudomonas putida* on clay minerals and iron oxide. *Colloids Surf. B Biointerfaces* **54**, 217–221 (2007).
34. Rong, X., Chen, W., Huang, Q., Cai, P. & Liang, W. *Pseudomonas putida* adhesion to goethite: Studied by equilibrium adsorption, SEM, FTIR and ITC. *Colloids Surf. B Biointerfaces* **80**, 79–85 (2010).
35. Xu, L.-C. & Logan, B. E. Adhesion forces between functionalized latex microspheres and protein-coated surfaces evaluated using colloid probe atomic force microscopy. *Colloids Surf. B Biointerfaces* **48**, 84–94 (2006).
36. Dufrière, Y. F. Using nanotechniques to explore microbial surfaces. *Nat. Rev. Microbiol.* **2**, 451–460 (2004).
37. Dufrière, Y. F. Application of atomic force microscopy to microbial surfaces: From reconstituted cell surface layers to living cells. *Micron* **32**, 153–165 (2001).
38. Mei, L., Ren, Y., Busscher, H. J., Chen, Y. & van der Mei, H. C. Poisson analysis of streptococcal bond-strengthening on saliva-coated enamel. *J. Dent. Res.* **88**, 841–845 (2009).
39. van der Mei, H. C., Rustema-Abbing, M., de Vries, J. & Busscher, H. J. Bond strengthening in oral bacterial adhesion to salivary conditioning films. *Appl. Environ. Microbiol.* <https://doi.org/10.1128/AEM.01119-08> (2008).
40. Lai, T., Chen, Y., Sun, J. & Guo, M. Material-related contact time dependence of adhesion force revealed by an AFM cantilever in a humid environment. *Appl. Surf. Sci.* **550**, 149357 (2021).
41. Abu-Lail, N. I. & Camesano, T. A. Role of ionic strength on the relationship of biopolymer conformation, DLVO contributions, and steric interactions to bioadhesion of *Pseudomonas putida* KT2442. *Biomacromolecules* **4**, 1000–1012 (2003).
42. Woche, S. K. *et al.* Soil wettability can be explained by the chemical composition of particle interfaces: An XPS study. *Sci. Rep.* **7**, 42877 (2017).
43. Baltrusaitis, J., Cwiertny, D. M. & Grassian, V. M. Adsorption of sulfur dioxide on hematite and goethite particle surfaces. *Phys. Chem. Chem. Phys.* **9**, 5542–5554 (2007).
44. Liu, C. & Zhao, Q. The CQ ratio of surface energy components influences adhesion and removal of fouling bacteria. *Biofouling* **27**, 275–285 (2011).
45. Sun, J., Rutherford, S. T., Silhavy, T. J. & Huang, K. C. Physical properties of the bacterial outer membrane. *Nat. Rev. Microbiol.* **20**, 236–248 (2022).
46. Nascimento, G. M. do. *Clays, Clay Minerals and Ceramic Materials Based on Clay Minerals*. (2016). <https://doi.org/10.5772/60492>.
47. Long, J., Xu, Z. & Masliyah, J. H. On the role of temperature in oil sands processing. *Energy Fuels* **19**, 1440–1446 (2005).
48. Bhattacharjee, S. & Elimelech, M. Surface element integration: A novel technique for evaluation of DLVO interaction between a particle and a flat plate. *J. Colloid Interface Sci.* **193**, 273–285 (1997).
49. Konopinski, D. I., Hudziak, S., Morgan, R. M., Bull, P. A. & Kenyon, A. J. Investigation of quartz grain surface textures by atomic force microscopy for forensic analysis. *Forensic Sci. Int.* **223**, 245–255 (2012).
50. Pinti, V., Marcolli, C., Zobrist, B., Hoyle, C. R. & Peter, T. Ice nucleation efficiency of clay minerals in the immersion mode. *Atmos. Chem. Phys.* **12**, 5859–5878 (2012).
51. Carstens, J. F., Bachmann, J. & Neuweiler, I. Effects of flow interruption on transport and retention of iron oxide colloids in quartz sand. *Colloids Surf. A Physicochem. Eng. Asp.* **520**, 532–543 (2017).
52. Hartmans, S., Smits, J. P., van der Werf, M. J., Volkering, F. & de Bont, J. A. Metabolism of styrene oxide and 2-phenylethanol in the styrene-degrading xanthobacter strain 124X. *Appl. Environ. Microbiol.* **55**, 2850–2855 (1989).
53. Abu Quba, A. A., Schaumann, G. E., Karagulyan, M. & Diehl, D. A new approach for repeated tip-sample relocation for AFM imaging of nano and micro sized particles and cells in liquid environment. *Ultramicroscopy* **211**, 112945 (2020).
54. Benítez, R., Bolós, V. J. & Toca-Herrera, J. *afmToolkit*: An R package for automated AFM force–distance curves analysis. *R. J.* <https://doi.org/10.32614/RJ-2017-045> (2017).
55. Elimelech, M., Gregory, J., Jia, X. & Williams, R. Particle deposition and aggregation, measurement, modeling and simulation. *Colloids Surf. A Physicochem. Eng. Asp.* **1**, 93–94 (1997).
56. van Oss, C. J., Giese, R. F. & Costanzo, P. M. DLVO and non-DLVO interactions in hectorite. *Clays Clay Miner.* **38**, 151–159 (1990).
57. Shani, C., Weisbrod, N. & Yakirevich, A. Colloid transport through saturated sand columns: Influence of physical and chemical surface properties on deposition. *Colloids Surf. A Physicochem. Eng. Asp.* **316**, 142–150 (2008).
58. Bachmann, J., Woche, S. K., Goebel, M.-O., Kirkham, M. B., & Horton, R. Extended methodology for determining wetting properties of porous media. *Water Resour. Res.* **39**(12), 1353 (2003).
59. Goebel, M. O., Woche, S. K., Abraham, P. M., Schaumann, G. E. & Bachmann, J. Water repellency enhances the deposition of negatively charged hydrophilic colloids in a water-saturated sand matrix. *Colloid Surf. A Physicochem. Eng. Asp.* **431**, 150–160 (2013).
60. Van Oss, C. J., Chaudhury, M. K. & Good, R. J. Interfacial Lifshitz–van der Waals and polar interactions in macroscopic systems. *Chem. Rev.* **88**, 927–941 (1988).
61. Norde, W. & Lyklema, J. Protein adsorption and bacterial adhesion to solid surfaces: A colloid-chemical approach. *Colloids Surf.* **38**, 1–13 (1989).
62. van Oss, C. J. *Interfacial Forces in Aqueous Media* (CRC Taylor & Francis, 2006).
63. Traini, D., Rogueda, P., Young, P. & Price, R. Surface energy and interparticle force correlation in model pMDI formulations. *Pharm. Res.* **22**, 816–825 (2005).
64. R Core Team. R: A language and environment for statistical computing. R Foundation for Statistical Computing, Vienna, Austria. Available online at <https://www.R-project.org/> (2021).

Acknowledgements

We thank the German Research Foundation (DFG) for funding this work as part of the project “Impact of bacterial biomass on the surface wettability of soil particles under varying moisture conditions” (DI 1907/2-1, GO 2329/2-1, MI 598/4-1). We also want to thank Susanne K. Woche (Leibniz Universität Hannover) for the contact angle and XPS measurements.

Author contributions

D.D., G.S., M.O.G., J.B., A.M., and M.Käs had the project idea and acquired the funding. A.A. developed the method for estimating the contact area. A.A., D.D., and G.S. performed the AFM experiments, analyzed the data, performed the statistical analyses and wrote the paper. M.O.G. and J.B. contributed with XPS, zeta potential and contact angle measurements, calculated the energy profiles based on the XDLVO theory and the work of adhesion. M.Kar, A.M. and M.Käs prepared the stressed and unstressed bacterial cell suspensions. All co-authors contributed to an internal review of the manuscript.

Funding

Open Access funding enabled and organized by Projekt DEAL.

Competing interests

The authors declare no competing interests.

Additional information

Supplementary Information The online version contains supplementary material available at <https://doi.org/10.1038/s41598-023-44256-7>.

Correspondence and requests for materials should be addressed to D.D.

Reprints and permissions information is available at www.nature.com/reprints.

Publisher's note Springer Nature remains neutral with regard to jurisdictional claims in published maps and institutional affiliations.



Open Access This article is licensed under a Creative Commons Attribution 4.0 International License, which permits use, sharing, adaptation, distribution and reproduction in any medium or format, as long as you give appropriate credit to the original author(s) and the source, provide a link to the Creative Commons licence, and indicate if changes were made. The images or other third party material in this article are included in the article's Creative Commons licence, unless indicated otherwise in a credit line to the material. If material is not included in the article's Creative Commons licence and your intended use is not permitted by statutory regulation or exceeds the permitted use, you will need to obtain permission directly from the copyright holder. To view a copy of this licence, visit <http://creativecommons.org/licenses/by/4.0/>.

© The Author(s) 2023

7 Synthesis and Conclusions

7.1 Relevance of relocation and inverse imaging methods for life and environmental sciences

The atomic force microscopy (AFM) tip modification process is normally complex and can introduce scan artifacts, which should be excluded from further evaluation using a proper validation method. The new approach for relocating the same region of interest using multiple AFM probes (Abu Quba *et al.*, 2020) as well as the novel method for the characterization of the modified probes by inverse imaging (Abu Quba *et al.*, 2021) have been shown to assist in developing probes modified with various materials like bacterial cells, nanosized goethite particles, and large quartz grains, enhancing the versatility of AFM applications. The improved method of fixing minerals to the tipless cantilever using tiny glue spot offers sharp mineral edges (tips) allowing precise placement of FD curves on cell centers by the minerals tips (Abu Quba *et al.*, 2023). In the framework of exploring the changes that take place directly at the cell surfaces due to stress, a special concern is the single-cell resolution offered by this modification process. This is crucial in attributing observed changes in cell-mineral interactions (CMI) specifically to stress effects, eliminating potential contributing factors such as contacting multiple cells (Huang *et al.*, 2015).

The use of inverse imaging is extended to determinate the cell-mineral contact area relative to the deformation depth which is essential for normalizing the adhesion forces (Lau *et al.*, 2009) between irregular interacting substances as detailed in chapter 6 (Abu Quba *et al.*, 2023). I suggest that this strategy has the potential to broaden the use of AFM across several fields such as biomedicine, microbiology, pharmacy as well as life and environmental sciences. For example, Wu *et al.*, discussed that the larger contact area between sandfish skin surface and a probe modified with sand led to a significantly higher adhesion compared to spherical or sharp probes (Wu *et al.*, 2018). However, this could not be confirmed as no estimation of the contact area was established owing to the irregularity of the sand probe. In another study focusing on adhesion between two calcite surfaces (Dziadkowiec *et al.*, 2021), only one probe was used to ensure that changes in adhesion with varying concentrations of solution Ca^{2+} were not artifacts i.e. due to changing the contact area if multiple probes were used. Using a single probe might limit the generalizability of interactions as revealed in my work (chapter 6) emphasizing the need to incorporate the effect of the contact geometry to allow comparison of results obtained by various probes. In accordance, direct comparison between results obtained by various probes

modified with drug particles might be misleading and required assumptions as the interaction forces might not only be affected by the kinetics of the interacting materials to bind but also by their geometries (Young *et al.*, 2006).

7.2 How to normalize adhesion? by tip radius or contact area?

A distinct contrast in rupture force is evident when comparing chemical force microscopy (CFM) tips with mineral tips. The formers exhibit a narrower rupture force range, typically falling within ~50 -175 pN, in contrast to the mineral tips with a broader range of ~ 200 - 700 pN (**Fig. 4a**). While the various chemical interactions surely play a role, the geometry of the tip, especially its “sharpness”, also contributes to the observed differences of rupture forces between the CFM/mineral tips and the cell surfaces. Hence, a sharp probe with a small radius leads to smaller average adhesion and rupture forces than a dull probe with large radius (Skulason & Frisbie, 2000, 2002). An order of magnitude more binding molecules of the dull tip was attributed to a significantly larger contact area (almost 16 times) than the sharp tip (Lehenkari *et al.*, 2000). In fact, the surface energy of the tip affects the extent of adhesion forces only moderately compared to the contact area (Wu *et al.*, 2018).

I suggest that the tip geometry has a direct influence on the configuration of adsorbed molecules. Molecules on the CFM tip surface farther from the apex stretch with separation, gradually rupturing with stretching the more central bonds until only a few ones remain (**Fig. 3a** and **Fig. 4b**). The finite part of the tip, approximated as a sphere (Rodriguez *et al.*, 2012), dominates surface interactions, allowing normalization of adhesion force by tip radius (nN/nm) (Abu Quba *et al.*, 2022).

However, cell molecules adsorbed on the dull mineral tips are likely to be in a relaxed state at position (4) and stretch up to the point of the final rupture event (6) when most of them break free together, resulting in a higher rupture force (**Fig. 3b** and **Fig. 4c**). Thus, almost the entire contact area contributes to the adhesion process and the use of P_{ad} is more appropriate in this case (Abu Quba *et al.*, 2023). While the adhesion force increases with increasing the cell-mineral contact area, P_{ad} starts with slight or moderate decrease with increasing the loading forces before reaching constant level (**Fig. SI 9a** and **b** and **Fig. SI 10a** and **b**, [Supplemental Information](#) chapter 6). Although this trend in P_{ad} has been previously reported (Lau *et al.*, 2009), the reasons behind it remain unclear. In only two cases, however, was a constant behavior of P_{ad} observed, which agrees with H4 (**Fig. SI 10a**).

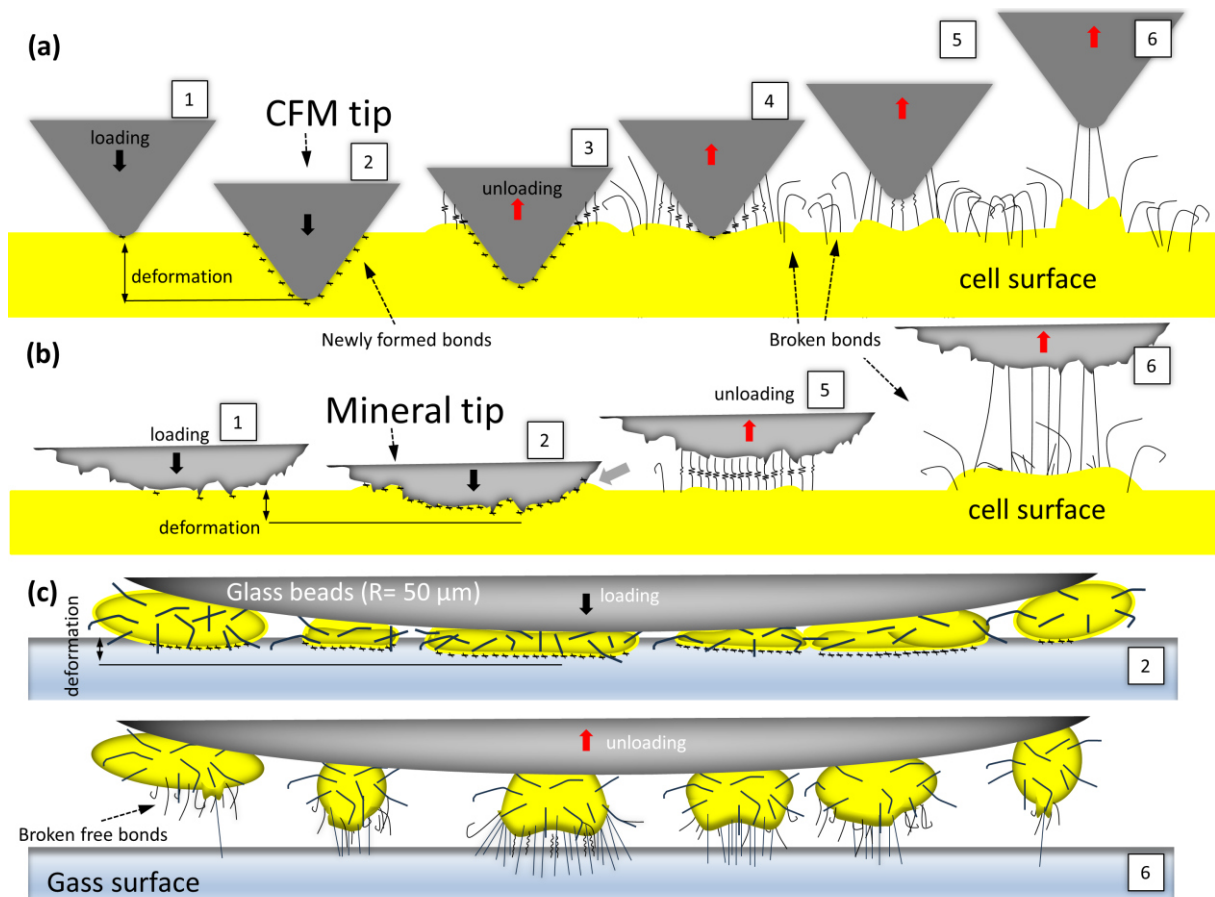


Fig. 3. Sketches illustrating the tip-sample interactions corresponding to the sequential steps addressed in the FD curve of **Fig. 2** (section 1.7), between (a) CFM tip and (b) mineral tip and a single bacterial cell. The configuration in (c) is reversed with the cells attached to the colloidal probe scanning against the sample surface.

I attribute this phenomenon to “size effect”. The flexibility of the cell membrane may allow little increase of the contact area (gray arrow, **Fig. 3b**). Since the contact area is small at low deformation, this increase of size will lead to overestimation of P_{ad} which explains its high initial levels. With increasing the loading forces, however, this contribution of the cell membrane diminishes and a better fit between the estimated contact area and the actual one results in the steady state behavior of P_{ad} . This concept is supported by the finding that unstressed cells, which have higher flexibility (Abu Quba *et al.*, 2022), exhibit a more significant P_{ad} decay compared to stressed cells (**Fig. SI 10a and b**). Similarly, the glue surface of double-sided tape, known for its ability to deform and elongate easily, shows a similar trend, sometimes with even higher decay rates than unstressed cells (**Fig. SI 10a and b**). Given the increasing importance of nanotechnology applications in life and environmental sciences, a challenging area for future research is therefore to understand how nanoscale mechanical properties of biological samples influence their adhesion function. In chapter 6, a loading force of 5 nN was employed for measuring CMI and capture the effect of stress. While lower loading

force might lead to an overestimation of P_{ad} , higher loading force might not allow single-cell resolution.

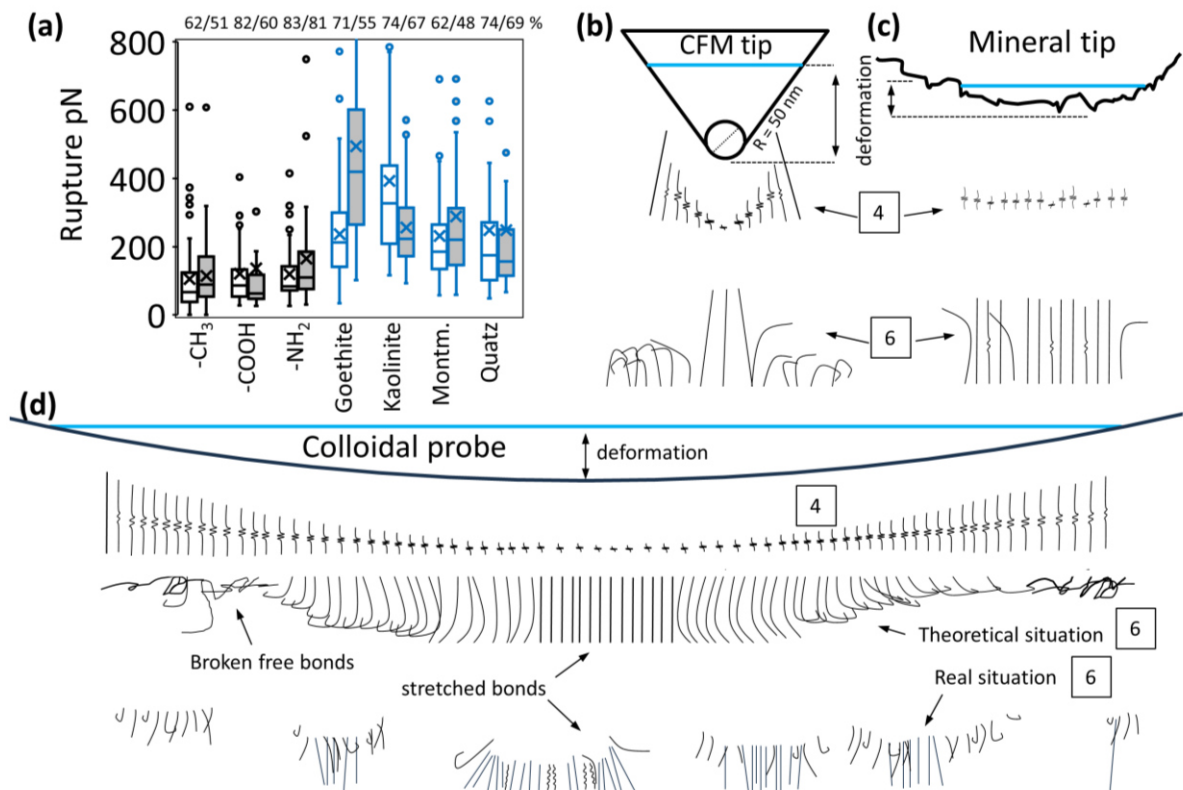


Fig. 4. (a) Box plots of rupture forces (position 6 in **Fig. 2**, section 1.7) for CFM (Abu Quba *et al.*, 2022) and mineral (Abu Quba *et al.*, 2023) tips, with numbers on the top of frequency (%) of events towards cells grown under unstressed (white) / stressed (gray) conditions. Configurations of the CFM (b) and mineral (c) tips elucidate that the lower rupture forces observed in (a), for CFM tips, are attributed to fewer intact bonds reaching position 6 compared to the relatively blunt mineral tips and (d) comparison between the theoretical and real situations of colloidal probe system highlighting discrepancies in bond distribution. Molecules that detach earlier (broken free bonds in (d)) gradually recover random orientation while the newly detached central bonds still have an orientation influenced by stretch direction.

The tip sharpness estimation involves calculating the aspect ratio (3D area / 2D area) relative to tip height using the 3D models of the tips (Abu Quba *et al.*, 2023) (**Fig. 5**). The tip area-height function was derived by plotting the 3D area against the height (Abu Quba *et al.*, 2023). Two approaches were also used to get a model for a CFM tip; both showing similar patterns. The first one involves estimating the tip radius using a blind tip reconstruction algorithm (Abu Quba *et al.*, 2021) and extrapolating the data beyond the tip radius from an inverse image of the CFM tip with a "sharper" characterizer representing the second method (green squares and black triangles in **Fig. 5**, respectively). The CFM tip exhibits a sharper profile evident by a rapid

increase in aspect ratio and a smaller increase in 3D area compared to dull mineral tips. Similarly, a standard AFM tip, like the SNL probe, appears sharper with a much smaller 3D area compared to both the CFM and mineral tips (yellow line, **Fig. 5**).

Based on that, I propose a normalization approach for adhesion forces detected by AFM: normalizing by the tip radius (Abu Quba *et al.*, 2022) for sharp tips and by the contact area (Abu Quba *et al.*, 2023) for dull tips. It is reasonable to establish that if the aspect ratio exceeds a value of ~ 2 at a height of 50 nm, the representative tip may be classified as “sharp”, (dashed red line, **Fig. 5**). However, this classification primarily holds true for single-cell investigations, as the determination of contact area becomes considerably more complex if the 3D area is already large at low levels of deformation (**Fig 3c**, **Fig 4d** and black dots in **Fig. 5**).

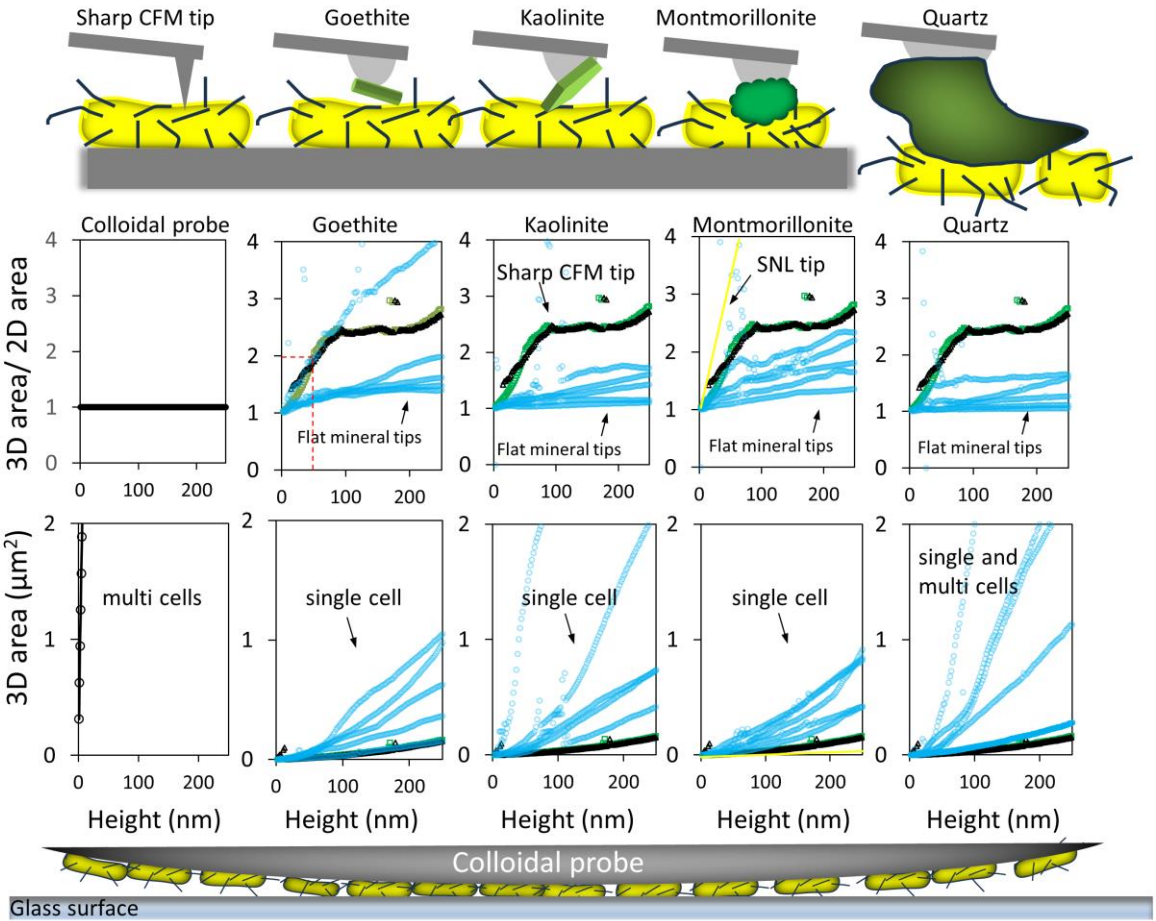


Fig. 5. Aspect ratio ($3D \text{ area} / 2D \text{ area}$) shown in the upper section and only 3D area in the lower section as a function of the height from the tip apex for various tips, as illustrated by the sketches. The mineral probes (blue dots), with relatively flat and larger tips, exhibit lower aspect ratios and larger 3D areas compared to the sharp SNL (yellow line) and CFM (black triangles and green squares) tips.

7.3 Theoretical model of bacterial growth under stress condition

Growth of bacteria under stress is a complex process, characterized by a sequence of events that are adapted to the changes of the environmental conditions. Once the cells regain access to resources essential for colonization, they develop a biofilm. Based on my work and other studies, a two step model elucidating bacterial behavior within a drying-rewetting cycle is proposed (**Fig. 6**).

Under relatively stress free conditions, cells with lower hydrophobicity (Karagulyan *et al.*, 2022) engage in molecular interactions with the mineral surfaces. An example of such interactions is the formation of bacterial footprints on host surfaces after cell detachment processes (Prakash *et al.*, 2003; El-Kirat-Chatel *et al.*, 2014b; Kimkes & Heinemann, 2020) (line scan, position 1, **Fig. 6**). These bridging polymers (El-Kirat-Chatel *et al.*, 2014a; b) play a role in reducing the surface wettability of minerals (Prakash *et al.*, 2003), thus, facilitating bacterial adhesion. While minerals with low wettability are particularly suitable for hosting cells as addressed in chapter 6 (Abu Quba *et al.*, 2023), hydrophilic minerals may initially offer primarily reversible attachment (Berne *et al.*, 2018). However, the formation of the footprints on the mineral surfaces enhances the binding ability towards cells indicating that adhesion may not be only a single binding event but occurs through cumulative processes.

Within the SOM, the kinetics involved in microbial biomass coordination and cluster formation should not be neglected. Initially, the enhanced cell-cell adhesion fosters association formation where multiple microbes share gel-like extracellular matrix (Birarda *et al.*, 2019) which may better protect microorganisms against external stressors compared to individual cells (Hirakawa & Tomita, 2013; Kreve & Reis, 2021) (black and white arrows at position 1 and 2, **Fig. 6**). As drought stress develops, these cellular associations migrate, while some individual cells establish interactions with the surrounding mineral surfaces. Forces propelling bacteria towards surfaces include not only external factors but also intrinsic microbial activities (section 1.4.3). An external factor contributing to this migration might stem from the reduction in volume of the bulk liquid within the soil network during drying. This can force bacteria to flow towards solid surfaces, thereby increasing the probability of initial cell-mineral interactions (position 2, **Fig. 6**). Continued drought imposes the reduction of exposure to the stress medium. A subpopulation of cells diffuses and condenses into the lower layers engaging in physical contact with the host surface (position 3, **Fig. 6**).

After cells initially attach, cell-mineral adhesion progressively becomes stronger over time due to several factors (position 3 to 4, **Fig. 6**). The enhancement of molecular interactions does not just originate from the increased contact areas but also the increased number of connectors (bridging molecules) during prolonged contact periods as demonstrated in chapter 6 for H4 and H5, respectively. This is often linked to the removal of water between the adhering cells and minerals (Xu & Logan, 2006; Chen *et al.*, 2014). It has been observed that the physical contact of the flagella with the surface can enhance adhesion through hydrophobic interactions particularly towards hydrophobic surfaces (Kimkes & Heinemann, 2020). These bond strengthening mechanisms occur quickly within seconds to minutes (Vadillo-Rodríguez *et al.*, 2004; Huang *et al.*, 2015; Carniello *et al.*, 2018). But these observations are primarily observed in *In vitro* conditions, lacking the dynamic cellular responses (Kimkes & Heinemann, 2020), which poses technical challenges for investigations. From my point of view, with the changes of the soil properties due to the shift in environmental conditions, adhesion could further strengthen. Consistent with H 1, that the cells favor molecular interactions with the hydrophobic $-CH_3$ surface than the hydrophilic ones like $-COOH$ and $-NH_2$ suggests that single cells become more repellent (chapter 5). Such change of the cell wall hydrophobicity is reflected by a reduced polarity of the entire microbial film as detected by the decrease of contact angles upon stress (Karagulyan *et al.*, 2022; Abu Quba *et al.*, 2022) which confirms H3. Thus, it could be suggested that the microbial colony adapts by shielding itself from water, thereby favoring adsorption onto mineral surfaces.

However, the characteristics of the mineral surfaces play a pivotal role in the formation of stable microbial coatings. Notably, minerals smaller in size compared to cells, like goethite, engage multiple particles with various orientations during interactions with the cells resulting in increased P_{ad} upon stress as expected in H6 (Abu Quba *et al.*, 2023). Montmorillonite with uniform and round porous domains also contributes to the stress induced increase of P_{ad} (Abu Quba *et al.*, 2023). But surfaces that are extremely flat, like the kaolinite sheets, pose a challenge for the proteins embedded in the cell outer membrane to adsorb to (Abu Quba *et al.*, 2023). Consequently, P_{ad} decreases (Abu Quba *et al.*, 2023) as the protein density increases by stress (Abu Quba *et al.*, 2022). An essential criterion for cell colonization under stress conditions is a certain level of repellency of the mineral surface (contact angle exceeding $\sim 20^\circ$). Surfaces that are completely wettable, like quartz, lack sufficient sites for hydrophobic junctions with the more hydrophobic stressed cells leading to no change of adhesion pressure upon stress (Abu Quba *et al.*, 2023). The demonstrated stronger adhesion of cells to less wettable minerals (Abu

Quba *et al.*, 2023), confirming hypothesis H7, suggests that minerals with lower wettability, like goethite, may host cells at higher rates compared to highly hydrophilic minerals, like quartz.

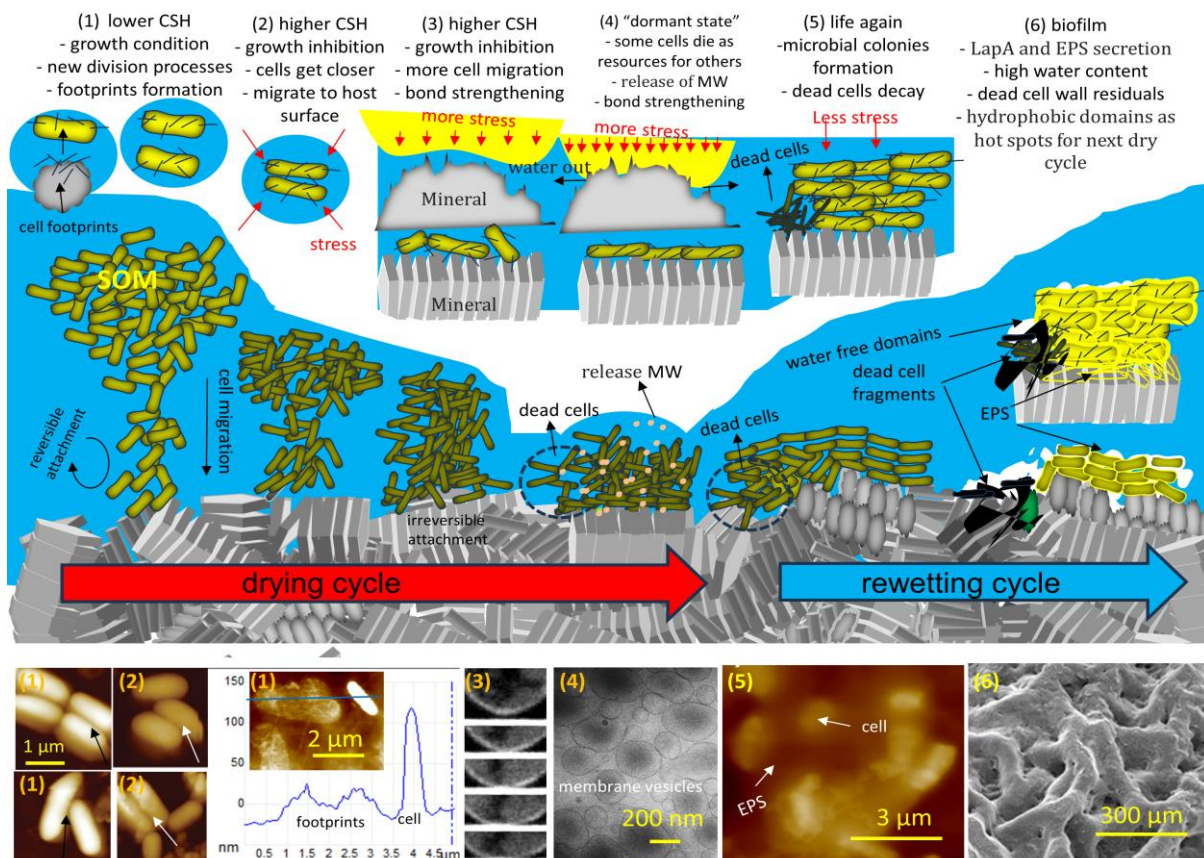


Fig. 6. Two step model illustrating bacterial growth over a drying-rewetting cycle. The sketch demonstrates the cumulative steps associated with biofilm formation on minerals surfaces from cells originally suspended in SOM. The lower bar presents findings supporting the proposed growth scenario. At position 1, the planktonic cells are in optimal condition for growth by division processes. AFM images at position 1 reveal the tendency of *B. subtilis* (up) and *P. fluorescens* (down) cells, with lower hydrophobicity, to remain isolated (indicated by black arrow). Some cells may recondition surrounding solid surfaces as shown after the removal of *P. putida* cell from epoxy glue (Abu Quba *et al.*, 2023) surface, line scan at position 1 (my unpublished results). As the dry stress develops, increased cell hydrophobicity prompts their association and migration towards the mineral surface. The AFM images of stressed cells show their tendency to form associations (observe the decrease in cell-cell spacing in AFM images at position 2, white arrow). Subsequently, bond strengthening progressively takes place for the cells that are already at the mineral surfaces. Fast processes like the increase of the contact area is shown by the SEM image (Gu *et al.*, 2017) at position 3 (potentially starting at position 2 as well). I propose that the whole microbial colony will structure to be densely packed increasing the number of cells adhering to the mineral surfaces with rising osmotic pressure (position 4). Throughout this transition (positions 1 to 4), the microbial colony actively defends stress by enhanced cell surface hydrophobicity, partial decay of cell subpopulations for biomass nutrition, and the release of outer membrane vesicles, reaching maximal release at position 4 shown by the SEM image (Baumgarten *et al.*, 2012). Upon rewetting, living biomass regains energy resources to continue their biological activities and form biofilm illustrated by organizational steps 5 and 6 supported by research (Donlan *et al.*, 1994; Otter *et al.*, 2015; Chitlapilly Dass & Wang, 2022; Parvin *et al.*, 2023). The AFM (Ripa *et al.*, 2020) and SEM (Epstein *et al.*, 2011) images show biofilm initiation at the respective steps 5 and 6. Notably, position 4 and 6 show distinct microbial configurations, each contributing various services to the soil ecosystem, as detailed in the text. Images reproduced by permission of IOP Publishing Ltd.

Bacteria simultaneously shrink in size (Abu Quba *et al.*, 2022) as drying progresses, possibly leading to an overall reduction of the biological coverage on minerals. In addition, the unexpected increase of cell stiffness (Abu Quba *et al.*, 2022) may hinder firm attachment of the outer membrane to the mineral surfaces. However, cell shrinkage is associated with an increase of protein to lipid ratio (Abu Quba *et al.*, 2022), which leads to a higher number of hydrophobic nanodomains per cell surface area. In turn, this may stimulate more molecular interactions between cells in the central layers of the colony and stronger adsorption at the cell-mineral interface, thereby improving the cohesion of the entire biological entity over the dry period. Speculatively, within the close vicinity of the surface hosting millions of cells (Clarke, 2016), the progressive structuring of densely packed cells, adapting to the gradual rise in cell hydrophobicity, might continually promote individual cell-surface contacts. Chapter 5 provides a detailed explanation of the mechanisms by which changes in cell size, stiffness, charge, and chemical composition lead to the development of hydrophobic characteristics on the cell surfaces. This adaptation supports H2 and may be further enhanced by additional contributions to the hydrophobic interactions, such as the release of outer membrane vesicles under stress (Baumgarten *et al.*, 2012).

Our work revealed growth inhibition across six tested bacterial strains due to exposure to both osmotic and matric stress (Karagulyan, 2022). Intermicrobial interactions often arise from competition of resources. Cells, especially in the bottom layers (Prakash *et al.*, 2003), might fail to meet minimal energy requirements for survival and could undergo degradation (Worrich *et al.*, 2016) or eventual cell death (Karagulyan, 2022) (position 4, **Fig. 6**). Their released products (Karagulyan, 2022), waste products from their neighbors (Prakash *et al.*, 2003) together with trapped nutrient (Westall *et al.*, 2000) within the microbial community as well as the organic molecules previously addressed, footprints (Kimkes & Heinemann, 2020), become potential substrates for metabolization (Kimkes & Heinemann, 2020; Karagulyan, 2022) by the surviving biomass, which stands a higher chance of persistence within this harsh micro-environment. It is plausible that cells adapt to a “dormant state” marked by a drastic reduction in cellular activity and motility, aiming to maintain their population as much as possible.

Up to this point, the microbial induced hydrophobizing effect of the mineral surfaces likely reaches its peak. First, the mineral surfaces become less accessible to water as they get covered by bacterial cells, imprinting their hydrophobic properties, consequently contributing to certain levels of soil water repellency (SWR) (Achtenhagen *et al.*, 2015; Karagulyan *et al.*, 2022; Abu Quba *et al.*, 2023). Second, the organic molecules released during cell envelope decay,

particularly lipids of the inner and outer membranes as well as the outer membrane proteins, may stabilize on the mineral surface in dry condition resulting to the formation of hydrophobic domains (Miltner *et al.*, 2012; Abu Quba *et al.*, 2022). Additionally, membrane vesicles (MV) produced by the cells could partially cover mineral surfaces, thereby reducing their surface energies (Baumgarten *et al.*, 2012; Mozaheb & Mingeot-Leclercq, 2020).

Upon rewetting, the subsequent process of biofilm development in aqueous dispersion has been intensively reviewed (Donlan *et al.*, 1994; Otter *et al.*, 2015; Chitlapilly Dass & Wang, 2022; Parvin *et al.*, 2023) and will not be covered here (position 5 and 6, **Fig. 6**). As extracellular polymeric substances (EPS) are produced (Westall *et al.*, 2000), the water content notably increases because EPS has a capacity for retaining water through hydrogen bonding (Prakash *et al.*, 2003). Consequently, the key characteristics and functions of the bacteria are modified (Marshall *et al.*, 1989; Otter *et al.*, 2015) as biofilms engage in physiological activities such as the degradation of organic matter (Cai *et al.*, 2019) and the cycling of different substances and metals (Flemming, 1993). This system significantly enhances resilience against stress, even under severe conditions (Fischer, 2009; Meisner *et al.*, 2017), by serving as a buffer that retains moisture in the bulk soil upon drying (Roberson & Firestone, 1992).

So far, at the end of the drying phase (position 4, **Fig. 6**), the microbial colony demonstrates a considerable level of hydrophobicity. After a rewetting phase, however, bacterial functions are predominantly dominated by their biofilm counterparts, characterized by hydrophobic domain residuals but with notably high water content (position 6, **Fig. 6**). My findings suggest a promising role of intact cells (potentially living biomass) in inducing SWR. This raises the question of whether bacteria can recover from the dry period and develop to form biofilms? Or, given the already established irreversible adhesion (Berne *et al.*, 2018; Carniello *et al.*, 2018), would the dynamic processes at the single-cell level not affect the integrity of the bacterial community leading to further accumulation of cell fragments, in turn, to the long-term hydrophobizing effects? In my opinion, the duration of droughts plays a role in determining the fate of the microbial colony. It essentially governs the rate of bacterial death, consequently impacting the preservation of organic matter against decay.

It was recently found that following prolonged periods of drying, even up to a year, bacterial growth starts rapidly upon rewetting and the growth rate soon matches that of conditions with continuous moisture (Meisner *et al.*, 2015, 2017). This resistance might be related to that in a dynamic soil environments (Smucker, 1993; Gao *et al.*, 2021), the accessibility of water and

nutrient to microorganisms increases creating favorable growth conditions through pronounced uptake processes (Soto González *et al.*, 2021). Particularly for bacteria immobilized on surfaces, unlike the suspended counterparts, already little enrichment of the nutrient levels leads to cellular growth processes (Kjelleberg *et al.*, 1982). Notably, multiple bacterial species can also resist for several months exhibiting resistance comparable to soil systems though in drier (Meisner *et al.*, 2017) conditions like on plastic or metallic air dry surfaces (Kramer *et al.*, 2006). These recent findings highlight a great ability of bacteria to withstand extended droughts likely with little losses of the living biomass.

A relevant experiment in the same project showed for two various soils that the fluctuations in moisture content caused by drying-rewetting events over a 90 day period were not reflected in changes of the soil hydrophobicity (Karagulyan, 2022). Based on this finding and considering recent literature insights, I propose the following hypothesis. In natural environments, bacteria demonstrate a greater resistance to water stress than previously understood, exhibiting a slow biomass loss. Therefore, temporal stress resulting from shifts in soil parameters (such as variations in precipitation intensity, frequency, and soil temperature) is accommodated by soil microorganisms. These microorganisms adjust their properties and behaviors, responding to the changed conditions, and subsequently recover to an unstressed state when the environmental conditions become more favorable.

While my proposed hypothesis regarding the elevation of bacterial surface hydrophobicity levels in dry conditions was confirmed, the implications of this phenomenon may not necessarily be harmful to soil health, as discussed in the introduction (section 1.1). Instead, the relative increase in cell surface hydrophobicity, enhancing survival ability, could potentially foster the drought tolerance of the entire ecological system maintaining plant productivity under stress conditions. Specifically, *P. fluorescens*, the most susceptible to increase hydrophobicity when subject to stress (Karagulyan *et al.*, 2022), is recognized as a root colonizer termed a "hidden hero" (Nishu *et al.*, 2022). This strain promotes plant growth and mitigates plant diseases through various processes, which get significantly activated under drought conditions, including: nitrogen fixation, phosphate solubilization, and the expression of materials related to plant growth (Nishu *et al.*, 2022). Similarly, the robust defense system enabling survival under soil stressors has positioned *B. subtilis* as a viable biofertilizer (Hashem *et al.*, 2019). Thus so, the continued study of dynamic soil-bacteria interactions holds huge promise. It may open a gateway for several strategies to enhance soil health through regulating these interactions to support plant productivity and resistance in stressful environmental conditions.

However, with global warming and climate change, an expected increase in soil temperature and salinity levels (Win *et al.*, 2018; Soto González *et al.*, 2021; Ebrahimi *et al.*, 2021) may create prolonged stress conditions that hinder microorganisms from full adaptation processes leading to a microbial degradation. Additionally, in hydrophobic soils characterized by preferential water flow paths (Morales *et al.*, 2010; Goebel *et al.*, 2011), prolonged exposure of soil microorganisms to dry conditions could impede their recovery when water becomes available again such as after cultivation activities. A study of the impacts of severe droughts, extending beyond seasonal changes, on cell wetting properties and the feedback on soil properties and crop yield should therefore be considered. This helps to understand how bacteria behave and function in such conditions enabling us to take measures in managing potential risks. Furthermore, exploring how the inhomogeneous water infiltration and distribution influence microbial interactions with soil materials may shed light on potential persistent hydrophilization effect of bacteria.

8 References

- Abu Quba, A.A., Goebel, M.-O., Karagulyan, M., Miltner, A., Kästner, M., Bachmann, J., Schaumann, G.E. & Diehl, D. 2022. Changes in cell surface properties of *Pseudomonas fluorescens* by adaptation to NaCl induced hypertonic stress. *FEMS Microbes*, **4**, xtac028.
- Abu Quba, A.A., Goebel, M.-O., Karagulyan, M., Miltner, A., Kästner, M., Bachmann, J., Schaumann, G.E. & Diehl, D. 2023. Hypertonic stress induced changes of *Pseudomonas fluorescens* adhesion towards soil minerals studied by AFM. *Scientific Reports*, **13**, 17146.
- Abu Quba, A.A., Schaumann, G.E., Karagulyan, M. & Diehl, D. 2020. A new approach for repeated tip-sample relocation for AFM imaging of nano and micro sized particles and cells in liquid environment. *Ultramicroscopy*, **211**, 112945.
- Abu Quba, A.A., Schaumann, G.E., Karagulyan, M. & Diehl, D. 2021. Quality control of direct cell–mineral adhesion measurements in air and liquid using inverse AFM imaging. *RSC Advances*, 5384–5392.
- Abu-Lail, N.I. & Beyenal, H. 2013. Chapter 5.2 - Characterization of Bacteria–Biomaterial Interactions, from a Single Cell to Biofilms. In: *Characterization of Biomaterials* (eds. Bandyopadhyay, A. & Bose, S.), pp. 207–253. Academic Press, Oxford.
- Achtenhagen, J., Goebel, M.-O., Miltner, A., Woche, S.K. & Kästner, M. 2015. Bacterial impact on the wetting properties of soil minerals. *Biogeochemistry*, **122**, 269–280.
- Adamczuk, A., Gryta, A., Skic, K., Boguta, P. & Jozefaciuk, G. 2022. Effect of Different Minerals on Water Stability and Wettability of Soil Silt Aggregates. *Materials (Basel, Switzerland)*, **15**, 5569.
- Aguayo, S., Donos, N., Spratt, D. & Bozec, L. 2015. Single-bacterium nanomechanics in biomedicine: unravelling the dynamics of bacterial cells. *Nanotechnology*, **26**, 062001.
- Allegrini, M., Ascoli, C., Baschieri, P., Dinelli, F., Frediani, C., Lio, A. & Mariani, T. 1992. Laser thermal effects on atomic force microscope cantilevers. *Ultramicroscopy*, **42–44**, 371–378.
- Alsteens, D., Beaussart, A., El-Kirat-Chatel, S., Sullan, R.M.A. & Dufrêne, Y.F. 2013. Atomic Force Microscopy: A New Look at Pathogens. *PLOS Pathogens*, **9**, e1003516.
- Alsteens, D., Gaub, H.E., Newton, R., Pfreundschuh, M., Gerber, C. & Müller, D.J. 2017. Atomic force microscopy-based characterization and design of biointerfaces. *Nature Reviews Materials*, **2**, 1–16.
- Amy, P.S., Durham, C., Hall, D. & Haldeman, D.L. 1993. Starvation-survival of deep subsurface isolates. *Current Microbiology*, **26**, 345–352.
- Anselme, K., Davidson, P., Popa, A.M., Giazzon, M., Liley, M. & Ploux, L. 2010. The interaction of cells and bacteria with surfaces structured at the nanometre scale. *Acta Biomaterialia*, **6**, 3824–3846.

- Awassa, J., Soulé, S., Cornu, D., Ruby, C. & El-Kirat-Chatel, S. 2022. Understanding the role of surface interactions in the antibacterial activity of layered double hydroxide nanoparticles by atomic force microscopy. *Nanoscale*, **14**, 10335–10348.
- Bachmann, J. & van der Ploeg, R.R. 2001. Isothermal and Nonisothermal Evaporation from Four Sandy Soils of Different Water Repellency. *Soil Science Society of America Journal*, **65**, 1599–1607.
- Bachmann, J., Söffker, S., Sepehrnia, N., Goebel, M.-O. & Woche, S.K. 2021. The effect of temperature and wetting–drying cycles on soil wettability: Dynamic molecular restructuring processes at the solid–water–air interface. *European Journal of Soil Science*, **72**, 2180–2198.
- Bailey, V.L., Smith, J.L. & Bolton, H. 2002. Fungal-to-bacterial ratios in soils investigated for enhanced C sequestration. *Soil Biology and Biochemistry*, **34**, 997–1007.
- Ball, B.C., O’sullivan, M.F. & Hunter, R. 1988. Gas diffusion, fluid flow and derived pore continuity indices in relation to vehicle traffic and tillage. *Journal of Soil Science*, **39**, 327–339.
- Baumgarten, T., Sperling, S., Seifert, J., von Bergen, M., Steiniger, F., Wick, L.Y. & Heipieper, H.J. 2012. Membrane vesicle formation as a multiple-stress response mechanism enhances *Pseudomonas putida* DOT-T1E cell surface hydrophobicity and biofilm formation. *Applied and Environmental Microbiology*, **78**, 6217–6224.
- Baumgartner, W., Hinterdorfer, P. & Schindler, H. 2000. Data analysis of interaction forces measured with the atomic force microscope. *Ultramicroscopy*, **82**, 85–95.
- Beaussart, A., El-Kirat-Chatel, S., Herman, P., Alsteens, D., Mahillon, J., Hols, P. & Dufrêne, Y.F. 2013. Single-Cell Force Spectroscopy of Probiotic Bacteria. *Biophysical Journal*, **104**, 1886–1892.
- Beaussart, A., Feuillie, C. & El-Kirat-Chatel, S. 2020. The microbial adhesive arsenal deciphered by atomic force microscopy. *Nanoscale*, **12**, 23885–23896.
- Berne, C., Ellison, C.K., Ducret, A. & Brun, Y.V. 2018. Bacterial adhesion at the single-cell level. *Nature Reviews. Microbiology*, **16**, 616–627.
- Birarda, G., Delneri, A., Lagatolla, C., Parisse, P., Cescutti, P., Vaccari, L. & Rizzo, R. 2019. Multi-technique microscopy investigation on bacterial biofilm matrices: a study on *Klebsiella pneumoniae* clinical strains. *Analytical and Bioanalytical Chemistry*, **411**, 7315–7325.
- Bowen, W.R., Lovitt, R.W. & Wright, C.J. 2001. Atomic Force Microscopy Study of the Adhesion of *Saccharomyces cerevisiae*. *Journal of Colloid and Interface Science*, **237**, 54–61.
- Braun, B., Böckelmann, U., Grohmann, E. & Szewzyk, U. 2010. Bacterial soil communities affected by water-repellency. *Geoderma*, **158**, 343–351.
- Bremer, E. & Krämer, R. 2019. Responses of Microorganisms to Osmotic Stress. *Annual Review of Microbiology*, **73**, 313–334.

- de Brogniez, D., Ballabio, C., Stevens, A., Jones, R.J.A., Montanarella, L. & van Wesemael, B. 2015. A map of the topsoil organic carbon content of Europe generated by a generalized additive model. *European Journal of Soil Science*, **66**, 121–134.
- Bronick, C.J. & Lal, R. 2005. Soil structure and management: a review. *Geoderma*, **124**, 3–22.
- Cai, P., Sun, X., Wu, Y., Gao, C., Mortimer, M., Holden, P.A., Redmile-Gordon, M. & Huang, Q. 2019. Soil biofilms: microbial interactions, challenges, and advanced techniques for ex-situ characterization. *Soil Ecology Letters*, **1**, 85–93.
- Caltabellotta, G., Iovino, M. & Bagarello, V. 2022. Intensity and persistence of water repellency at different soil moisture contents and depths after a forest wildfire. *Journal of Hydrology and Hydromechanics*, **70**, 410–420.
- Cao, T., Tang, H., Liang, X., Wang, A., Auner, G.W., Salley, S.O. & Ng, K.Y.S. 2006. Nanoscale investigation on adhesion of *E. coli* to surface modified silicone using atomic force microscopy. *Biotechnology and Bioengineering*, **94**, 167–176.
- Carniello, V., Peterson, B.W., van der Mei, H.C. & Busscher, H.J. 2018. Physico-chemistry from initial bacterial adhesion to surface-programmed biofilm growth. *Advances in Colloid and Interface Science*, **261**, 1–14.
- Carter, M.R. & Gregorich, E.G. (Eds). 2007. *Soil Sampling and Methods of Analysis*. 2nd ed. CRC Press, Boca Raton.
- Chau, H.W., Goh, Y.K., Vujanovic, V. & Si, B.C. 2012. Wetting properties of fungi mycelium alter soil infiltration and soil water repellency in a γ -sterilized wettable and repellent soil. *Fungal Biology*, **116**, 1212–1218.
- Chen, Y., Busscher, H.J., van der Mei, H.C. & Norde, W. 2011. Statistical Analysis of Long- and Short-Range Forces Involved in Bacterial Adhesion to Substratum Surfaces as Measured Using Atomic Force Microscopy. *Applied Environmental Microbiology*, **77**, 5065–5070.
- Chen, R., Fan, Y., Dong, X., Ma, X., Feng, Z., Chang, M. & Li, N. 2021. Impact of pH on interaction between the polymeric flocculant and ultrafine coal with atomic force microscopy (AFM). *Colloids and Surfaces A: Physicochemical and Engineering Aspects*, **622**, 126698.
- Chen, Y., Harapanahalli, A.K., Busscher, H.J., Norde, W. & van der Mei, H.C. 2014. Nanoscale cell wall deformation impacts long-range bacterial adhesion forces on surfaces. *Applied and Environmental Microbiology*, **80**, 637–643.
- Chen, Y., Norde, W., van der Mei, H.C. & Busscher, H.J. 2012. Bacterial cell surface deformation under external loading. *mBio*, **3**, e00378-12.
- Chen, G. & Zhu, H. 2004. Impact of lipopolysaccharide coating on clay particle wettability. *Colloids and Surfaces. B, Biointerfaces*, **35**, 143–147.
- Chenu, C., Le Bissonnais, Y. & Arrouays, D. 2000. Organic matter influence on clay wettability and soil aggregate stability. *Soil Science Society of America Journal*, **64**, 1479–1486.

- Chitlapilly Dass, S. & Wang, R. 2022. Biofilm through the Looking Glass: A Microbial Food Safety Perspective. *Pathogens*, **11**, 346.
- Clarke, E. 2016. Levels of selection in biofilms: multispecies biofilms are not evolutionary individuals. *Biology & Philosophy*, **31**, 191–212.
- Cramer, A., Benard, P., Zarebanadkouki, M., Kaestner, A. & Carminati, A. 2023. Microplastic induces soil water repellency and limits capillary flow. *Vadose Zone Journal*, **22**, e20215.
- Dague, E., Alsteens, D., Latgé, J.-P., Verbelen, C., Raze, D., Baulard, A.R. & Dufrêne, Y.F. 2007. Chemical Force Microscopy of Single Live Cells. *Nano Letters*, **7**, 3026–3030.
- Davari, M., Fahmideh, S. & Mosaddeghi, M.R. 2022. Rapid assessment of soil water repellency indices using Vis-NIR spectroscopy and pedo-transfer functions. *Geoderma*, **406**, 115486.
- DeBano, L.F. 1981. *Water repellent soils: a state-of-the-art*. Pacific Southwest Forest and Range Experiment Station, Berkeley, California.
- Dekker, L.W. & Jungerius, P.D. 1990. Water repellency in the dunes with special reference to the Netherlands. In: *Dunes of the European coasts: Geomorphology - Hydrology - Soils*, pp. 173–183.
- Deng, Y., Sun, M. & Shaevitz, J.W. 2011. Direct Measurement of Cell Wall Stress Stiffening and Turgor Pressure in Live Bacterial Cells. *Physical Review Letters*, **107**, 158101.
- Diao, M., Taran, E., Mahler, S.M. & Nguyen, A.V. 2014. Comparison and evaluation of immobilization methods for preparing bacterial probes using acidophilic bioleaching bacteria *Acidithiobacillus thiooxidans* for AFM studies. *Journal of Microbiological Methods*, **102**, 12–14.
- Diehl, D. 2013. Soil water repellency: Dynamics of heterogeneous surfaces. *Colloids and Surfaces A: Physicochemical and Engineering Aspects*, **432**, 8–18.
- Doerr, S.H., Llewellyn, C.T., Douglas, P., Morley, C.P., Mainwaring, K.A., Haskins, C., Johnsey, L., Ritsema, C.J., Stagnitti, F., Allinson, G., Ferreira, A.J.D., Keizer, J.J., Ziogas, A.K., Diamantis, J., Doerr, S.H., Llewellyn, C.T., Douglas, P., Morley, C.P., Mainwaring, K.A., Haskins, C., Johnsey, L., Ritsema, C.J., Stagnitti, F., Allinson, G., Ferreira, A.J.D., Keizer, J.J., Ziogas, A.K. & Diamantis, J. 2005. Extraction of compounds associated with water repellency in sandy soils of different origin. *Soil Research*, **43**, 225–237.
- Doerr, S.H., Shakesby, R.A. & Walsh, R.P.D. 2000. Soil water repellency: its causes, characteristics and hydro-geomorphological significance. *Earth-Science Reviews*, **51**, 33–65.
- Donlan, R.M., Pipes, W.O. & Yohe, T.L. 1994. Biofilm formation on cast iron substrata in water distribution systems. *Water Research*, **28**, 1497–1503.
- Dufrêne, Y.F. 2008. Atomic force microscopy and chemical force microscopy of microbial cells. *Nature Protocols*, **3**, 1132–1138.

- Dufrêne, Y.F. 2014. Atomic Force Microscopy in Microbiology: New Structural and Functional Insights into the Microbial Cell Surface. *mBio*, **5**, 10.1128/mbio.01363-14.
- Dufrêne, Y.F., Ando, T., Garcia, R., Alsteens, D., Martinez-Martin, D., Engel, A., Gerber, C. & Müller, D.J. 2017. Imaging modes of atomic force microscopy for application in molecular and cell biology. *Nature Nanotechnology*, **12**, 295–307.
- Dykhuizen, D. 2005. Species Numbers in Bacteria. *Proceedings. California Academy of Sciences*, **56**, 62–71.
- Dziadkowiec, J., Ban, M., Javadi, S., Jamtveit, B. & Røyne, A. 2021. Ca²⁺ Ions Decrease Adhesion between Two (104) Calcite Surfaces as Probed by Atomic Force Microscopy. *ACS Earth and Space Chemistry*, **5**, 2827–2838.
- Ebrahimi, F., Salehi, A., Movahedi Dehnavi, M., Mirshekari, A., Hamidian, M. & Hazrati, S. 2021. Biochemical response and nutrient uptake of two arbuscular mycorrhiza-inoculated chamomile varieties under different osmotic stresses. *Botanical Studies*, **62**, 22.
- Edwards, K.J. & Rutenberg, A.D. 2001. Microbial response to surface microtopography: the role of metabolism in localized mineral dissolution. *Chemical Geology*, **180**, 19–32.
- Efremov, Y.M., Wang, W.-H., Hardy, S.D., Geahlen, R.L. & Raman, A. 2017. Measuring nanoscale viscoelastic parameters of cells directly from AFM force-displacement curves. *Scientific Reports*, **7**, 1541.
- Elbourne, A., Chapman, J., Gelmi, A., Cozzolino, D., Crawford, R.J. & Truong, V.K. 2019. Bacterial-nanostructure interactions: The role of cell elasticity and adhesion forces. *Journal of Colloid and Interface Science*, **546**, 192–210.
- El-Kirat-Chatel, S., Beaussart, A., Alsteens, D., Jackson, D.N., Lipke, P.N. & Dufrêne, Y.F. 2013. Nanoscale analysis of caspofungin-induced cell surface remodelling in *Candida albicans*. *Nanoscale*, **5**, 1105–1115.
- El-Kirat-Chatel, S., Beaussart, A., Boyd, C.D., O'Toole, G.A. & Dufrêne, Y.F. 2014a. Single-Cell and Single-Molecule Analysis Deciphers the Localization, Adhesion, and Mechanics of the Biofilm Adhesin LapA. *ACS Chemical Biology*, **9**, 485–494.
- El-Kirat-Chatel, S., Boyd, C.D., O'Toole, G.A. & Dufrêne, Y.F. 2014b. Single-Molecule Analysis of *Pseudomonas fluorescens* Footprints. *ACS Nano*, **8**, 1690–1698.
- Epstein, A.K., Pokroy, B., Seminara, A. & Aizenberg, J. 2011. Bacterial biofilm shows persistent resistance to liquid wetting and gas penetration. *Proceedings of the National Academy of Sciences*, **108**, 995–1000.
- Fageria, N.K. & Moreira, A. 2011. Chapter Four - The Role of Mineral Nutrition on Root Growth of Crop Plants. In: *Advances in Agronomy* (ed. Sparks, D.L.), pp. 251–331. Academic Press.
- Faulkner, M., Zhao, L.-S., Barrett, S. & Liu, L.-N. 2019. Self-Assembly Stability and Variability of Bacterial Microcompartment Shell Proteins in Response to the Environmental Change. *Nanoscale Research Letters*, **14**, 54.

- Feng, B., Liu, H., Li, Y., Liu, X., Tian, R., Li, R. & Li, H. 2020. AFM measurements of Hofmeister effects on clay mineral particle interaction forces. *Applied Clay Science*, **186**, 105443.
- Fierer, N., Schimel, J.P. & Holden, P.A. 2003. Influence of Drying–Rewetting Frequency on Soil Bacterial Community Structure. *Microbial Ecology*, **45**, 63–71.
- Fischer, T. 2009. Substantial rewetting phenomena on soil respiration can be observed at low water availability. *Soil Biology and Biochemistry*, **41**, 1577–1579.
- Flemming, H.-C. 1993. Biofilms and Environmental Protection. *Water Science and Technology*, **27**, 1–10.
- Francius, G., Polyakov, P., Merlin, J., Abe, Y., Ghigo, J.-M., Merlin, C., Beloin, C. & Duval, J.F.L. 2011. Bacterial Surface Appendages Strongly Impact Nanomechanical and Electrokinetic Properties of Escherichia coli Cells Subjected to Osmotic Stress. *PLOS ONE*, **6**, e20066.
- Frisbie, C.D., Rozsnyai, L.F., Noy, A., Wrighton, M.S. & Lieber, C.M. 1994. Functional Group Imaging by Chemical Force Microscopy. *Science*, **265**, 2071–2074.
- Fundamentals of Soil Physics - 1st Edition. (At: <https://www.elsevier.com/books/fundamentals-of-soil-physics/hillel/978-0-08-091870-9>. Accessed: 7/2/2023).
- Furtak, K. & Gajda, A.M. 2018. Activity and Variety of Soil Microorganisms Depending on the Diversity of the Soil Tillage System. In: *Sustainability of Agroecosystems* (ed. Oliveira, A.B. de). InTech.
- Gao L.I.N., Zhi-yuan L.I. & Jian-bo L.I. 2021. Dynamic soil-structure interaction under complex soil environment. *Chinese Journal of Geotechnical Engineering*, **43**, 1573–1580.
- Girvan, M.S., Bullimore, J., Pretty, J.N., Osborn, A.M. & Ball, A.S. 2003. Soil Type Is the Primary Determinant of the Composition of the Total and Active Bacterial Communities in Arable Soils. *Applied and Environmental Microbiology*, **69**, 1800–1809.
- Goebel, M.-O., Bachmann, Jör., Reichstein, M., Janssens, I.A. & Guggenberger, G. 2011. Soil water repellency and its implications for organic matter decomposition – is there a link to extreme climatic events? *Global Change Biology*, **17**, 2640–2656.
- Goebel, M.-O., Woche, S.K., Bachmann, J., Lamparter, A. & Fischer, W.R. 2007. Significance of Wettability-Induced Changes in Microscopic Water Distribution for Soil Organic Matter Decomposition. *Soil Sci. Soc. Am. J.*, **71**, 1593–1599.
- Green, J.-B.D., Idowu, A. & Chan, S.S.F. 2003. Modified tips: molecules to cells. *Materials Today*, **6**, 22–29.
- Gu, J., Valdevit, A., Chou, T.-M. & Libera, M. 2017. Substrate effects on cell-envelope deformation during early-stage Staphylococcus aureus biofilm formation. *Soft Matter*, **13**, 2967–2976.

- Gultekinoglu, M., Jin Oh, Y., Hinterdorfer, P., Duman, M., Çatçat, D. & Ulubayram, K. 2016. Nanoscale characteristics of antibacterial cationic polymeric brushes and single bacterium interactions probed by force microscopy. *RSC Advances*, **6**, 17092–17099.
- Gupta, S.C. & Larson, W.E. 1979. Estimating soil water retention characteristics from particle size distribution, organic matter percent, and bulk density. *Water Resources Research*, **15**, 1633–1635.
- Hachicho, N., Birnbaum, A. & Heipieper, H.J. 2017. Osmotic stress in colony and planktonic cells of *Pseudomonas putida* mt-2 revealed significant differences in adaptive response mechanisms. *AMB Express*, **7**, 62.
- Hallett, P.D. 2001. Microbial derived water repellency in golf course soil. *International Turfgrass Society Research Journal*, **9**, 518–524.
- Hallett, P.D. 2007. An introduction to soil water repellency. *Proceedings of the 8th International Symposium on Adjuvants for Agrochemicals (ISAA2007)*, **6**, 9.
- Hallett, P.D., Baumgartl, T. & Young, I.M. 2001. Subcritical Water Repellency of Aggregates from a Range of Soil Management Practices. *Soil Science Society of America Journal*, **65**, 184–190.
- Hallett, P.D. & Young, I.M. 1999. Changes to water repellence of soil aggregates caused by substrate-induced microbial activity. *European Journal of Soil Science*, **50**, 35–40.
- Harper, R.J. & Gilkes, R.J. 1994. Soil attributes related to water repellency and the utility of soil survey for predicting its occurrence. *Soil Research*, **32**, 1109–1124.
- Hashem, A., Tabassum, B. & Fathi Abd_Allah, E. 2019. *Bacillus subtilis*: A plant-growth promoting rhizobacterium that also impacts biotic stress. *Saudi Journal of Biological Sciences*, **26**, 1291–1297.
- Heidar Barghi, M. 2019. *Use of capillary action to control soil moisture*. D_ph, University of Birmingham. (At: <https://etheses.bham.ac.uk/id/eprint/9055/>. Accessed: 8/2/2023).
- Hinsa, S.M., Espinosa-Urgel, M., Ramos, J.L. & O'Toole, G.A. 2003. Transition from reversible to irreversible attachment during biofilm formation by *Pseudomonas fluorescens* WCS365 requires an ABC transporter and a large secreted protein. *Molecular Microbiology*, **49**, 905–918.
- Hirakawa, H. & Tomita, H. 2013. Interference of bacterial cell-to-cell communication: a new concept of antimicrobial chemotherapy breaks antibiotic resistance. *Frontiers in Microbiology*, **4**, (At: <https://www.frontiersin.org/articles/10.3389/fmicb.2013.00114>. Accessed: 12/11/2023).
- Hizal, F., Choi, C.-H., Busscher, H.J. & van der Mei, H.C. 2016. Staphylococcal Adhesion, Detachment and Transmission on Nanopillared Si Surfaces. *ACS Applied Materials & Interfaces*, **8**, 30430–30439.
- Horne, D.J. & McIntosh, J.C. 2000. Hydrophobic compounds in sands in New Zealand—extraction, characterisation and proposed mechanisms for repellency expression. *Journal of Hydrology*, **231–232**, 35–46.

- Huang, Q., Wu, H., Cai, P., Fein, J.B. & Chen, W. 2015. Atomic force microscopy measurements of bacterial adhesion and biofilm formation onto clay-sized particles. *Scientific Reports*, **5**, 16857.
- Jaschke, M., Butt, H.-J., Manne, S., Gaub, H.E., Hasemann, O., Krimphove, F. & Wolff, E.K. 1996. The atomic force microscope as a tool to study and manipulate local surface properties. *Biosensors and Bioelectronics*, **11**, 601–612.
- John, A.-K., Schmalzer, M., Khanna, N. & Landmann, R. 2011. Reversible Daptomycin Tolerance of Adherent Staphylococci in an Implant Infection Model. *Antimicrobial Agents and Chemotherapy*, **55**, 3510–3516.
- Jost, A.P.-T. & Waters, J.C. 2019. Designing a rigorous microscopy experiment: Validating methods and avoiding bias. *Journal of Cell Biology*, **218**, 1452–1466.
- Jozefczuk, S., Klie, S., Catchpole, G., Szymanski, J., Cuadros-Inostroza, A., Steinhauser, D., Selbig, J. & Willmitzer, L. 2010. Metabolomic and transcriptomic stress response of *Escherichia coli*. *Molecular Systems Biology*, **6**, 364.
- Kabiri, V., Raiesi, F. & Ghazavi, M.A. 2016. Tillage effects on soil microbial biomass, SOM mineralization and enzyme activity in a semi-arid Calcixerepts. *Agriculture, Ecosystems & Environment*, **232**, 73–84.
- Karagulyan, M. 2022. *Impact of bacterial biomass on soil particle wettability under various moisture conditions*. Doctoral Thesis, Hannover : Institutionelles Repositorium der Leibniz Universität Hannover. (At: <https://www.repo.uni-hannover.de/handle/123456789/11921>. Accessed: 26/5/2023).
- Karagulyan, M., Goebel, M.-O., Diehl, D., Abu Quba, A.A., Kästner, M., Bachmann, J., Wick, L.Y., Schaumann, G.E. & Miltner, A. 2022. Water Stress-Driven Changes in Bacterial Cell Surface Properties. *Applied and Environmental Microbiology*, **88**, e00732-22.
- Keller, T. & Håkansson, I. 2010. Estimation of reference bulk density from soil particle size distribution and soil organic matter content. *Geoderma*, **154**, 398–406.
- Kimkes, T.E.P. & Heinemann, M. 2020. How bacteria recognise and respond to surface contact. *FEMS Microbiology Reviews*, **44**, 106.
- Kjelleberg, S., Humphrey, B.A. & Marshall, K.C. 1982. Effect of interfaces on small, starved marine bacteria. *Applied and Environmental Microbiology*, **43**, 1166–1172.
- Ko, D., Yoo, G., Yun, S.-T., Jun, S.-C. & Chung, H. 2017. Bacterial and fungal community composition across the soil depth profiles in a fallow field. *Journal of Ecology and Environment*, **41**, 34.
- Koebnik, R., Locher, K.P. & Van Gelder, P. 2000. Structure and function of bacterial outer membrane proteins: barrels in a nutshell. *Molecular Microbiology*, **37**, 239–253.
- Kramer, A., Schwebke, I. & Kampf, G. 2006. How long do nosocomial pathogens persist on inanimate surfaces? A systematic review. *BMC Infectious Diseases*, **6**, 130.

- Kreve, S. & Reis, A.C.D. 2021. Bacterial adhesion to biomaterials: What regulates this attachment? A review. *The Japanese Dental Science Review*, **57**, 85–96.
- Lal, R. 2009. Challenges and opportunities in soil organic matter research. *European Journal of Soil Science*, **60**, 158–169.
- Lambert, J.-F. 2008. Adsorption and Polymerization of Amino Acids on Mineral Surfaces: A Review. *Origins of Life and Evolution of Biospheres*, **38**, 211–242.
- Lang, F. 2007. Mechanisms and Significance of Cell Volume Regulation. *Journal of the American College of Nutrition*, **26**, 613S–623S.
- Lau, P.C.Y., Dutcher, J.R., Beveridge, T.J. & Lam, J.S. 2009. Absolute Quantitation of Bacterial Biofilm Adhesion and Viscoelasticity by Microbead Force Spectroscopy. *Biophysical Journal*, **96**, 2935–2948.
- Lauber, C.L., Strickland, M.S., Bradford, M.A. & Fierer, N. 2008. The influence of soil properties on the structure of bacterial and fungal communities across land-use types. *Soil Biology and Biochemistry*, **40**, 2407–2415.
- Lázaro, B. 2015. Halloysite and kaolinite: two clay minerals with geological and technological importance. *Rev. Real. Acad. Ciencias, Zaragoza*, 7–38.
- Lehenkari, P.P., Charras, G.T., Nykänen, A. & Horton, M.A. 2000. Adapting atomic force microscopy for cell biology. *Ultramicroscopy*, **82**, 289–295.
- Lévy, R. & Maaloum, M. 2001. Measuring the spring constant of atomic force microscope cantilevers: thermal fluctuations and other methods. *Nanotechnology*, **13**, 33.
- Lewin, M., Mey-Marom, A. & Frank, R. 2005. Surface free energies of polymeric materials, additives and minerals. *Polymers for Advanced Technologies*, **16**, 429–441.
- Li, M., Xi, N. & Liu, L. 2021. Peak force tapping atomic force microscopy for advancing cell and molecular biology. *Nanoscale*, **13**, 8358–8375.
- Long, J., Xu, Z. & Masliyah, J.H. 2006. Role of illite–illite interactions in oil sands processing. *Colloids and Surfaces A: Physicochemical and Engineering Aspects*, **281**, 202–214.
- Longo, G. & Kasas, S. 2014. Effects of antibacterial agents and drugs monitored by atomic force microscopy. *WIREs Nanomedicine and Nanobiotechnology*, **6**, 230–244.
- van Loosdrecht, M.C.M., Norde, W., Lyklema, J. & Zehnder, A.J.B. 1990. Hydrophobic and electrostatic parameters in bacterial adhesion. *Aquatic Sciences*, **52**, 103–114.
- Lu, H. & Schulten, K. 1999. Steered molecular dynamics simulation of conformational changes of immunoglobulin domain I27 interpret atomic force microscopy observations. *Chemical Physics*, **247**, 141–153.
- Majid, N., Bahar, M.M., Harper, R., Megharaj, M. & Naidu, R. 2023. Influence of biotic and abiotic factors on the development of non-wetting soils and management approaches: A review. *Soil Security*, **11**, 100091.

- Mao, J., Nierop, K.G.J., Dekker, S.C., Dekker, L.W. & Chen, B. 2019. Understanding the mechanisms of soil water repellency from nanoscale to ecosystem scale: a review. *Journal of Soils and Sediments*, **19**, 171–185.
- Markiewicz, P. & Goh, M.C. 1994. Atomic force microscopy probe tip visualization and improvement of images using a simple deconvolution procedure. *Langmuir*, **10**, 5–7.
- Marshall, P.A., Loeb, G.I., Cowan, M.M. & Fletcher, M. 1989. Response of microbial adhesives and biofilm matrix polymers to chemical treatments as determined by interference reflection microscopy and light section microscopy. *Applied and Environmental Microbiology*, **55**, 2827–2831.
- Medilanski, E., Kaufmann, K., Wick, L.Y., Wanner, O. & Harms, H. 2002. Influence of the Surface Topography of Stainless Steel on Bacterial Adhesion. *Biofouling*, **18**, 193–203.
- Meinders, J.M., van der Mei, H.C. & Busscher, H.J. 1995. Deposition Efficiency and Reversibility of Bacterial Adhesion under Flow. *Journal of Colloid and Interface Science*, **176**, 329–341.
- Meisner, A., Leizeaga, A., Rousk, J. & Bååth, E. 2017. Partial drying accelerates bacterial growth recovery to rewetting. *Soil Biology and Biochemistry*, **112**, 269–276.
- Meisner, A., Rousk, J. & Bååth, E. 2015. Prolonged drought changes the bacterial growth response to rewetting. *Soil Biology and Biochemistry*, **88**, 314–322.
- Meister, A., Gabi, M., Behr, P., Studer, P., Vörös, J., Niedermann, P., Bitterli, J., Polesel-Maris, J., Liley, M., Heinzelmann, H. & Zambelli, T. 2009. FluidFM: Combining Atomic Force Microscopy and Nanofluidics in a Universal Liquid Delivery System for Single Cell Applications and Beyond. *Nano Letters*, **9**, 2501–2507.
- Meyer, E. 1992. Atomic force microscopy. *Progress in Surface Science*, **41**, 3–49.
- Michel, J.P., Wang, Y.X., Kiesel, I., Gerelli, Y. & Rosilio, V. 2017. Disruption of Asymmetric Lipid Bilayer Models Mimicking the Outer Membrane of Gram-Negative Bacteria by an Active Plasticin. *Langmuir*, **33**, 11028–11039.
- Miller, C.M., Kim, Y.C. & Mittal, J. 2016. Protein Composition Determines the Effect of Crowding on the Properties of Disordered Proteins. *Biophysical Journal*, **111**, 28–37.
- Miltner, A., Bombach, P., Schmidt-Brücken, B. & Kästner, M. 2012. SOM genesis: microbial biomass as a significant source. *Biogeochemistry*, **111**, 41–55.
- Mitik-Dineva, N., Wang, J., Mocanasu, R.C., Stoddart, P.R., Crawford, R.J. & Ivanova, E.P. 2008. Impact of nano-topography on bacterial attachment. *Biotechnology Journal*, **3**, 536–544.
- Mitik-Dineva, N., Wang, J., Truong, V.K., Stoddart, P.R., Malherbe, F., Crawford, R.J. & Ivanova, E.P. 2009. Differences in colonisation of five marine bacteria on two types of glass surfaces. *Biofouling*, **25**, 621–631.
- Morales, V.L., Parlange, J.Y. & Steenhuis, T.S. 2010. Are preferential flow paths perpetuated by microbial activity in the soil matrix? A review. *Journal of Hydrology*, **393**, 29.

- Mozaheb, N. & Mingeot-Leclercq, M.-P. 2020. Membrane Vesicle Production as a Bacterial Defense Against Stress. *Frontiers in Microbiology*, **11**, (At: <https://www.frontiersin.org/articles/10.3389/fmicb.2020.600221>. Accessed: 16/3/2023).
- Mulansky, S., Saballus, M., Friedrichs, J., Bley, T. & Boschke, E. 2017. A novel protocol to prepare cell probes for the quantification of microbial adhesion and biofilm initiation on structured bioinspired surfaces using AFM for single-cell force spectroscopy. *Engineering in Life Sciences*, **17**, 833–840.
- Müller, D.J., Schoenenberger, C.A., Schabert, F. & Engel, A. 1997. Structural changes in native membrane proteins monitored at subnanometer resolution with the atomic force microscope: a review. *Journal of Structural Biology*, **119**, 149–157.
- Murphy, B. 2015. Key soil functional properties affected by soil organic matter - evidence from published literature. *IOP Conference Series: Earth and Environmental Science*, **25**, 012008.
- Navarro-Pedreño, J., Almendro-Candel, M.B. & Zorpas, A.A. 2021. The Increase of Soil Organic Matter Reduces Global Warming, Myth or Reality? *Sci*, **3**, 18.
- Neal, A.L., Bank, T.L., Hochella, M.F. & Rosso, K.M. 2005. Cell adhesion of *Shewanella oneidensis* to iron oxide minerals: Effect of different single crystal faces. *Geochemical Transactions*, **6**, 77.
- Neuman, K.C. & Nagy, A. 2008. Single-molecule force spectroscopy: optical tweezers, magnetic tweezers and atomic force microscopy. *Nature Methods*, **5**, 491–505.
- Nimmo, J.R. 2013. Porosity and Pore Size Distribution☆. In: *Reference Module in Earth Systems and Environmental Sciences*. Elsevier.
- Nimmo, J. & Shillito, R. 2023. Infiltration of Water Into Soil. In: *Oxford Research Encyclopedia of Environmental Science*.
- Nishu, S.D., No, J.H. & Lee, T.K. 2022. Transcriptional Response and Plant Growth Promoting Activity of *Pseudomonas fluorescens* DR397 under Drought Stress Conditions. *Microbiology Spectrum*, **10**, e00979-22.
- Oh, Y.J., Jo, W., Yang, Y. & Park, S. 2007. Influence of culture conditions on *Escherichia coli* O157:H7 biofilm formation by atomic force microscopy. *Ultramicroscopy*, **107**, 869–874.
- Oren, A. 1999. Bioenergetic aspects of halophilism. *Microbiology and molecular biology reviews: MMBR*, **63**, 334–348.
- Otter, J.A., Vickery, K., Walker, J.T., deLancey Pulcini, E., Stoodley, P., Goldenberg, S.D., Salkeld, J.A.G., Chewins, J., Yezli, S. & Edgeworth, J.D. 2015. Surface-attached cells, biofilms and biocide susceptibility: implications for hospital cleaning and disinfection. *Journal of Hospital Infection*, **89**, 16–27.
- Park, J.S. & Lin, H. 2022. Soil Water Retention Curve and Hydraulic Conductivity of Fungi-Treated Sand. 624–634.

- Parvin, F., Rahman, M.A., Deva, A.K., Vickery, K. & Hu, H. 2023. Staphylococcus aureus Cell Wall Phenotypic Changes Associated with Biofilm Maturation and Water Availability: A Key Contributing Factor for Chlorine Resistance. *International Journal of Molecular Sciences*, **24**, 4983.
- Petersen, L.W., Moldrup, P., Jacobsen, O.H. & Rolston, D.E. 1996. Relations between specific surface area and soil physical and chemical properties. *Soil Science*, **161**, 9–21.
- Pethica, J.B. & Oliver, W.C. 1987. Tip Surface Interactions in STM and AFM. *Physica Scripta*, **1987**, 61.
- Prakash, B., Veeregowda, B.M. & Krishnappa, G. 2003. Biofilms: A survival strategy of bacteria. *Current Science*, **85**, 1299–1307.
- Qiu, Y., Chien, C.-C., Maroulis, B., Bei, J., Gaitas, A. & Gong, B. 2022. Extending applications of AFM to fluidic AFM in single living cell studies. *Journal of Cellular Physiology*, **237**, 3222–3238.
- Ramos, J.-L. (Ed). 2004. *Pseudomonas: Volume 1 Genomics, Life Style and Molecular Architecture*. Springer US, Boston, MA. (At: <https://link.springer.com/10.1007/978-1-4419-9086-0>. Accessed: 29/3/2023).
- Ricci, D. & Braga, P.C. 2004. Recognizing and Avoiding Artifacts in AFM Imaging. In: *Atomic Force Microscopy: Biomedical Methods and Applications* (eds. Braga, P.C. & Ricci, D.), pp. 25–37. Humana Press, Totowa, NJ.
- Rijnaarts, H.H.M., Norde, W., Lyklema, J. & Zehnder, A.J.B. 1999. DLVO and steric contributions to bacterial deposition in media of different ionic strengths. *Colloids and Surfaces B: Biointerfaces*, **14**, 179–195.
- Ripa, R., Shen, A.Q. & Funari, R. 2020. Detecting Escherichia coli Biofilm Development Stages on Gold and Titanium by Quartz Crystal Microbalance. *ACS Omega*, **5**, 2295–2302.
- Roberson, E.B. & Firestone, M.K. 1992. Relationship between Desiccation and Exopolysaccharide Production in a Soil Pseudomonas sp. *Applied and Environmental Microbiology*, **58**, 1284–1291.
- Rodriguez, R.D., Lacaze, E. & Jupille, J. 2012. Probing the probe: AFM tip-profiling via nanotemplates to determine Hamaker constants from phase–distance curves. *Ultramicroscopy*, **121**, 25–30.
- Roper, M.M. 2004. The isolation and characterisation of bacteria with the potential to degrade waxes that cause water repellency in sandy soils. *Soil Research*, **42**, 427–434.
- Rousk, J., Bååth, E., Brookes, P.C., Lauber, C.L., Lozupone, C., Caporaso, J.G., Knight, R. & Fierer, N. 2010. Soil bacterial and fungal communities across a pH gradient in an arable soil. *The ISME Journal*, **4**, 1340–1351.
- Roy, J.L., McGill, W.B. & Rawluk, M.D. 1999. Petroleum residues as water-repellent substances in weathered nonwettable oil-contaminated soils. *Canadian Journal of Soil Science*, **79**, 367–380.

- Salifu, E. & El Mountassir, G. 2021. Fungal-induced water repellency in sand. *Géotechnique*, **71**, 608–615.
- Salifu, E., El Mountassir, G., Minto, J.M. & Tarantino, A. 2022. Hydraulic behaviour of fungal treated sand. *Geomechanics for Energy and the Environment*, **30**, 100258.
- Seaton, F.M., Jones, D.L., Creer, S., George, P.B.L., Smart, S.M., Lebron, I., Barrett, G., Emmett, B.A. & Robinson, D.A. 2019. Plant and soil communities are associated with the response of soil water repellency to environmental stress. *Science of The Total Environment*, **687**, 929–938.
- Sheng, X., Ting, Y.P. & Pehkonen, S.O. 2007. Force measurements of bacterial adhesion on metals using a cell probe atomic force microscope. *Journal of Colloid and Interface Science*, **310**, 661–669.
- Shibata-Seki, T., Tajima, K., Takahashi, H., Seki, H., Masai, J., Goto, H., Kobatake, E., Akaike, T. & Itoh, N. 2015. AFM characterization of chemically treated corneal cells. *Analytical and Bioanalytical Chemistry*, **407**, 2631–2635.
- Silveira, É.L. da, Pereira, R.M., Scaquitto, D.C., Pedrinho, E.A.N., Val-Moraes, S.P., Wickert, E., Carareto-Alves, L.M. & Lemos, E.G. de M. 2006. Bacterial diversity of soil under eucalyptus assessed by 16S rDNA sequencing analysis. *Pesquisa Agropecuária Brasileira*, **41**, 1507–1516.
- Six, J., Frey, S.D., Thiet, R.K. & Batten, K.M. 2006. Bacterial and Fungal Contributions to Carbon Sequestration in Agroecosystems. *Soil Science Society of America Journal*, **70**, 555–569.
- Skulason, H. & Frisbie, C.D. 2000. Rupture of Hydrophobic Microcontacts in Water: Correlation of Pull-Off Force with AFM Tip Radius. *Langmuir*, **16**, 6294–6297.
- Skulason, H. & Frisbie, C.D. 2002. Contact Mechanics Modeling of Pull-Off Measurements: Effect of Solvent, Probe Radius, and Chemical Binding Probability on the Detection of Single-Bond Rupture Forces by Atomic Force Microscopy. *Analytical Chemistry*, **74**, 3096–3104.
- Smucker, A.J.M. 1993. Soil Environmental Modifications of Root Dynamics and Measurement. *Annual Review of Phytopathology*, **31**, 191–218.
- Soto González, H.H., Peñuelas-Rubio, O., Argente-Martínez, L., Leyva Ponce, A., Herrera Andrade, M.H., Hasanuzzaman, M., González Aguilera, J. & Eduardo Teodoro, P. 2021. Salinity effects on water potential and the normalized difference vegetation index in four species of a saline semi-arid ecosystem. *PeerJ*, **9**, e12297.
- Spagnoli, C., Beyder, A., Besch, S. & Sachs, F. 2008. Atomic force microscopy analysis of cell volume regulation. *Physical review. E, Statistical, nonlinear, and soft matter physics*, **78**, 031916.
- Spengler, C., Thewes, N., Jung, P., Bischoff, M. & Jacobs, K. 2017. Determination of the nano-scaled contact area of staphylococcal cells. *Nanoscale*, **9**, 10084–10093.

- Sullan, R.M.A., Beaussart, A., Tripathi, P., Derclaye, S., El-Kirat-Chatel, S., Li, J.K., Schneider, Y.-J., Vanderleyden, J., Lebeer, S. & Dufrêne, Y.F. 2013a. Single-cell force spectroscopy of pili-mediated adhesion. *Nanoscale*, **6**, 1134–1143.
- Sullan, R.M.A., Churnside, A.B., Nguyen, D.M., Bull, M.S. & Perkins, T.T. 2013b. Atomic force microscopy with sub-picoNewton force stability for biological applications. *Methods*, **60**, 131–141.
- Sun, Z., Boneschanscher, M.P., Swart, I., Vanmaekelbergh, D. & Liljeroth, P. 2011. Quantitative Atomic Force Microscopy with Carbon Monoxide Terminated Tips. *Physical Review Letters*, **106**, 046104.
- Talà, L., Fineberg, A., Kukura, P. & Persat, A. 2019. Pseudomonas aeruginosa orchestrates twitching motility by sequential control of type IV pili movements. *Nature Microbiology*, **4**, 774–780.
- Thewes, N., Loskill, P., Jung, P., Peisker, H., Bischoff, M., Herrmann, M. & Jacobs, K. 2014. Hydrophobic interaction governs unspecific adhesion of staphylococci: a single cell force spectroscopy study. *Beilstein Journal of Nanotechnology*, **5**, 1501–1512.
- Thewes, N., Loskill, P., Spengler, C., Hümbert, S., Bischoff, M. & Jacobs, K. 2015. A detailed guideline for the fabrication of single bacterial probes used for atomic force spectroscopy. *The European Physical Journal. E, Soft Matter*, **38**, 140.
- Tisdall, J.M. 1995. Formation of Soil Aggregates and Accumulation of Soil Organic Matter. In: *Structure and Organic Matter Storage in Agricultural Soils*. CRC Press.
- Toca-Herrera, J.L. 2019. Atomic Force Microscopy Meets Biophysics, Bioengineering, Chemistry, and Materials Science. *Chemsuschem*, **12**, 603–611.
- Touhami, A., Jericho, M.H. & Beveridge, T.J. 2004. Atomic Force Microscopy of Cell Growth and Division in Staphylococcus aureus. *Journal of Bacteriology*, **186**, 3286–3295.
- Trache, A. & Meininger, G.A. 2008. Atomic Force Microscopy (AFM). *Current Protocols in Microbiology*, **8**, 2C.2.1-2C.2.17.
- Tuleva, B.K., Ivanov, G.R. & Christova, N.E. 2002. Biosurfactant Production By A New Pseudomonas Putida Strain. *Zeitschrift für Naturforschung C*, **57**, 356–360.
- Tuson, H.H. & Weibel, D.B. 2013. Bacteria-surface interactions. *Soft matter*, **9**, 4368–4380.
- Uddin, F. 2008. Clays, Nanoclays, and Montmorillonite Minerals. *Metallurgical and Materials Transactions A*, **39**, 2804–2814.
- Vadillo-Rodríguez, V., Busscher, H.J., Norde, W., de Vries, J. & van der Mei, H.C. 2004. Atomic force microscopic corroboration of bond aging for adhesion of Streptococcus thermophilus to solid substrata. *Journal of Colloid and Interface Science*, **278**, 251–254.
- Vahabi, S., Nazemi Salman, B. & Javanmard, A. 2013. Atomic Force Microscopy Application in Biological Research: A Review Study. *Iranian Journal of Medical Sciences*, **38**, 76–83.

- Variola, F. 2015. Atomic force microscopy in biomaterials surface science. *Physical Chemistry Chemical Physics*, **17**, 2950–2959.
- Vasileva-Tonkova, E., Galabova, D., Stoimenova, E. & Lalchev, Z. 2006. Production and properties of biosurfactants from a newly isolated *Pseudomonas fluorescens* HW-6 growing on hexadecane. *Zeitschrift Fur Naturforschung. C, Journal of Biosciences*, **61**, 553–559.
- Vogelmann, E.S., Reichert, J.M., Prevedello, J., Consensa, C.O.B., Oliveira, A.E., Awe, G.O. & Mataix-Solera, J. 2013. Threshold water content beyond which hydrophobic soils become hydrophilic: The role of soil texture and organic matter content. *Geoderma*, **209**, 177–187.
- Waraich, E.A., Ahmad, R. & Ashraf, M.Y. 2011. Role of Mineral Nutrition in Alleviation of Drought Stress in Plants. *Australian Journal of Crop Science*, **5**, 764–777.
- Watanabe, K. & Flury, M. 2008. Capillary bundle model of hydraulic conductivity for frozen soil. *Water Resources Research*, **44**, (At: <https://onlinelibrary.wiley.com/doi/abs/10.1029/2008WR007012>. Accessed: 26/9/2023).
- Weber, P.L., Hermansen, C., Norgaard, T., Pesch, C., Moldrup, P., Greve, M.H., Müller, K., Arthur, E. & de Jonge, L.W. 2021. Moisture-dependent Water Repellency of Greenlandic Cultivated Soils. *Geoderma*, **402**, 115189.
- Westall, F., Steele, A., Toporski, J., Walsh, M., Allen, C., Guidry, S., McKay, D., Gibson, E. & Chafetz, H. 2000. Polymeric substances and biofilms as biomarkers in terrestrial materials: Implications for extraterrestrial samples. *Journal of Geophysical Research: Planets*, **105**, 24511–24527.
- Westra, K.L. & Thomson, D.J. 1994. Atomic force microscope tip radius needed for accurate imaging of thin film surfaces. *Journal of Vacuum Science & Technology B: Microelectronics and Nanometer Structures Processing, Measurement, and Phenomena*, **12**, 3176–3181.
- Win, K.T., Tanaka, F., Okazaki, K. & Ohwaki, Y. 2018. The ACC deaminase expressing endophyte *Pseudomonas* spp. Enhances NaCl stress tolerance by reducing stress-related ethylene production, resulting in improved growth, photosynthetic performance, and ionic balance in tomato plants. *Plant Physiology and Biochemistry*, **127**, 599–607.
- Worrich, A., König, S., Banitz, T., Centler, F., Frank, K., Thullner, M., Harms, H., Miltner, A., Wick, L.Y. & Kästner, M. 2016. Bacterial Dispersal Promotes Biodegradation in Heterogeneous Systems Exposed to Osmotic Stress. *Frontiers in Microbiology*, **7**, (At: <https://www.frontiersin.org/articles/10.3389/fmicb.2016.01214>. Accessed: 14/11/2023).
- Wu, W., Lutz, C., Mersch, S., Thelen, R., Greiner, C., Gomard, G. & Hölscher, H. 2018. Characterization of the microscopic tribological properties of sandfish (*Scincus scincus*) scales by atomic force microscopy. *Beilstein Journal of Nanotechnology*, **9**, 2618–2627.

- Xia, Y., Chen, X., Zheng, X., Deng, S., Hu, Y., Zheng, S., He, X., Wu, J., kuzyakov, Y. & Su, Y. 2020. Preferential uptake of hydrophilic and hydrophobic compounds by bacteria and fungi in upland and paddy soils. *Soil Biology and Biochemistry*, **148**, 107879.
- Xu, L.-C. & Logan, B.E. 2006. Adhesion forces between functionalized latex microspheres and protein-coated surfaces evaluated using colloid probe atomic force microscopy. *Colloids and Surfaces. B, Biointerfaces*, **48**, 84–94.
- Xu, L.-C. & Siedlecki, C.A. 2012. Submicron-textured biomaterial surface reduces staphylococcal bacterial adhesion and biofilm formation. *Acta Biomaterialia*, **8**, 72–81.
- Yamashita, H., Taoka, A., Uchihashi, T., Asano, T., Ando, T. & Fukumori, Y. 2012. Single-Molecule Imaging on Living Bacterial Cell Surface by High-Speed AFM. *Journal of Molecular Biology*, **422**, 300–309.
- Yan, Y., Geng, Y. & Hu, Z. 2015. Recent advances in AFM tip-based nanomechanical machining. *International Journal of Machine Tools and Manufacture*, **99**, 1–18.
- Yang, Q., Ma, Q., Herum, K.M., Wang, C., Patel, N., Lee, J., Wang, S., Yen, T.M., Wang, J., Tang, H., Lo, Y.-H., Head, B.P., Azam, F., Xu, S., Cauwenberghs, G., McCulloch, A.D., John, S., Liu, Z. & Lal, R. 2019. Array atomic force microscopy for real-time multiparametric analysis. *Proceedings of the National Academy of Sciences*, **116**, 5872–5877.
- Young, P.M., Tobyn, M.J., Price, R., Buttrum, M. & Dey, F. 2006. The use of colloid probe microscopy to predict aerosolization performance in dry powder inhalers: AFM and in vitro correlation. *Journal of Pharmaceutical Sciences*, **95**, 1800–1809.
- Zeng, G., Müller, T. & Meyer, R.L. 2014. Single-Cell Force Spectroscopy of Bacteria Enabled by Naturally Derived Proteins. *Langmuir*, **30**, 4019–4025.
- Zhang, W., Stack, A.G. & Chen, Y. 2011. Interaction force measurement between E. coli cells and nanoparticles immobilized surfaces by using AFM. *Colloids and Surfaces. B, Biointerfaces*, **82**, 316–324.

9 Annex

9.1 List of abbreviations

AFM: Atomic force microscope

CA: Contact angle

CMA: Cell-mineral association

CFM: Chemical force microscopy

DMT: Derjaguin–Müller–Toporov

EPS: Extracellular polymeric substances

ESEM: Environmental scanning electron microscope

FD: Force-distance

LPS: Lipopolysaccharides

MV: Membrane vesicles

OD: Optical density

P_{ad} : Adhesion pressure

PFQNM: PeakForce Quantitative Nanomechanical Mapping

ROI: Region-of-interest

SNL: Sharp Nitride Lever

SOM: Soil organic matter

SWR: Soil water repellency

XDLVO: Extended Derjaguin–Landau–Verwey–Overbeek

XPS: X-ray photoelectron spectroscopy

9.2 List of figures

Fig. 1. Top left: single bacterial cell scanned with increased loading force from 5 to 75 nN in increments of 5 nN. High loading forces lead to cell deformation, which affects the quality of cell profiling negatively. The inset (top left) shows a subsequent scan of the cell at 5 nN, where the cell remains undamaged. Adhesion is influenced by the loading force, as seen in the brighter color of the adhesion channel (top right) and increased adhesion forces along the line scan (bottom) which is aligned with the direction of increased loading force (blue arrow).

Fig. 2. FD curve (left) obtained between a CFM probe and a bacterial cell with sketches of tip-cell configuration (right) at the corresponding positions (numbers). The black curve illustrates the approach of the probe towards the cell surface, marking the point of initial tip-cell contact (1). Continuing the approach, the tip deforms the surface until reaching a predefined force setpoint (2). Subsequent retraction (red curve) shows force reduction, reaching zero (3), followed by a slight negative (attractive) force at the cell surface position (4). This is followed by a maximum adhesion peak (5). Then, a gradual unbinding of adsorbed molecules occurs reaching the rupture of the final bond leading to a complete separation (6). Note: Positions 1, 3, and 4 merge to the same point when there is no energy dissipation on the cell surface.

Fig. 3. Sketches illustrating the tip-sample interactions corresponding to the sequential steps addressed in the FD curve of **Fig. 2** (section 1.7), between (a) CFM tip and (b) mineral tip and a single bacterial cell. The configuration in (c) is reversed with the cells attached to the colloidal probe scanning against the sample surface.

Fig. 4. (a) Box plots of rupture forces (position 6 in **Fig. 2**, section 1.7) for CFM (Abu Quba *et al.*, 2022) and mineral (Abu Quba *et al.*, 2023) tips, with numbers on the top of frequency (%) of events towards cells grown under unstressed (white) / stressed (gray) conditions. Configurations of the CFM (b) and mineral (c) tips elucidate that the lower rupture forces observed in (a), for CFM tips, are attributed to fewer intact bonds reaching position 6 compared to the relatively blunt mineral tips and (d) comparison between the theoretical and real situations of colloidal probe system highlighting discrepancies in bond distribution. Molecules that detach earlier (broken free bonds in (d)) gradually recover random orientation while the newly detached central bonds still have an orientation influenced by stretch direction.

Fig. 5. Aspect ratio (3D area / 2D area) shown in the upper section and only 3D area in the lower section as a function of the height from the tip apex for various tips, as illustrated by the

sketches. The mineral probes (blue dots), with relatively flat and larger tips, exhibit lower aspect ratios and larger 3D areas compared to the sharp SNL (yellow line) and CFM (black triangles and green squares) tips.

Fig. 6. Two step model illustrating bacterial growth over a drying-rewetting cycle. The sketch demonstrates the cumulative steps associated with biofilm formation on minerals surfaces from cells originally suspended in SOM. The lower bar presents findings supporting the proposed growth scenario. At position 1, the planktonic cells are in optimal condition for growth by division processes. AFM images at position 1 reveal the tendency of *B. subtilis* (up) and *P. fluorescens* (down) cells, with lower hydrophobicity, to remain isolated (indicated by black arrow). Some cells may recondition surrounding solid surfaces as shown after the removal of *P. putida* cell from epoxy glue (Abu Quba *et al.*, 2023) surface, line scan at position 1 (my unpublished results). As the dry stress develops, increased cell hydrophobicity prompts their association and migration towards the mineral surface. The AFM images of stressed cells show their tendency to form associations (observe the decrease in cell-cell spacing in AFM images at position 2, white arrow). Subsequently, bond strengthening progressively takes place for the cells that are already at the mineral surfaces. Fast processes like the increase of the contact area is shown by the SEM image (Gu *et al.*, 2017) at position 3 (potentially starting at position 2 as well). I propose that the whole microbial colony will structure to be densely packed increasing the number of cells adhering to the mineral surfaces with rising osmotic pressure (position 4). Throughout this transition (positions 1 to 4), the microbial colony actively defends stress by enhanced cell surface hydrophobicity, partial decay of cell subpopulations for biomass nutrition, and the release of outer membrane vesicles, reaching maximal release at position 4 shown by the SEM image (Baumgarten *et al.*, 2012). Upon rewetting, living biomass regains energy resources to continue their biological activities and form biofilm illustrated by organizational steps 5 and 6 supported by research (Donlan *et al.*, 1994; Otter *et al.*, 2015; Chitlapilly Dass & Wang, 2022; Parvin *et al.*, 2023). The AFM (Ripa *et al.*, 2020) and SEM (Epstein *et al.*, 2011) images show biofilm initiation at the respective steps 5 and 6. Notably, position 4 and 6 show distinct microbial configurations, each contributing various services to the soil ecosystem, as detailed in the text. Images reproduced by permission of IOP Publishing Ltd.



Abd Alaziz Abu Quba

**Master of Material Science,
Researcher in Environmental Sciences**

LANGUAGES

Arabic	Mother tongue
English	Fluent
German	Good

EDUCATION

2012-2016	Master of Materials Science (TU Darmstadt) Master Degree in Materials Science. DAAD Scholarship holder.
2012	Entrepreneurship course (Syrian Enterprise & Business Centre) Full scholar year in Superior Knowledge by Intensive Labor Learning Schemes (SKILLS) in collaboration with ETF "European Training Foundation".
2006-2011	Bachelor of Engineering (Damascus University) Mechanical Design and Material Science Engineering degree.

EDUCATIONAL EXPERIENCE & PROJECTS

2017-Present	Research Assistant (RPTU Kaiserslautern-Landau) <u>Institute for Environmental Sciences, RPTU Kaiserslautern-Landau, Germany.</u> I work on the BACSWR project: impact of bacterial biomass on the surface wettability of soil particles under varying moisture conditions. Research interests: 1) soil wetting dynamics and specially Soil Water Repellency (SWR), 2) physicochemical properties of natural abiotic and biological substances at the nano and macro scale, 3) interaction between mineral and soil bacteria at the single cell level. Development of Atomic Force Microscopy (AFM) approaches for the study of natural substances under environmental conditions. Applied AFM in fluids, employing various probes including standard sharp, home-modified, and chemically modified tips. AFM modes: Tapping Mode, PeakForce Quantitative Nanomechanics Mapping (PFQNM) Mode, force spectroscopy with constant force or constant height with delay in air and fluids.
---------------------	----------------------------------------------------------------------------------------------------------------------------------------------------------------------------------------------------------------------------------------------------------------------------------------------------------------------------------------------------------------------------------------------------------------------------------------------------------------------------------------------------------------------------------------------------------------------------------------------------------------------------------------------------------------------------------------------------------------------------------------------------------------------------------------------------------------------------------------------------------------------------------------------------------------------------------------------------------------------------------------------------

- Jun 2016-Dec 2017** **Master Thesis** (*TU Darmstadt*)
 Impact of severe plastic deformation (SPD) processes on the microstructure evolution and mechanical properties of Cu-X alloys (used techniques: Micro/ Nano Indentation and Scanning Electron Microscope (SEM, BSE, EBSD))
 Cooperation with: Piter the Great St. Petersburg Polytechnic University, St. Petersburg, 195251, Russia.
- Apr 2015-Dec 2015** **Internship & Workstudent** (*Fraunhofer institute IISB, Erlangen*)
 Worked with the nanotechnology group, use of scanning probe microscopy in contact mode with TUNA extension (conductive atomic force microscopy (cAFM) and scanning spreading resistance microscopy (SSRM)) to characterize focused ion beam induced electric damage on semiconductor materials such as (Si, SiC). Used current-voltage spectroscopy (ramp) to study the Schottky contacts of the diodes.
- Apr 2013-Jun 2013** **Advanced Research Lab** (*TU Darmstadt, Physical Metallurgy group*)
 Study of the dislocation structure and density of CaF₂ and SrTiO₃ single crystals using indentation tests and etch pit technique (using: Micro/ Nano Indentation, Laser Microscope, AFM, SEM).
- Jun 2011-Dec 2011** **Bachelor Thesis** (*Damascus University*)
 Design of a forklift to transport products automatically. The forklift follows a black line (track) such that it moves the product from the beginning to the end of the line. I programmed the forklift using a Programmable Logic Controller (PLC).
- 2017-Present** **Teacher Assistant** (*RPTU Kaiserslautern-Landau*)
 Supervisor for lab experiments to check environmental contaminants:
Lab 1: Extraction of polycyclic aromatic hydrocarbons (PAHs) from soil samples and the analysis of PAHs through high performance liquid chromatography (HPLC).
Lab 2: Extraction of the aromatic hydrocarbons benzene, toluene, and p-Xylene (BTEX) from aqueous samples and the analysis of BTEX through gas chromatography.
Lab 3: Extraction of copper from soil sample with aqua regia digestion and the analysis using atomic absorption spectrometry (AAS).
- 2013- 2016** **Teacher Assistant** (*TU Darmstadt, Physics of Surfaces group*)
 Supervisor of lab experiments to check surface properties of materials:
Lab 1: Surface characterization with Magnetic Force Microscopy (MFM) using AFM lift (Interleave) mode including calculating the magnetic stray field of old and new hard disc drive domains.
Lab 2: Studying the wettability and calculating of the surface energies of several hydrophilic and hydrophobic materials with contact angle technique.

TECHNICAL SKILLS

Microscopy: Atomic Force Microscope in air and fluids (FM, AM, SSRM, cAFM, PFQNM, MFM and lithography). I used AFM for bacterial cells, minerals particles and cell-mineral interactions at the single-cell level. I also used AFM for magnetic, nanoparticles, semiconductors, perovskite, glass and glue surfaces. Scanning Electron Microscope (SEM, SE, BSE, EBSD and EDX). Optical (bright, dark) field microscopy and laser microscopy. Live/Dead cell imaging with fluorescence microscopy.

Analytical methods: Elemental analysis with atomic absorption spectrometry (AAS). Sessile and pendant drop techniques for contact angle and surface tension. Time dependent contact angle. Basic experience with Focused Ion Beam (FIB), Transmission Electron Microscopy (TEM), High Performance Liquid Chromatography (HPLC), Gas Chromatography (GC), Pulsed Laser Deposition (PLD), X-ray crystallography (XRD), optical sensors, light sensors, rotary sensor (encoder), stepper motors.

Mechanical tests: micro-hardness, nanoindentation, tensile strength, compression, fracture toughness, fatigue, Charpy test.

Software: NanoScope, Gwyddion, Nanosurf naio, AutoCAD, SolidWorks, Abaqus finite element analysis (FEA), Microsoft Office, Origin. Programmable Logic Controller (PLC), Microcontroller.

PUBLICATIONS

"Hypertonic stress-induced changes of *Pseudomonas fluorescens* adhesion towards soil minerals studied by AFM."

Scientific Reports 13.1 (2023): 17146.

Abd Alaziz Abu Ouba, Marc-Oliver Goebel, Mariam Karagulyan, Anja Miltner, Matthias Kästner, Jörg Bachmann, Gabriele E. Schaumann, Doerte Diehl.

"Changes in cell surface properties of *Pseudomonas fluorescens* by adaptation to NaCl induced hypertonic stress."

FEMS microbes 4 (2023): xtac028.

Abd Alaziz Abu Ouba, Marc-Oliver Goebel, Mariam Karagulyan, Anja Miltner, Matthias Kästner, Jörg Bachmann, Gabriele E. Schaumann, Doerte Diehl.

"Water Stress-Driven Changes in Bacterial Cell Surface Properties."

Applied and Environmental Microbiology 88.21 (2022): e00732-22.

Mariam Karagulyan, Marc-Oliver Goebel, Doerte Diehl, Abd Alaziz Abu Ouba , Matthias Kästner , Jörg Bachmann², Lukas Y Wick, Gabriele E Schaumann , Anja Miltner.

"Quality control of direct cell-mineral adhesion measurements in air and liquid using inverse AFM imaging."

RSC advances 11.10 (2021): 5384-5392.

Abu Ouba Abd Alaziz, Gabriele E. Schaumann, Mariam Karagulyan, and Doerte Diehl.

"A new approach for repeated tip-sample relocation for AFM imaging of nano and micro sized particles and cells in liquid environment."

Ultramicroscopy 211 (2020): 112945.

Abu Quba Abd Alaziz, Gabriele E. Schaumann, Mariam Karagulyan, and Doerte Diehl.

"Detailed characterisation of focused ion beam induced lateral damage on silicon carbide samples by electrical scanning probe microscopy and transmission electron microscopy."

Journal of applied physics 123.12 (2018).

Stumpf, F., Abu Quba, A. A., Singer, P., Rumler, M., Cherkashin, N., Schamm-Chardon, S., Cours, R. & Rommel, M.

"Validation of a field deployable reactor for in situ formation of NOM-engineered nanoparticle corona."

Environmental Science: Nano 7.2 (2020): 486-500.

Tayyebi Sabet Khomami, N., Philippe, A., Abu Quba, A. A., Lechtenfeld, O. J., Guigner, J. M., Heissler, S., & Schaumann, G. E.

"The influence of severe plastic deformation on microstructure formation of Cu-based alloys."

Naumov, A. A., Borisov, A. S., Durst, K., & Abu Quba, A. A. (2016).

CONFERENCES

"Hypertonic stress-induced changes of *Pseudomonas fluorescens* adhesion towards soil minerals studied by AFM." (oral presentation)

DBG Jahrestagung, Halle (Saale), Germany, 2023.

Abd Alaziz Abu Quba, Marc-Oliver Goebel, Jörg Bachmann, Mariam Karagulyan, Anja Miltner, Matthias Kästner, Gabriele E. Schaumann, Dörte Diehl.

"Use of Atomic Force Microscopy for Measuring Cell-Mineral Adhesion." (oral presentation)

DBG Jahrestagung, Trier, Germany, 2022.

Abd Alaziz Abu Quba, Marc-Oliver Goebel, Jörg Bachmann, Mariam Karagulyan, Anja Miltner, Matthias Kästner, Gabriele E. Schaumann, Dörte Diehl.

"Use of Atomic Force Microscopy for Measuring Cell-Mineral Adhesion." (oral presentation)

Eurosoil, online conference, 2021.

Abd Alaziz Abu Quba, Marc-Oliver Goebel, Jörg Bachmann, Mariam Karagulyan, Anja Miltner, Matthias Kästner, Gabriele E. Schaumann, Dörte Diehl.

"Application of chemical force microscopy for bacterial-induced soil water repellency." (oral presentation)

DBG Jahrestagung, Bern, Switzerland, 2019.

Abd Alaziz Abu Quba, Marc-Oliver Goebel, Jörg Bachmann, Mariam Karagulyan, Anja Miltner, Matthias Kästner, Gabriele E. Schaumann, Dörte Diehl.

"Application of chemical force microscopy for bacterial-induced soil water repellency." (oral presentation)

Biohydrology Conference, Valencia, Spain 2019.

Abd Alaziz Abu Quba, Marc-Oliver Goebel, Jörg Bachmann, Mariam Karagulyan, Anja Miltner, Matthias Kästner, Gabriele E. Schaumann, Dörte Diehl.

"Direct measurement of cell-mineral interactions of natural soil materials using atomic force microscopy (AFM) – Method development." (Poster)

NC-AFM, Finland, Porvoo, 2018.

Abd Alaziz Abu Quba, Marc-Oliver Goebel, Jörg Bachmann, Mariam Karagulyan, Anja Miltner, Matthias Kästner, Gabriele E. Schaumann, Dörte Diehl.

CO-AUTHOR in CONFERENCES

"Bacterial cell-mineral associations and their stability under varying moisture conditions."

EGU23, Vienna, Austria, 2023.

Marc-Oliver Goebel, Mariam Karagulyan, Anja Miltner, Abd Alaziz Abu Quba, Dörte Diehl, Gabriele E. Schaumann, Matthias Kästner, and Jörg Bachmann.

"Contribution of bacterial biomass to soil particle wettability."

ISMOM conference, Seville, Spain, 2019.

Marc-Oliver Goebel, Mariam Karagulyan, Anja Miltner, Abd Alaziz Abu Quba, Dörte Diehl, Gabriele E. Schaumann, Matthias Kästner, and Jörg Bachmann.

"Role of bacterial biomass in the development of soil water repellency."

WCSS21 conference, Rio de Janeiro, Brazil, 2018.

Marc-Oliver Goebel, Mariam Karagulyan, Anja Miltner, Abd Alaziz Abu Quba, Dörte Diehl, Gabriele E. Schaumann, Matthias Kästner, and Jörg Bachmann.

"Impact of osmotic and matric stress on surface properties of bacteria."

ISME17 conference, Leipzig, Germany, 2018.

Mariam Karagulyan, Lukas Y. Wick, Jörg Bachmann, Marc-Oliver Goebel, Dörte Diehl, Abd Alaziz Abu Quba, Matthias Kästner, Anja Miltner.

"The influence of severe plastic deformation on microstructure formation of Cu-based alloys."

ICPNS conference, Seattle, USA, 2016

Anton A. Naumov; Anatolii S. Borisov, Peter the Great St. Petersburg Polytechnic University; Karsten Durst; Abd Alaziz Abu Quba.

"Experimental characterisation of FIB induced lateral damage on silicon carbide samples."

MNE International Conference on Micro and Nano Engineering, Hague, Netherlands, 2015.

Florian Stumpf, Maximilian Rumler, Abd Alaziz Abu Quba, Philipp Singer, Mathias Rommel.